GUANIDINIUM BASED ANION EXCHANGE MEMBRANES FOR SOLID POLYMER ALKALINE FUEL CELL APPLICATIONS

by

SYED DAWAR SAJJAD

Presented to the Faculty of the Graduate School of

The University of Texas at Arlington in Partial Fulfillment

of the Requirements

for the Degree of

DOCTOR OF PHILOSOPHY

THE UNIVERSITY OF TEXAS AT ARLINGTON

December 2015

Acknowledgements

First and foremost I would like to express my sincere gratitude towards my supervisor Dr. Fuqiang Liu, for his encouragement, academic and moral support throughout the rough road of completing this research. At various stages of this program, I was faced with some daunting times and it was his compassion and reassurance which kept me going in those testing days. I am particularly grateful to him for his genuine kindness and support.

My thesis committee remained a great source of guidance during my research. I am grateful to Dr. Yi Hong, Dr. Pranesh Aswath, Dr. Yaowu Hao and Dr. Kyungsuk Yum for their invaluable teachings and words of wisdom.

I want to recognize the Department of Materials Science and Engineering for permitting me to benefit from all their facilities and for providing me the opportunity to carry out my research without any hindrance. I also want to thank all the department staff, particularly Jennifer and Beth for all their help and support.

I am highly indebted to my lab mates for their assistance over the years. A special mention to Dr. Chiajen Hsu, Dr. Dong Liu, Dr. Noor, Zi, Amir and Yi for their wonderful support.

I am most grateful to my beloved wife Ghazal for her unwavering support and the confidence she instilled in me. It is due to the sacrifices she made for me that I have been able to achieve this milestone. I am grateful to my family members,

especially my mother for her unbelievable faith in me and her countless prayers for my well-being and success. My father has sacrificed a lot for my education. I thank him for always being my biggest source of inspiration. I would also like to mention my brother for having my back and supporting me whenever I have needed him. I also thank my father-in-law and mother-in-law for their continuous motivation and prayers as well as my Aunt Shahnaz for being my home away from home.

However, lastly I would like to thank Allah for letting this opportunity come my way and for always showing me light whenever the night was dark.

In the words Ali ibn Abi Talib (A.S), "Knowledge gives life to the soul"

November 19, 2015

Abstract

GUANIDINIUM BASED ANION EXCHANGE MEMBRANES FOR SOLID POLYMER ALKALINE FUEL CELL APPLICATIONS

Syed Dawar Sajjad, PhD

The University of Texas at Arlington, 2015

Supervising Professor: Fuqiang Liu

Fuel Cells and low temperature traditional PEM Fuel Cells in particular suffer from the acute yet long standing issues of cost and performance. This has severely hindered the commercialization of fuel cells but Alkaline Anion Exchange Membrane Fuel Cells (AAEMFCs) pose as a breakthrough technology by offering improved conversion efficiency (a virtue of fast kinetics in the alkaline media) and lower costs (from the prospect of using non-noble metal catalysts). However, before systematic testing of non-noble metal catalysis is tested on this system, it is imperative to develop a reliable anion exchange membrane which lies at the heart of the fuel cell and solve their inherent problems of low conductivity and fast degradation.

In this work, a series of novel AEMs are developed based on the guanidinium functional group. A bottom-up approach is taken starting with the synthesis of the prepolymer. The guanidine polymer is synthesized through a polycondensation reaction between a guanidinium salt and two different diamines. The guanidinium functional group is attached directly to the polymer backbone to enhance both ionic conductivity and durability. As a result of this configuration and the resonance stabilized structure of guanidinium, it exhibited superior stability compared to commercial quaternary ammonium AEMs after being exposed in extreme conditions of 5 M KOH solution at 55°C for 50 h. This prepolymer is then subject to minor post modification such as crosslinking or tethering a lipophilic element to its main chain for suitable physio-chemical and mechanical properties. In addition, to achieve these optimum properties along with the required electrochemical performance, the membranes are eventually fabricated using two different approaches.

The composite membrane is fabricated by incorporating guanidinium based polymer solution into a porous polytetrafluoroethylene (PTFE) film. Polymer crosslinking helped reinforce the mechanical strength of the membranes and interlock the guanidinium moieties to the porous PTFE. The hybrid blend membranes were obtained by blending the prepolymer with chitosan, another strengthening agent. Whereas the composite membrane displayed an outstanding ionic conductivity 80 mS cm^{-1} (at 20°C in deionized water), the hybrid blend

membranes exhibited relatively lower values due to the effect from the blend components. However, the selectivity (ratio of ionic conductivity to methanol permeability) of the hybrid blend membranes is found to be superior even when compared to commercial membranes. Similarly, when used in a direct methanol alkaline fuel cells (DMAFCs) it fared even better than a commercial AEM reference reaching to an OCV of 0.69 V compared to the 0.47V of Tokuyama A201 at room temperature. Overall, the developed membranes demonstrate superior performance and therefore pose great promise for direct methanol anion exchange fuel cell (DMAFC) applications.

Furthermore, through an experimental micro/nano phase analysis backed by simulation, the hydroxide transport process is highlighted which before now has not been well understood or experimentally probed in the past. The hydroxide transport is hypothesized to take place through the development of an alternating nanoscale ravine-ridged structure with increase in hydration of the membranes. This mechanism be transferrable to other guanidinium based membranes and extendible to other types of AEMs as well.

Table of Contents

List of Illustrations

List of Tables

Chapter 1

Introduction

Energy consumption that relies on combustion of fossil fuels is forecast to have a severe impact on both future world economics and ecology. Electrochemical energy devices are under serious consideration as alternative energy/power sources because they are potentially sustainable, environmentally friendly and economically competitive. The best candidate for electrochemical energy storage and conversion are namely batteries, fuel cells, and electrochemical capacitors (ECs). All three of them consist of two electrodes in contact with an electrolyte and they thus share the same common feature, i.e., the electrochemical reactions processes taking place at the boundary of the electrode/electrolyte interface and separated electron and ion transport. However, their principle and actual mechanisms of energy storage and conversion are different. In batteries and fuel cells, electrical energy is generated by conversion of chemical energy via redox reactions at the anode and cathode while electrochemical capacitors (supercapacitors) in contrast, may have energy not delivered via redox reactions, but double-layer charging/discharging

The Ragone plot in **Figure 1-1** is used to compare the usefulness and applications of these three electrochemical devices. The units for the "specific energy" or "energy density" on the horizontal axis are watt-hours per kilogram

(Wh/kg)] and watt-hours per liter (Wh/L)] respectively. Supercapacitors being limited to high-power systems have found applications in niche markets as memory protection in several electronic devices. Fuel cells on the other hand are considered high-energy systems and have been considered for several stationary and mobile applications like their competing batteries which possess intermediate energy and power characteristics.

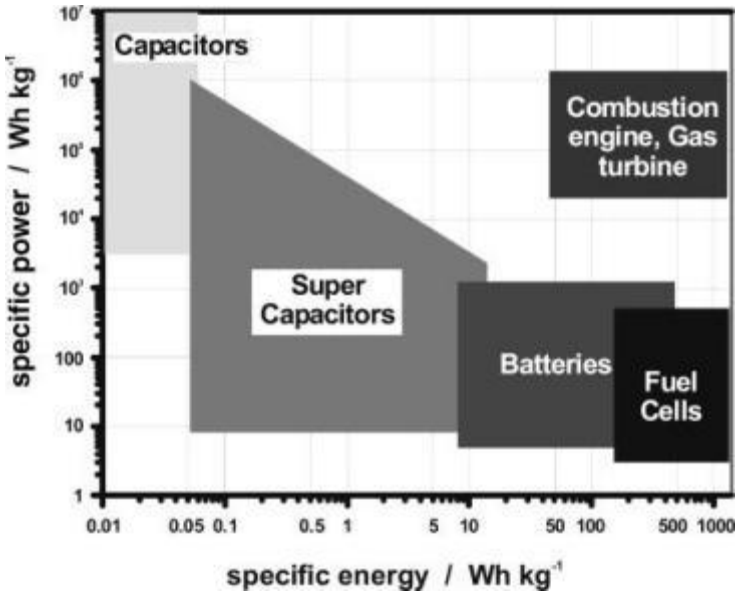

Figure 1-1: Simplified Ragone plot of the energy storage domains [1]

The difference between batteries and fuel cells is related to the locations of energy storage and conversion. Batteries are closed systems. They are sealed devices so that their materials can be protected from degradation reactions with moisture and air. They are comprised of an anode and cathode being the charge-

transfer medium and they are the ones that take an active role in the redox reaction as “active masses”. Hence, energy storage and conversion occur in the same compartment. In contrast a fuel cell is a reactor where reactants have to be continuously provided and products are removed constantly. Fuel cells are hence, open systems where the anode and cathode are just charge-transfer media and the active masses undergoing the redox reaction are delivered from outside the cell. The active masses are thus provided either from a tank for example, fuels such as hydrogen and hydrocarbons or from the environment, for example, oxygen from air. This means that energy storage (in the tank) and energy conversion (in the fuel cell) are thus locally separated.

The main impetus to develop fuel cells is that they offer the cleanest power generation possible. They also operate quietly and can be located close to the application. Compared to gasoline engines or thermal power plants, they produce much less greenhouse emissions and can be more efficient in conversion of the energy in a fuel into power. Fuel cells are best suited as a steady energy sources and are an ideal power source for remote site locations and places where an assured uninterrupted electrical supply is required. However, they can also be used for applications that require varying power demands, such as automotive applications in hybrid configurations. **Table 1-1** below compares the various pros and cons associated with use of fuel cells.

Table 1-1: Advantages & disadvantages of using fuel cells compared with other mainstream technologies

Advantages	Disadvantages
efficient energy conversion	complex to operate
modular construction	best as primary energy source
nonpolluting	impurities in gas stream shorten life
low maintenance	pulse demands shorten cell life
silent	expensive
safe	limited availability
high energy density	low durability; low power density per volume

In addition the chemical energy stored in hydrogen and several hydrocarbon fuels is significantly higher than that found in common battery materials. This fact provides strong motivation to develop fuel cells for a variety of applications. For example, the direct conversion of methanol fuel cells (5-25 W) are proposed for portable electronics as a replacement for Li ion and Ni-MH batteries. The more promising commercial applications of fuel cells appear to be as a stationary power source for central and distributed power stations (megawatts) and as mobile power for portable electronic devices and automobiles.

Direct methanol fuel cells for portable electronic devices such as notebook computers seem close to commercial reality and will compete with batteries for this market. The key challenge for each will be to meet the cost-performance barrier in a small size as well as governmental regulations. It is estimated that the fuel cell market for distributed power and demonstration projects and contracts amounted to about $100 million for 2003[2]. Research and development contracts to develop fuel cells for automotive propulsion and stationary energy storage are an order of magnitude larger.

Fuel cells, which originally were intended to replace combustion engines and combustion power sources due to possible higher energy conversion efficiencies and lower environmental impacts, are now under development to replace batteries to power cellular telephones and notebook computers and for stationary energy storage. The motivation for fuel cells to enter the battery market is simple. With operation times of typically <3000 h and, at least to an order of magnitude, similar costs, batteries are less strong competitors for fuel cells.

However despite all this research and development, fuel cells find it difficult to compete with gas/steam turbines and combustion engines because of inferior power and energy performance, much higher costs and insufficient stability (durability and lifetime). All these factors hinge upon the catalyst and membrane components of the fuel cell which are the most important functionally and also the most expensive. Hence, this study aims to utilize the relatively newer alkaline

anion exchange membrane fuel cells (AAEMFCs) which have the ability to at least theoretically by-pass these barriers. It can combat these large pitfalls which have restricted other types of fuel cells mainly because of the anion exchange membrane used here. The anion exchange membrane used in alkaline environment offers the best kinetics amongst all other types of fuel cells granting better performance to the system. Equally important is the possibility of using cheaper non-noble metal catalysts which will not only lower the cost of fabrication significantly but also ensure better stability in the alkaline environment.

This study uses this type of fuel cells (AAEMFCs) with guanidinium as the functional material in the base polymer for fabricating the anion exchange membranes. Guanidinium by virtue of its high basicity has exhibited one of the best anionic conductivity values and long term durability due to its resonance-stabilization promises greater. Hence, this polymer is uniquely modified to create novel anion exchange membranes in search of breakthrough in fuel cell technology in this work.

This PhD dissertation begins with a broad description of polymer electrolyte membrane based fuel cells and the anion exchange type (hydroxide conducting) in particular along with their selection criteria. It discusses and justifies the importance of implementing AEMFCs and compares the superiority of the guanidinium group with other functional head groups in literature. The last part of

the background in Chapter 2 talks about relevant fundamentals in membrane transport and discusses the proposed functional mechanism of AEMs.

Chapter 3-5 covers the experimental methodologies in fabricating the membranes and their structural as well as electrochemical characterizations. This also includes a concluding fuel cell study to test their performance in end application

Chapter 6 covers a Micro/Nano Phase Analysis of the membranes and guanidinium based prepolymer. It also includes a numerical study supported by AFM images to understand the mechanism of hydroxide transport through Guanidinium based AEMs. This is essential because the literature on this subject is still not mature as AEMs are still in a developing phase compared to their analogue PEMs which are highly developed and commercialized and their transport phenomena are well understood. Lastly, Chapter 7 summarizes the key findings of this work and proposes future work to build upon this study.

Chapter 2

Background & Objective of Study

2.1 Literature Review for AEMFCs

2.1.1 Evolution of Alkaline Fuel Cells

Fuel Cells are a fairly old technology and their invention is attributed to Sir William Grove in as early as 1839. Performance and costs issues compounded by tough competition from fossil based fuels prompted the evolution of this basic concept into a number of different fuel cells illustrated in **Figure 2-1**.

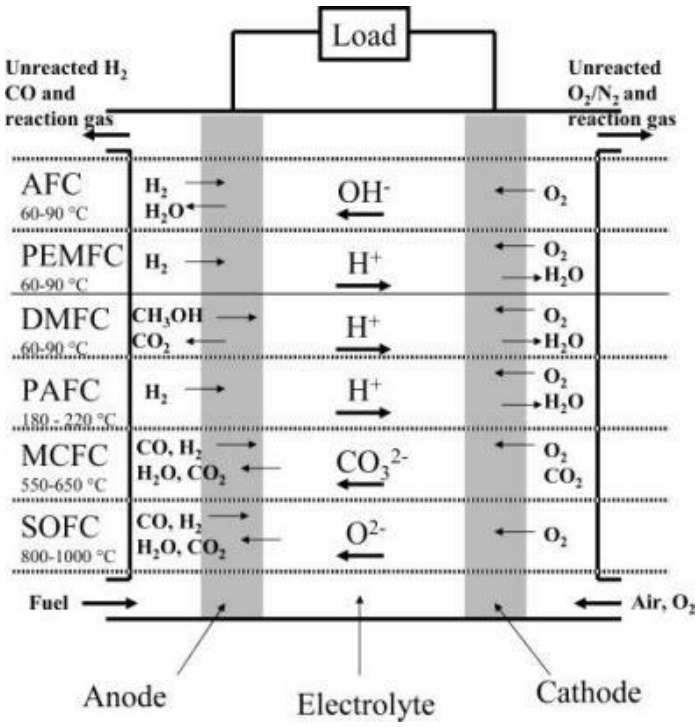

Figure 2-1: Comparison of reactions that occur in various fuel cell systems [1]

Out of these, alkaline fuel cells (AFCs) have the best performance (for temperatures lower than 200^{o}C) by virtue of their superior electro-kinetics. In fact one of the first poignant application of fuel cells (**Figure 2-2**) was undertaken by NASA in their space missions using AFCs as a source of reliable with low volume and weight, at virtually unconstrained cost.

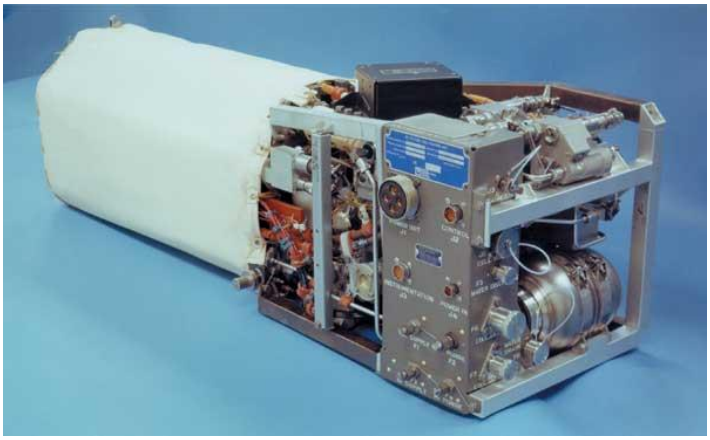

Figure 2-2: The alkaline fuel cell system as used on the space shuttles [3]

But a big drawback is that unless ultra-pure oxygen can be supplied, traditional AFCs undergo electrolyte electrode degradation caused by the formation of carbonate/bicarbonate (CO_3^{2-}/ HCO_3^-) in the liquid alkaline electrolyte on reaction of OH^- ions with CO_2 contamination in the oxidant gas stream [4, 5]. The solid carbonate or bicarbonate crystals form in the electrolyte-filled pores of the electrodes thus blocking them and also mechanically disrupt and destroy the active layers. The formation of carbonate/bicarbonate reactions is described as:

$$CO_2 + 2OH^- \rightarrow CO_3^{2-} + H_2O$$

$$CO_2 + OH^- \rightarrow HCO_3^-$$

This has severely limited the applications of AFCs. However, this issue caused by carbonate precipitates on the electrodes can be avoided in utilizing a new generation of alkaline fuel cells called the alkaline anion exchange membrane fuel cells (AEMFCs). This type of fuel cell uses a membrane electrode assembly utilizing a solid polymer electrolyte membrane (instead of liquid aq. KOH) similar to proton exchange membrane fuel cells (PEMFCs). However, the membrane conducts anions instead of protons as used in PEMFCs. Hence, AEMFCs likely combine two important advantages: the solid polymer electrolyte doesn't offer any cation in the liquid phase to take part in the formation carbonates, yet facile kinetics of the AFCs can still be used.

2.1.2 PEMFCs Vs AEMFCs

Figure 2-3 shows the difference in the schematics of PEMFCs and AEMFCs. The make-up of the membrane electrode assembly is similar but the main difference is in the actual polymer electrolyte membranes. The membrane in the PEMFC is proton-conducting while the membrane in the AEMFC is hydroxide-conducting. Hence, there is a difference in their respective electrode reactions as shown below:

(a) PEMFC:

Anode: $H_2 \rightarrow 2H^+ + 2e^-$

Cathode: $\frac{1}{2} O_2 + 2H^+ + 2e^- \rightarrow H_2O$

(b) AAEMFC:

Anode: $2H_2 + 4OH^- \rightarrow 4H_2O + 4e^-$

Cathode: $(3/2)\ O_2 + 3H_2O + 6e^- \rightarrow 6OH^-$

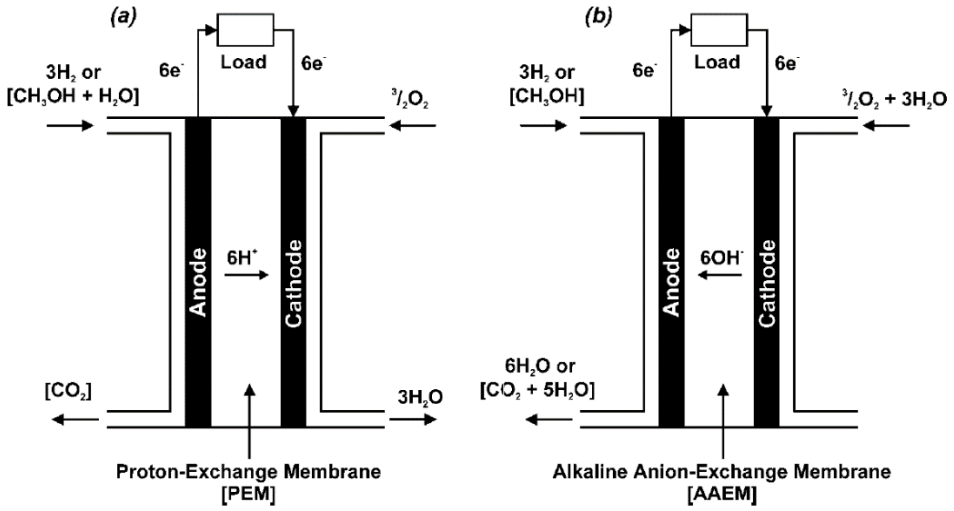

Figure 2-3: Differences between PEMFC & AEMFCs [6]

This change in transport of hydroxide ions instead of protons in AEMFCs, though seemingly a small difference, it leads to a serious of both positive and negative repercussions on the entire fuel cell system. These are listed in Table 2-1.

Table 2-1: Advantages & disadvantages incurred by using AEMFCs instead of PEMFCs

Advantages of AEMFCs:	**Disadvantages for AEMFCs**
Fuel crossover is reduced	Inherent mobility of OH^- is lower than a H^+
Choice of larger variety of fuels	AEMs have degradations and long term stability issues
Superior kinetics	
Non-noble metal catalysts potential	

The immediate advantage that is incurred by switching from PEMFCs to AEMFCs as already highlighted is the more facile oxygen reduction reaction (ORR) in alkaline environments than in acidic environments. The alkaline environment leads to a further two pronged effect by facilitating the use of less expensive non-noble metal catalysts with high stability in alkaline environments [7] and enhancing the electro-oxidation kinetics for many liquid fuels (including non-conventional choices such as sodium borohydride) in the alkaline environment [6]. Hence, the flexibility in terms of fuel and catalyst choice widens and allows selection of better highly selective catalysts that are more tolerant to fuel crossover. To add to this effect, due to hydroxide flow from the cathode to anode, now the electroosmotic drag associated with this ion transport opposes the crossover of

liquid fuel in AEMFCs, thereby permitting the use of more concentrated liquid fuels.

2.1.3 Direct Alkaline Methanol Fuel Cells

These can be considered a subset of AEMFCs. The use of AEMS in what are traditionally called Direct Methanol Fuel Cells (DMFCs) may solve several problems PEMs struggled for with decades, while still allowing the electro-kinetic advantages of AFCs. The utility of DMFCs stems mainly from the higher volumetric energy density and reversible efficiencies of methanol compared with liquid hydrogen (see **Table 2-2**). Another factor is the relative ease of conversion of the current petroleum distribution networks to methanol compared with the costly whole new distribution structure and infrastructure required for hydrogen.

Table 2-2: Fuels for AEM fuel cells with standard thermodynamic voltages and energy densities. [6, 8]

Fuel	**E^o/V**	**W_e/kWhkg^{-1}**	**W_e/kWh dm^{-3}**	**η_{rev}**
Hydrogen	1.23	39	2.6 (liquid hydrogen)	0.83
Methanol	1.21	6.1	4.8	0.97
Ethanol	1.15	8	6.3	0.97
Propanol	1.07	8.6	6.8	0.93
Ethylene Glycol	1.22	5.3	5.9	0.99

The use of AEMs in DMFCs allows other advantages. The ion transport within the membrane will be from the cathode to the anode, opposing the direction of, and hence reducing the level of, methanol crossover from anode to cathode. In reality, water will actually be electro-osmotically transported from the cathode to the anode, which is the reverse of the situation found with PEM-based DMFCs. As the water is now produced at the anode and consumed at the cathode, the water management regime is hence drastically improved. The two factors above avert the long standing problem of catastrophic flooding at the cathode from electro-osmosis of water in PEM-based DMFCs, reducing mass-transport-derived voltage losses.

Finally, DMFCs are amenable to a great number of portable applications as well by virtue of the good energy density of liquid methanol, even when compared to most state of the art batteries (5–10 times that of batteries). Another benefit of using DMFCs instead of batteries is ‘‘instant’’ refueling when utilizing a plug-in methanol cartridge. Hence, in this study we have chosen DMFCs as the fuel cell system to test our fabricated AEMs. However, there is a need to address the two problems stated in table before these membranes can be successfully utilized in high demand applications such as fuel cell. The next section which is a detailed literature review on AEMs discusses these problems and their solutions.

2.1.4 Kinetics of AEMFCs & Non-Noble Catalysts

Superior cathode kinetics and ohmic polarization just two of the numerous advantages AEMFCs bring over their competing PEMFCs. It is however, important

to discuss how these inherently fast kinetics of oxygen reduction reactions in particular are obtained. In doing so we first need to discuss the nature of the oxygen reduction reaction.

The oxygen reduction in aqueous alkaline media is a complicated multistep electrocatalytic reaction with many proposed intermediates such as O, OH, O^{2-}, and HO_2^-. This leads to a great number of possible pathways as illustrated by the model in **Figure 2-4**. It shows the general scheme that can explain the observed ORR behavior in alkaline media. The model looks seemingly complicated but the pathways can be divided into three groups. Two of these lead to OH^- as the final product signifying complete reduction, with transfer of four electrons and one leads to peroxide signifying partial reduction, with transfer of two electrons. Hence, they are correspondingly described as 'direct' and 'series' pathways. In the latter, hydrogen peroxide is produced (HO_2^- in alkaline media) as an intermediate which is eventually reduced to OH^-. It is widely accepted that proton transfer to O_2, producing adsorbed HO_2 or HO_2^-, occurs before cleavage of the O–O bond during the ORR on Pt-group metals. Formation of an intermediate adsorbed HO_2 species is likely in both two- and four-electron pathways, but the interpretation of this species is different in alkaline media than in acidic media. In alkaline conditions, the much lower working potential of an ORR electrode is likely to facilitate desorption of HO_2 as the HO_2^- ion. However, in acidic media desorption becomes much more difficult due to its higher working potential. HO_2 desorption is restricted

so that further protonation (to produce H_2O_2) is required in order for peroxide desorption to finally occur.

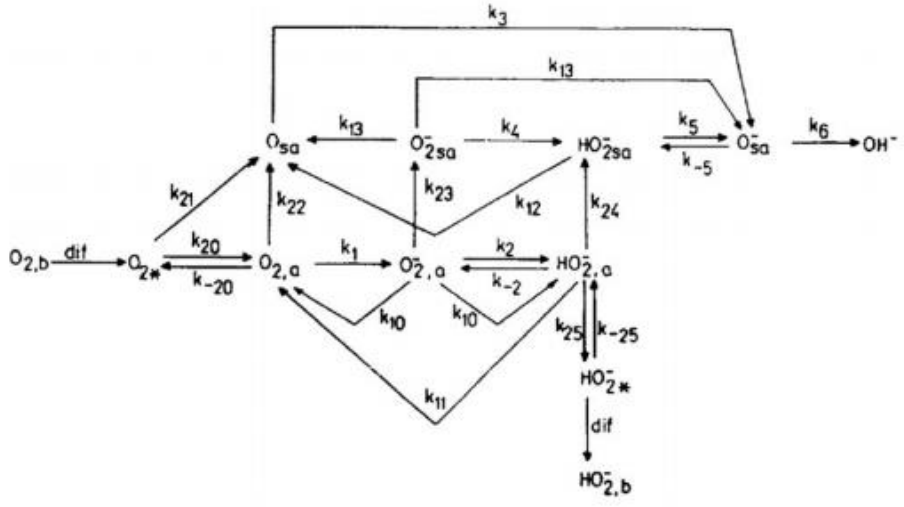

Figure 2-4: General scheme for O_2 reduction in alkaline solutions. [9]

The pH is considered to play a remarkable role in electro-kinetics since a long time but the fundamental reason remained elusive. Also according to the Nernst equation, the working potential range shifts by -59 mV for every increase of 1 pH unit while the working potential range when measured on an absolute scale such as the standard hydrogen electrode (SHE) it shifts by nominally 0.83 V as a result of a change from a 1 N solution of strong acid to a 1 N solution of strong base [10]. This changes the local double layer structure and the electric field at the electrode–electrolyte interface, leading to changes in adsorption & desorption

strengths even for neutral species (hinted at in the previous paragraph). The effect of pH was aptly exhibited in a reference where the effect of pH on the oxygen electro-reduction of Ag (111) surface, by comparing the ORR activity in 0.1 M KOH and 0.1 M $HClO_4$ solutions (pH difference = 12 units) was investigated [11]. The authors would attribute their results to the influence of adsorbed anions from the supporting electrolyte not directly involved in the oxygen electroreduction reaction (spectator species). Their inhibiting effect is manifested by blocking the active sites required for adsorption onto Platinum surface of oxygen electro-reduction reaction intermediates. Spendelow & Wieckowski covered the same reasoning in an excellent review [10] on the subject again stating that the enhanced activity in alkaline media is attributed to the lack of specifically adsorbing spectator ions in alkaline solutions, and the higher coverage of adsorbed OH at low potential (a requirement for methanol oxidation). The effect of the alkaline media in terms of kinetics cannot however be denied. Tripković et al. exemplify this by achieving kinetics much higher in alkaline than in acid solution. The kinetics were improved by a factor of 30 for Pt (and 20 for Pt_2Ru_3) at 333 K and 0.5 V [12]. Again, the pH effect is attributed to the pH competitive adsorption of oxygenated species with anions from supporting electrolytes.

Combined with the less corrosive nature of the alkaline environment, AEMFCs promise not only greater longevity but also use of non-noble catalysts. Hence, alkaline direct methanol direct fuel cells have been established using non-

precious metals, such as silver catalysts [13] and perovskite-type oxides [14]. In addition, a variety of catalytic materials have been investigated for application as oxygen cathodes in alkaline media. These include carbon, various transition metals, coinage metals, metal macrocycles, including porphyrins, and phthalocyanines, and metal oxides, including manganese dioxide as well as various spinels [12]. Individual details will not be provided here as the focus of this dissertation is the AEM and not the electro-catalyst.

2.2 Literature Review of AEMs

Utilizing AEMs in fuel cell application place certain material requirements on the membranes particularly with regard to their performance, structural integrity and longevity. The basic requirements for developing AEMs for fuel cell application are summarized below:

1) Efficient hydroxyl transport & high ionic conductivity
2) Correct selectivity for the active ions
3) Outstanding chemical stability in alkaline conditions
4) Good barrier to electrons to provide effective separation between anode and cathode
5) Thin membranes (<100 μm) in order to keep good mechanical stability when immersed in water and also to decrease the cost of the system

6) Good mechanical and thermal integrity during both manufacturing and operation
7) Low cost

The first set of requirements relate to the properties of the ion exchange group while the second relate to how these ion exchange groups are incorporated in the bulk composition and the method of fabricating the membrane. These two criteria are respectively discussed in sections 2.2.1-3.

2.2.1 Anion Exchange Functional Groups

Historically, AEMs have been used mainly in electrodialysis for the desalination of brackish water and for the production of table salt from seawater. However, development of AEM materials has been a subject of extensive research activities in the last decade. The ion exchange group, chemical structure, crosslinking, and polymer chain flexibility of AEMs are all believed to play important roles in both conductivity and durability. Among the recent development of different kinds of AEMs [15-25], a number of ion exchange groups have been investigated and are illustrated in **Figure 2-5**. From left to right in the top row these are pyridinium, ammonium, phosphonium and sulfonium and in the bottom row these are guanidinium and imidazolium.

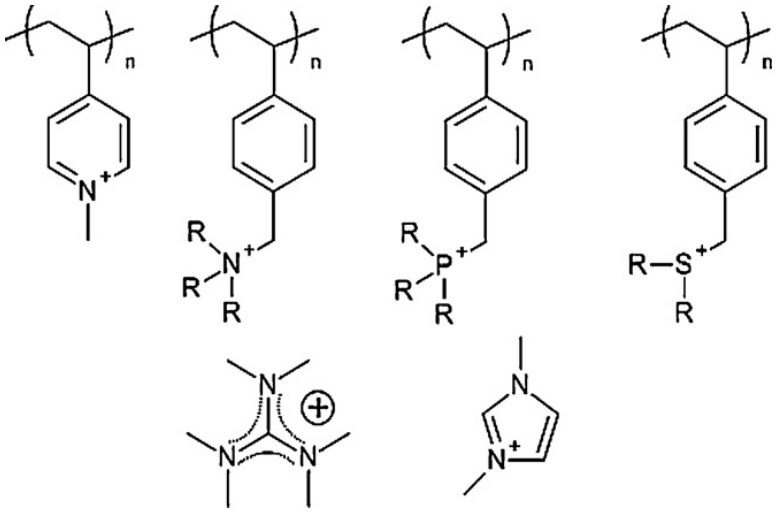

Figure 2-5: Chemical structures of common anion-exchange sites [26].

However, the majority of the research involves the use of quaternary ammonium as anion exchange sites [27-29]. These membranes generally exhibit a much lower conductivity at the same ion exchange capacity (IEC) when compared to proton exchange membranes (PEMs). The mobility of hydroxide anions is generally considered to be nearly half of that of protons which contributes significantly to this loss in conductivity [30, 31]. Despite this, great strides have been made to significantly improve conductivity values by enhancing micro-phase separation as demonstrated by Hickner *et al.* [24]. Zhang *et al.* [18] also employed this approach through a non-choromethylation and pre-quaternary-amination route to fabricate membranes which displayed conductivities between 65–87 mS cm^{-1} at 20–60 ^{o}C. However, their membranes showed extensive swelling and doubtful

chemical stability which highlights the underlying needs for future AEM development.

2.2.1.1 Efficacy of guanidinium as ion exchange groups

Recently, investigation of guanidinium moieties as anion exchange sites [31-34] has yielded promising results to overcome the above-mentioned technical difficulties. The high basicity of guanidinium has led to conductivity values as high as 67 mS cm^{-1} at 20°C and 74 mS cm^{-1} at 60 °C [32]. Besides, membrane stability can be potentially improved due to the inherent charge delocalization from the π-electron conjugated system of the resonance structure shown in **Figure 2-6** [32, 35]. However, guanidinium moieties as ion-exchange groups have been mostly attempted as side-chain groups in AEMs [32, 33, 36].

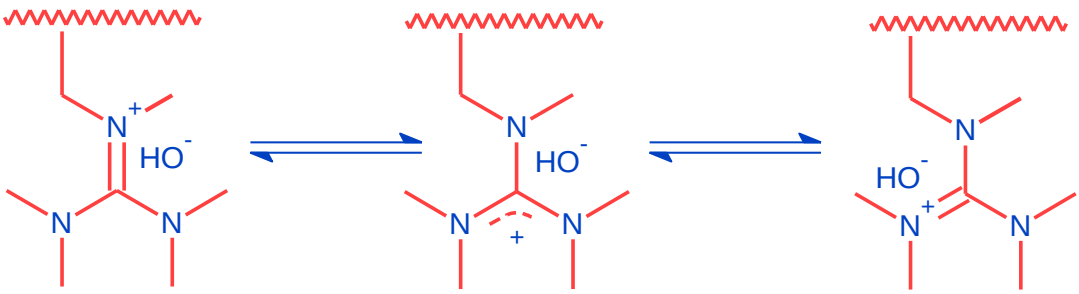

Figure 2-6: The electron delocalization in the guanidinium group

We propose to study integrated network membranes containing guanidinium moieties in polymer backbone to enhance both membrane

conductivity and durability. Considering the branched nature of the moieties, the polymer electrolyte with guanidinium groups (**Figure 2-7**) tethered to the polymer backbone potentially provides a higher IEC and better polymer integrity, improving both membrane conductivity and chemical/electrochemical stability. Due to the simple nature of the starting monomers and their proposed polymer structure, the resulting findings may also be extrapolated for other guanidinium based systems thus acting as a model for guanidinium ion exchange groups and proving the feasibility of these materials as promising AEM materials in alkaline fuel cells. Furthermore, to the best knowledge of the investigators, no modification to the guanidine polymers has been done to meet the comprehensive requirements in an alkaline fuel cell MEA, e.g., solubility, conductivity, and mechanical properties.

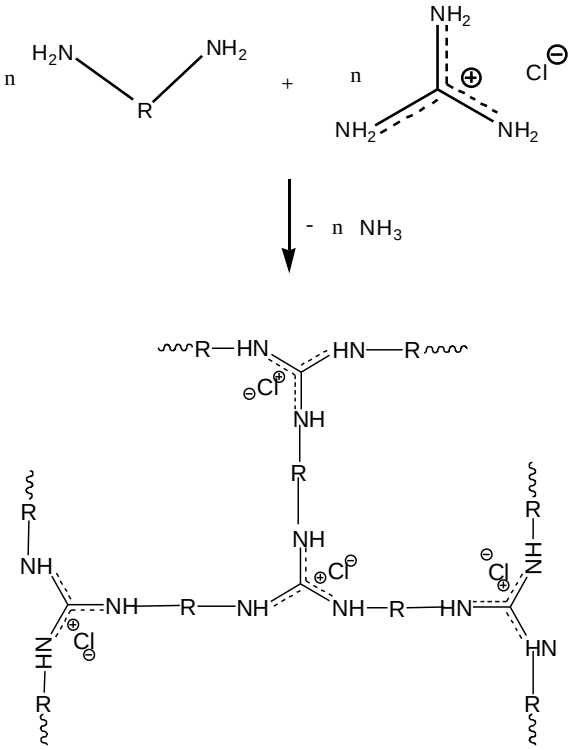

Figure 2-7: The reaction for the proposed guanidine polymer with network structure

2.2.2 Classification of AEMs

Once the preferred ion exchange groups have been shortlisted, they still have to be incorporated into robust membranes for utilization in high-end applications such as fuel cells. This is another area which has impeded AEM progress. Whereas for PEMs Nafion and other sulfonated polymers represent strong and stable membranes enabling their commercialization, AEMs have comparatively struggled in the synthesis and fabrication process. This has not

stopped researchers from trying and the combination of different materials and techniques used has led to the following classifications for AEMs. Looking at **Figure 2-8**, there are three broad classification namely interpenetrated polymer networks, heterogeneous and homogenous membranes.

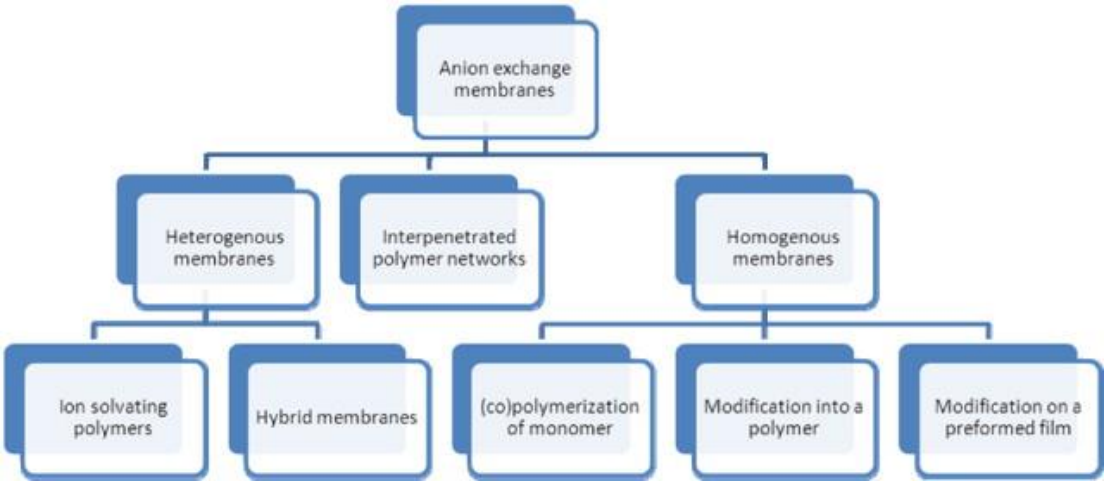

Figure 2-8: Tree diagram of different AEMs [37]

2.2.2.1 Heterogeneous membranes

Heterogenous membranes have the ion exchange group embedded in an inert material. This type of membrane is further divided into two types: ion solvating membrane and hybrid ones, depending on the nature of the inert material. If the inert material is in the form of a salt it is called ion solvating. Ion solvating membranes usually comprise of a matrix (water soluble polymer), a hydroxide salt (mostly KOH) and some plasticizer. The alkaline salt is responsible for the electrochemical properties while the polymer matrix contributes towards the

mechanical properties. The ionic conductivity is dependent on the interactions between the hydroxide salt and cations.

The hybrid membrane on the other hand has the inert compound in the form of an inorganic material. Hence they are usually composed of organic and inorganic segments. The organic part provides the electrochemical properties and the inorganic part (siloxane or silane) contributes to the mechanical properties of the membrane. These membranes are mostly formed through the sol-gel process; although, other methods like intercalation, blending etc. can also be used.

2.2.2.2 Interpenetrating Polymer Network

IPN or Interpenetrating Polymer Network is a combination of two polymers in network form of which at least one polymer is synthesized or cross-linked in the immediate presence of the other without any covalent bonds between them. One of the polymers is conductive while the other is hydrophobic (doesn't swell when in contact with water). The combination of having conductive polymer transports anions and hydrophobic polymer providing good chemical, thermal and mechanical properties leads to strong membranes with an excellent mixture of said properties. These membranes which are usually heterogeneous blends often swell in solvents without dissolving in them. [8].

2.2.2.3 Homogeneous Membranes

Having the simplest concept, the most extensive work and research has been done on these type of AEMs. They can be considered as one phase systems. The cationic charges are covalently bound to the polymer backbone as sidegroups and to maintain the electro-neutrality of the polymer a mobile counter ion is associated with each ionic functional group. The further three sub-classifications simply are related to the method of fabricating the membrane.

2.2.3 Stability of the ion exchange group

The main cause of the degradation of the various cationic groups at the anion-exchange sites (**Figure 2-9**) is the basicity of the medium [20]. Among these different species, quaternary ammonium groups are more chemically and thermally stable than quaternary phosphonium and tertiary sulfonium groups. It has been shown that these cations tend to degrade under aqueous conditions at high pH, due to the hydroxide counter ions, following two main degradation pathways (**Figure 2-9**) when temperature increases: elimination [38] and nucleophilic substitution mechanisms [39].

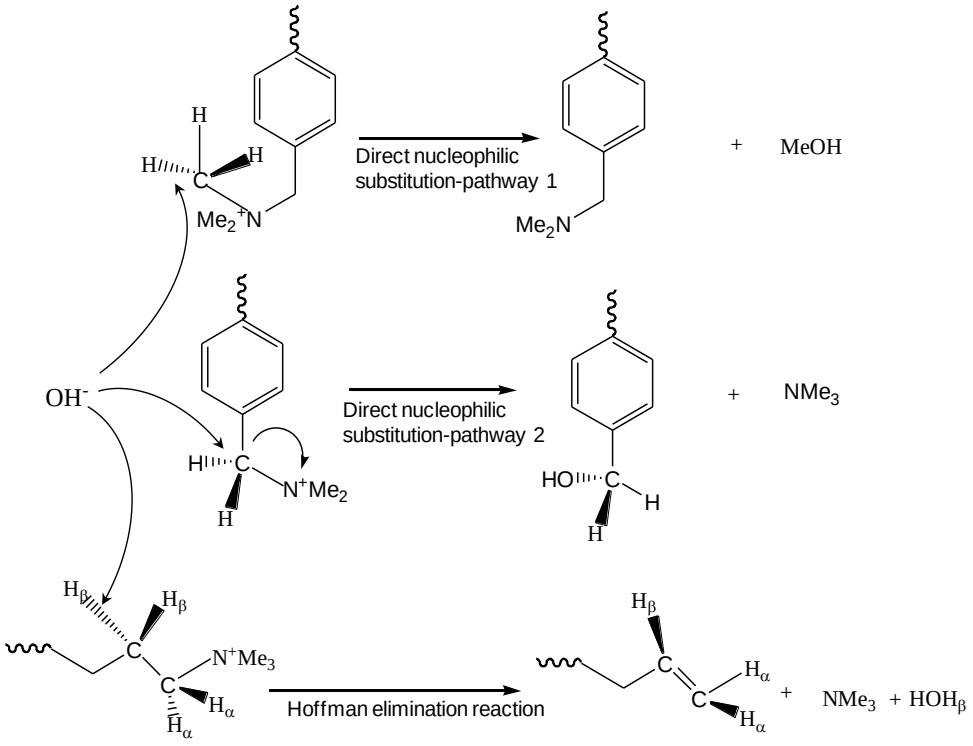

Figure 2-9: Degradation mechanisms for quaternary-ammonium AEMs

The extent of both elimination [38] and nucleophilic substitution [26] degradation mechanisms is determined by the nature of the ion exchange functional groups (in this and in most cases quaternary ammonium since they are the ones most deeply investigated up till now). The E2 elimination reaction known as "Hofmann Elimination" occurs when a substituent in the β-position of the nitrogen atom has at least one hydrogen atom. The alkalized quaternary ammonium group is correspondingly cleaved yielding an amine and an olefin as part of the degradation products. The nucleophilic substitution route for degradation

corresponds to two S_N2 reactions between an OH^- anion and a carbon atom in the α-position of the ammonium group. Again two products are generated: an amine and this time an alcohol. As mentioned, several factors inherent to the structure of the polymer allow the competition between these mechanisms. Thus, on the one hand, if no hydrogen is located on the α-carbon, the degradation mainly consists in a S_N2 substitution. On the other hand, highly nucleophilic or hindered bases and the presence of a carbon atom in β-position of the ammonium preferentially lead to an E2 elimination reaction.

Hence, chemical degradation of AEMs stems largely from nucleophilic attack of hydroxide ions on the fixed cationic sites, which results directly in a loss of ion-exchange groups, and a subsequent decrease in OH- conductivity. Degradation mechanisms of AEMS have virtually always been studied on quaternary-ammonium groups, even though research on new ion exchange groups has increased dramatically [17, 40-43]. Though recent membrane degradation studies [23, 44, 45] on quaternary ammonium groups have provided some fundamental understandings that may be applied to other types of AEMs, but with considerable limitation. For example, membrane conditions that lead to poor solvation of OH^- ions may enhance chemical degradation of the cations. Chemical stability is less dependent on modification of the alkyl groups that attach to the cationic moieties [46]. Of course, the above statements may be valid for non-

quaternary-ammonium AEMs in some sense, as the nucleophilic attack by OH^- ions contributes to the chemical degradation in most of cases.

The stability of the guanidinium groups due to their inherent charge delocalization is expected to surpass that of the quaternary ammonium groups. Indeed early studies in literature do point towards greater stability. For example, when guanidinium moieties were inserted onto poly (arylene ether sulfone) (PES) [41], higher ionic conductivity was observed due to their higher basicity and hydrophilicity. In addition, the decrease in this ionic conductivity was negligible when chemical stability tests were performed on the membrane. Finally they also showed better thermal stability compared to their ammonium bearing equivalents [41, 47].

However, it is well known from studies on quaternary ammonium based AEMs that ion exchange groups acting in pendent positions may not be very stable. For example, guanidinium groups anchored to polymer side chains (as in the above references) may be easily lost if the single bond attached to the base polymers is cleaved by hydroxide ion attack, as shown in **Figure 2-10**.

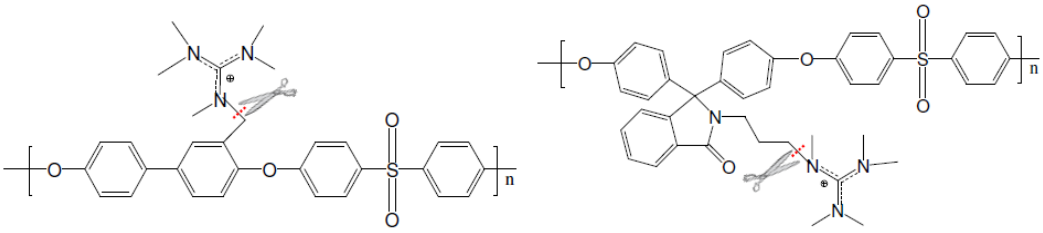

Figure 2-10: Guanidinium AEM materials: (l) poly(arylene ether sulfone) with tethered pentamethylguanidine [41], & (r) hexaalkylguanidinium groups anchored on poly(aryl ether sulofone) [47]

This is because when ion exchange groups are tethered in the polymer backbone, chemical degradation due to either Hoffman elimination or direct nucleophilic substitution [48] is not possible. We propose to study integrated network membranes containing guanidinium moieties in polymer backbone to by-pass these degradation mechanisms. This coupled with the high basicity, resonance stabilization of the π-system and the "Y-delocalization" of the guanidinium group is expected to enhance both membrane conductivy and durability. Indeed our preliminary chemical durability experiments (Chapter 4.3.6) [49] under harsh alkaline conditions corroborated this hypothesis. Guanidinium integrated network membranes showed superior hydroxide resistance compared to the commercialized quaternary ammonium based Tokuyama A201.

Although the studies cited in this section have made important contributions toward developing guanidinium AEMs, the full range of possible application owing

to the desirable properties of guanidine-based polymer materials, especially those related to high hydroxide ion conductivity and chemical stability, remains uncertain in an alkaline AEM fuel cell environment. The knowledge gained from this work will provide a greater understanding of the fundamental aspects of hydroxide conduction and AEM degradation, and could open up new opportunities in the synthesis of novel membrane electrode materials in alkaline AEM fuel cells.

2.3 Hydroxide Conductivity Mechanism

An AEMFC works by allowing passage of anions usually hydroxide ions to pass through its anion exchange membrane. This conduction and mobility of the hydroxide ions through the membrane is hence an underlying principal of AEMFC operation. The importance of investigation in this area can be summarized by the following arguments:

i. There is very little prior study on any possible mechanisms and hence our understanding of this subject is inadequate

ii. Understanding of hydroxide conductivity is key to developing AEMs with higher conductivities

iii. It may help in designing AEMs with better secondary properties such as degree of swelling & mechanical integrity

iv. It may also help in tuning reaction parameters to get better performance from the AEMs

The present literature on the mechanism for hydroxide ion transport is still in its infancy. However, many simulations and experiments have been conducted to establish reliable models for proton exchange through H_3O^+ in water. Given the similar dependence of ionic conductivity values for both PEMs and AEMs on experimental conditions such as temperature, degree of hydration etc, it is reasonable to deduce that they would share some combination of the same mechanism. The mechanisms are namely: Grotthuss mechanism, diffusive transport, convection and surface hopping.

2.3.1 Grotthuss Mechanism

The Grotthuss mechanism by virtue of the transport rates it can provide is thought to be the most dominating mechanism for proton transport. Since OH^- exhibits Grotthuss behavior in aqueous solutions comparable to protons [50, 51], it is assumed that this behavior is responsible for transporting the majority of the OH^- [52].

The mechanism however is different than transfer of protons. It is postulated that the hydroxyl anions tend to have stable solvation shells that re-organize the solvent molecules and disturb the hydrogen bond network (whereas in contrast, the hydrogen ions are naturally integrated into the hydrogen bonding network of water). Basically, the hydroxyl ions are transported through the membrane along a chain of water molecules through hydrogen bond formation and cleavage of the hydrogen bond. In fact, it is claimed that the transfer of hydrated

hydroxyl ion is accompanied by a hyper-coordinating water molecule. It has been proposed [51] that the movement of the hydrated hydroxyl ion is accompanied by a hyper-coordinating water molecule. The subsequent arrival of another electron-donating water molecule leads to hydrogen bond rearrangements, re-orientations and hydrogen ion transfer resulting in the formation of a fully tetrahedrally coordinated water molecule.

2.3.2 Diffusive Transport

This type of transport occurs in the presence of a concentration and/or electrical potential gradient. Due to their similar molecular weights comparable en masse diffusion coefficients can be anticipated for both OH^- and H_3O^+ in water [52].

2.3.3 Convection

Convection occurs via permeation and osmotic drag. Convective flow of water molecules across the membrane appears as hydroxides moving through the membrane, drag water molecules with them through the membrane.

2.3.4 Surface site hopping

Surface site hopping of hydroxyl anions occurs on the ion exchange functional groups (e.g. quaternary ammonium groups) present on the membrane and is generally thought of a secondary transport process [37]. The reason for this is on the basis of length scales in the system while also considering coulombic interactions between the functional groups and their OH^- carriers that will try to

promote the electroneutrality. The water present in the system acts as a permanent dipole and interacts with the fixed charges of the membrane. This strong coordination of water molecules around the ion exchange functional groups imparts a reduction of the possibility of the ionic species to interact with the ion exchange functional groups on the membrane.

Figure 2-11 shows the how transport mechanism (described) for PEMs can be adopted for quaternary amine based AEMs.

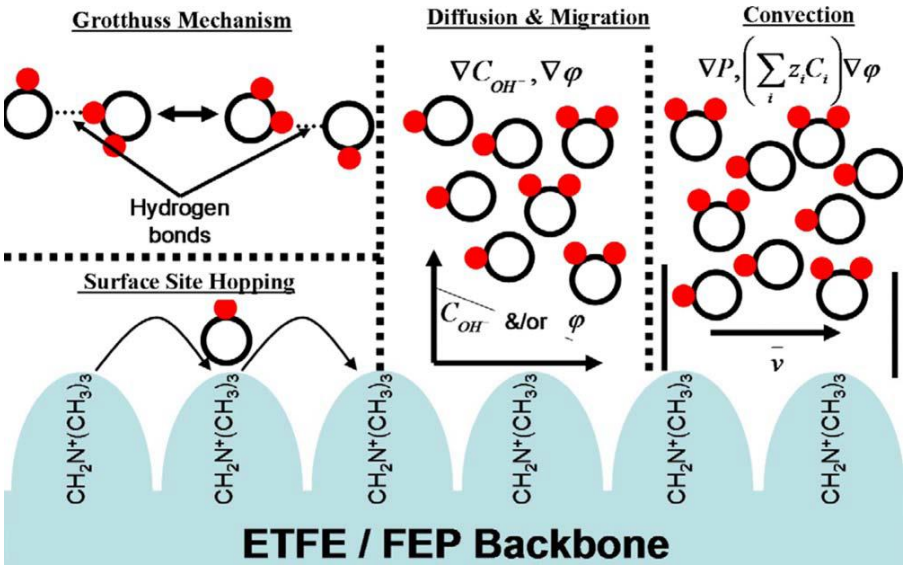

Figure 2-11: Schematic representation of the different transport mechanisms that may be observed in an AEM [52]

These mechanisms namely Grotthuss, diffusion, convection and surface hopping which have been described in detail above although over here they

illustrated with reference to quaternary ammonium groups, they can be applied to guanidinium functional groups as well both depend on hydroxide conductivity. Hence, the aim of this chapter is to understand the fundamental nature of hydroxide conduction through the guanidinium functionlized membranes used in this dissertation supported by the mechanisms and theories of both other AEMs and PEMs reported in literature. To accomplish this task the structure of the AEMs are studied at the nanoscale using atom force microscope (AFM) under different hydration conditions and this is followed by a computer simulation to recreate these structures whilst estimating the contributing hydroxide conductivities.

2.4 Objective of Study

The objective of this research is to develop a family of robust anion exchange membranes with guanidinium moieties incorporated in the polymer backbones for high performance alkaline fuel cells. The strong basic nature and resonance structure of the guanidinium functional group would lead to high hydroxide conductivities and superior thermal and chemical stability.

To test this hypothesis, a bottom-up approach is taken starting with successful synthesis of said guanidinium based polymers and their modifications for fabricating versatile anion exchange membranes and including development for the end-product fuel cell applications.

Development of these anion exchange membranes represent and will help achieve a breakthrough technology for fuel cells which have been strongly impeded by constraints of performance and cost. By utilizing the more facile kinetics of the alkaline media and prospects of using cheaper non-noble catalysts, this study hopes to remove these two-pronged problems which have plagued the fuel industry since its inception.

In addition, there is far little information known regarding the hydroxide transport mechanism through anion-exchange membranes. This dissertation includes a fundamental study by microstructure analysis coupled with meaningful simulation to gauge a better understanding of this process. Understanding the transport properties of guandinium based membranes and anion exchange membranes in particular will contribute greatly to the tailoring of ionic conductivity and design of superior performing yet stronger future membrane.

Chapter 3

Synthesis of Prepolymer & Fabrication of AEMs

3.1 Introduction

A bottom-up approach is taken where the polymer material is first synthesized from scratch with the monomers via polycondensation. This prepolymer is used as is or modified through crosslinking/blending etc before being used to fabricate the anion exchange membranes. Because the prepolymer is mechanically weak by itself, it is therefore supported by a PTFE substrate to make a composite membrane (Scheme 1) or blended with a stronger polymer (chitosan) to yield hybrid blended membranes (Scheme 2). **Figure 3-1** illustrates this:

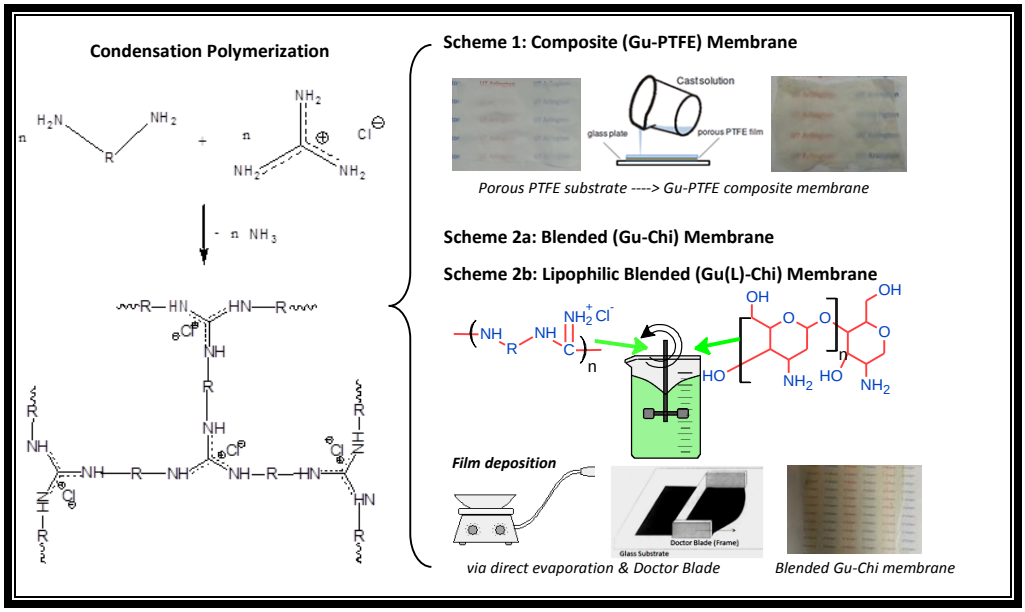

Figure 3-1: Overview of the polymer synthesis and fabrication process for different membranes

The polymer synthesis parameters and mechanism along with the membrane fabrication procedure are detailed in length in the following sections.

3.2 Synthesis of Guanidinium based prepolymer

Guanidinium-based polymers were synthesized through a condensation reaction between guanidine hydrochloride salt (GHCl) and two different diamines (HMDA and AEE) as shown in **Figure. 3-1**. While **Figure 3-2** shows structure of the two diamines which are different to serve as a good comparison but similar enough as an effective control agent to each other.

Hexamethylenediamine, HMDA:

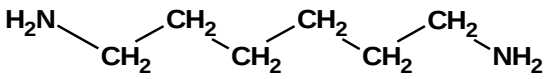

1, 2- Bis(2-aminoethoxy) ethane, AEE:

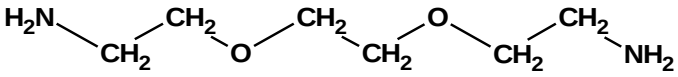

Figure 3-2: Structures of the two diamines used in the polymerization

Equimolar mixture of the diamines and GHCl was first put into a flask equipped with a reflux condenser. A heating mantle was hooked with a PID

controller and the arrangement is shown in Figure The mixture was mechanically stirred while the reaction was conducted at 100°C for 1 h, 140°C for 2h, and then 180°C for 4h, before it was allowed to cool down. At 140 ^{o}C, the flask was attached to a vacuum to suck and accelerate the removal of ammonia in order to facilitate the condensation reaction. While at 180 ^{o}C, the reaction flask was purged by a slow flow of Argon to maintain an inert atmosphere and prevent polymer degradation.

The weight of the polymer product is obtained by measuring the mass of the final flask (with the polymer product) and subtracting it with the weight of the empty flask prior to adding any reagents.

The polymer is hard to extract manually. But since it is water soluble, it is therefore dissolved in water and removed from the flask. This polymer solution was slowly heated over a hot plate with temperature kept at approximately 50 ^{o}C. Since the total polymer product is known, the polymer/water ratio can be calculated at any time by measuring the total weight of the solution. Required amounts of polymer solution are then extracted for various modifications such as crosslinking and polymer blending in order to eventually fabricate anion exchange membranes.

Figure 3-3: Experimental setup for synthesis of the polymer

3.2.1 Mechanism of Polycondenstation reaction

Hexamethylene diamine (HMDA) and guanidine hydrochloride (GHCl) react to form polyhexamethyleneguanidine hydrochloride (PHMGHC) and ammonia. The synthesis route was derived and modified from references [53, 54] albeit for antimicrobial applications. It is also water-soluble as discussed previously and possesses pronounced antiseptic and fungicidal properties.

The starting materials, GHCl & HMDA however, due to the presence of amino groups are strong bases capable of binding even with weak acid. GHCl has been described as a complex compound, in which a positive charge is delocalized over nitrogen atoms and the chlorine anion is bound electrostatically [55].

However, according to an alternative concept, a positive charge is localized on the carbon atom of the GHCl molecule, which is proved by the absence of absorption bands in the ammonium region of 2700–2250 cm^{-1} of the GHCl IR spectrum [56]. Furthermore, quantum chemical calculations of GHCl by the semi empirical method or semi-rule of thumb also shows the presence of positive charge on the carbon atom in contrast to positive charge delocalized on nitrogen atoms [57]. Therefore, the mechanism of HMDA and GHCl polycondensation was suggested; it represents transamination reaction and realizes as nucleophylic substitution mechanism [57, 58].

3.3 Fabrication of Composite Membranes

The synthesized polymers were dissolved in an aqueous solution with 5wt% of DMSO and subsequently transferred to a beaker. The polymer solution was then mixed vigorously for five minutes prior to being transferred to a porous PTFE film (kindly supplied from Phillips Scientific Inc. with porosity of 90% and thickness of 25.4 μm). For some polymer samples, solution viscosity increased more dramatically during the bulk condensation polymerization process, thus inhibiting further growth of polymer chains. In order to increase the molecular weight as reported elsewhere [53], EP was added to the polymer solution (in equimolar ratio to the initial monomers) prior to transferring to the porous PTFE substrate. In this

way, impregnation into the porous substrate and crosslinking of the polymers could occur simultaneously.

The setup for adding the polymer solution to the porous PTFE and forming the composite membrane is illustrated in **Figure 3-4**, according to our previous reports [59, 60]. The PTFE with the polymer solution was heat-treated on a hot plate. The temperature increased slowly to ensure evaporation of the solvents without forming bubbles. After being maintained at 100 ^{o}C for 12 hours, the membranes were transferred to a vacuum oven where they were heated to 130 ^{o}C for 24 hours. After cooling down to room temperature, the membranes were thoroughly washed and submerged in 1 M KOH for 48 hours to allow sufficient time for hydroxide ion exchange and functionalization of the membranes.

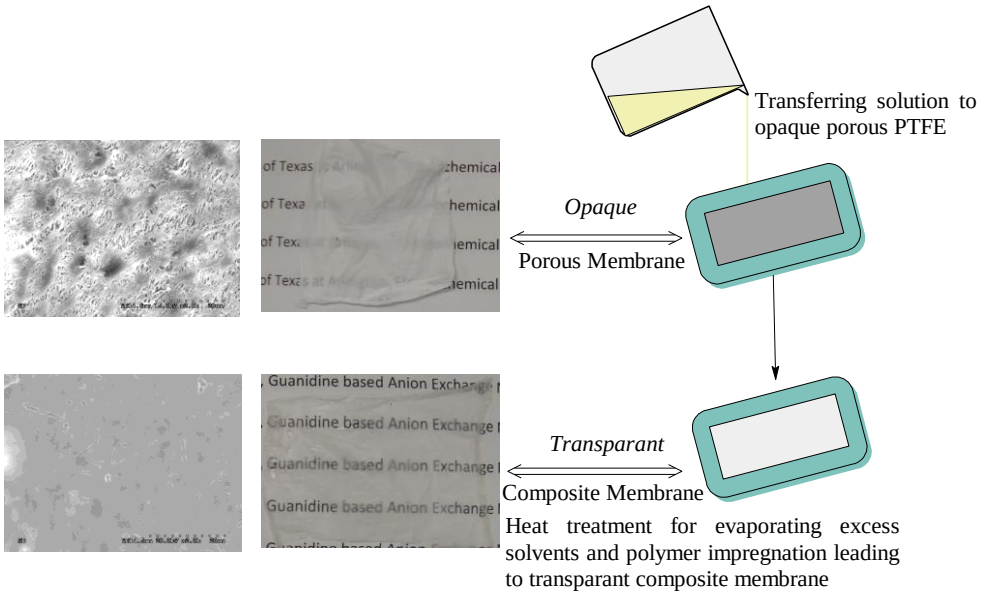

Figure 3-4 Impregnation of PTFE substrate with polymer ionomer solution

3.4 Fabrication of Hybrid Blended Gu-Chi Membranes

In scheme 2, Chitosan is blended with the guanidinium based prepolymer to improve the mechanical integrity of the final membrane. Chitosan is chosen as a suitable blend material for several reasons:

1) It has high molecular weight and so good strength
2) It has excellent film making properties and hence is conducive to make membranes
3) It is stable and has previously been used for AEMs
4) It is a cheap and abundant material

In addition, lipophilic blended Guanidinium-chitosan membranes were also made. This includes the additional step of incorporating a long chained stearate group to the structure. The rationale for doing this is again an improvement in the membrane mechanical properties and changing its dissolution properties. The details of this and of the blending process illustrated in **Figure 3-5** are discussed in the following sections.

Scheme 2a: Blended (Gu-Chi) Membrane

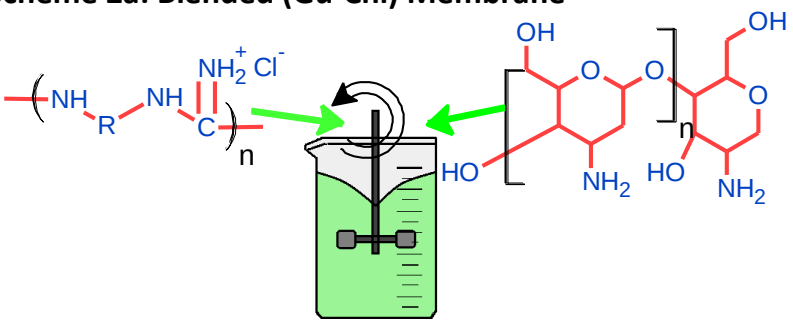

Scheme 2b: Lipophilic Blended (Gu(L)-Chi) Membrane

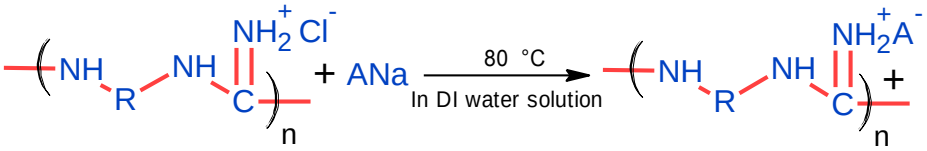

Where: A = $CH_3(CH_2)_{16}COO$

R = $(CH_2)_60_2$

Figure 3-5: Scheme for making the hybrid blended Gu-Chi membranes

3.4.2 Hybrid (Gu-Chi) Blend membranes (Scheme 2a)

5.6 g of guanidinium polymer was blended in a solution comprising of different amount of chitosan (5.6 g and 2.2 g). Initially the guanidinium polymer and chitosan were separately dissolved in deionized water and a slightly acidic solution (~1% acetic acid), respectively. After being completely dissolved, they were mixed and mechanically blended via a mechanical stirrer at approx. 70 ^{o}C as shown in **Figure 3-5**. With the evaporation of most of the solvent, the blend formed sticky slurry which was used to cast membranes on a flat glass slab by a doctor blade (**see Figure 3-6**). The casted membranes were then heat treated in an oven at 70 ^{o}C for 6 h before putting it in a vacuum oven at 110 ^{o}C for 10 h.

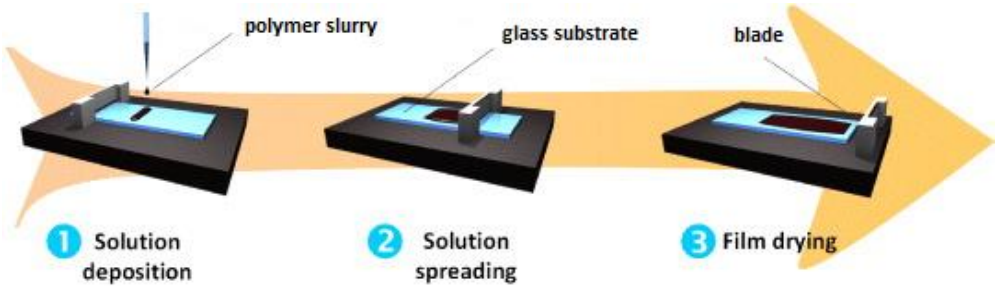

Figure 3-6: Thin film deposition through use of doctor blade

The membranes were then thoroughly washed and submerged in 1 M KOH (aq) for 48 h to allow for complete hydroxide ion exchange and functionalization of the membranes. Afterwards they were subsequently washed and stored in

deionized water for at least 24 h before use in a fuel cell or other characterization tests.

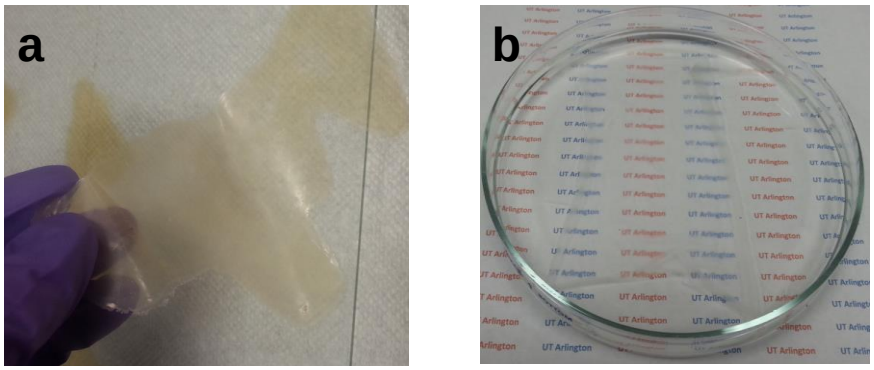

Figure 3-7: (a) Dry non-activated Gu-Chi5; (b) Activated wet Gu-Chi5.6

3.4.3 Hybrid Lipophilic [Gu(L)-Chi] blend membranes (Scheme 2b)

This type of membrane was fabricated to further modify and in particular improve the integrity of the membrane, which would decrease its fuel permeability. Also, the precipitation reaction with sodium stearate yielded the polymer insoluble in water and soluble in methanol instead (**Table 3-1**). This promises a route for future ionomer and membrane development as dissolution and swelling of the materials in MEAs are considered to result in primarily loss of mechanical strength, increasing fuel crossover, and eventually failure of fuel cells.

Table 3-1: Solubility of different polymer material in water, alkali and methanol. The 'ticks' denote soluble while 'crosses' denote insoluble

Material	**Water**	**Alkali**	**Methanol**
Guanidine Prepolymer	✓	✓	×
Gu-PTFE	×	×	×
Gu-Chi	×	×	×
Gu(L)	×	×	✓
Gu(L)-Chi	×	×	×

An equal mass of sodium stearate and guanidinium polymer was dissolved in water and then mixed with each other (Scheme 2b of **Figure 3-5**). The temperature of the mixture was raised to 70 ^{o}C while continuously mixing the solution to allow the precipitation reaction (color of the mixture changes abruptly as shown in **Figure 3-8**) to occur until most of the solvent has evaporated. The remaining white solid was insoluble in water and had no odor. After it was separated and dried, 5.6g of this lipophilic guanidinium polymer was dissolved in methanol and added to a solution of water containing 2.5g of chitosan. The mixture was again blended at 70 ^{o}C, but this time the membrane film was achieved by slow evaporation of excess solvent as the blend proved too viscous under application of a doctor blade. Finally, the same heat treatment and hydroxide functionalization procedure to the one described in the previous section was applied.

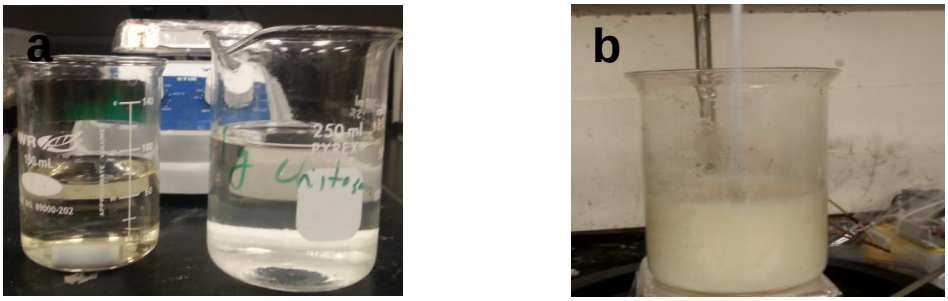

Figure 3-8: a) Lipophilic treated guanidine water dissolved in water (l) with chitosan dissolved in 1% acetic acid solution b) The two solutions in 'a' mixed to yield milky white blend which is mechanically stirred & heated at 60 oC

3.5 Conclusion

A series of novel composite and hybrid blended AEMs are synthesized by incorporating guanidinium-based polymers into a porous polytetrafluoroethylene (PTFE) film. The guanidinium-based polymers are polymerized using a simple condensation process between a guanidinium salt and two different diamines so that the guanidinium cations are attached directly to the polymer backbone to enhance both conductivity and durability.

Two diverse yet straightforward techniques are used to fabricate the AEMs. The composite membrane is supported by a porous PTFE substrate. The prepared solution based on the guanidinium prepolymer is used to penetrate these pores. Crosslinking is also attempted to obtain better interlocking with the substrate.

Similarly, the prepolymer is blended with chitosan and this slurry is used to obtain hybrid blended membranes. Chitosan is used as the mechanical reinforcement while the prepolymer contains the ion exchange group.

Chapter 4

Structural & Chemical Study

4.1 Introduction

Research is designed to develop a new family of AEMs – integrated network membranes with guanidinium moieties as ion-exchange groups in the polymer backbone. The membranes are then subject to structural, chemical and electrochemical characterization as required for AEMFC applications. The figure below gives an overview of the necessary tasks to meet the research aims of this project. They include polymer synthesis, membrane fabrication and characterization followed by fuel cell and electrochemical studies including stability assessments:

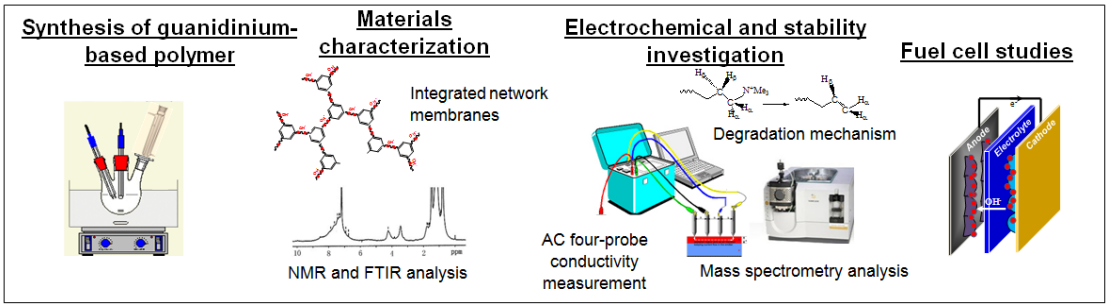

Figure 4-1: Overview of the experimental tasks for meeting the objectives of the proposal

4.2 Experimental Setup

4.2.1 FTIR

FTIR spectra of the blend membranes and starting materials were recorded using Thermo Nicolet 6700 FTIR Spectrometer in ATR mode with a resolution of 16 cm^{-1} within the range of 800-4000 cm^{-1}.

4.2.2 NMR

The polymers were initially dried in vacuum at 60^{o}C for 16 h as well as freeze dried to remove any trace of DI water. ^{1}H and ^{13}C NMR spectra for the different monomers and resulted polymers were measured at 300 MHz on a JNM ECS 300 spectrometer (JEOL, Tokyo, Japan) to verify their chemical structures. DMSO-d_6 was used as the solvent, and tetramethylsilane was used as an internal standard.

4.2.3 SEM

The morphology and microstructure of all the membranes were observed by means of a scanning electron microscope (Hitachi S-3000N Variable Pressure SEM). The samples were sputtered with silver before studying them under the SEM.

4.2.4 Raman

Studies using Raman spectroscopy were performed on a Thermo Scientific DXR Raman microscope at a wavelength of 780 nm and 100 mW in the range of 200-3400 cm^{-1}.

4.2.5 Mechanical Strength of Membranes

Mechanical properties such as tensile strength, total elongation and fracture strength were measured with a MTS advantage^{TM} tension tester at room temperature. A programmed elongation rate of 10 mm/min was adopted until break. Membrane sample dimensions were approximately of 3 mm x 14.5 mm.

4.2.6 Thermal Analysis

TGA/DTA from TA Instruments (SDT Q600) with heating rate 10 ^{o}C min^{-1} under N_2 flow rate of 60 ml min^{-1} was used to assess the thermal stability of the guanidine polymers.

4.3 Characterization of Guanidinium Prepolymer

^{1}H NMR spectra for the monomers were shown in **Figure 4-2 i-ii)**. The two diamines, AEE (**Figure 4-2i)** and HMDA (**Figure 4-2ii**), showed their characteristic peaks at δ =3.46 ppm (peak 4) and δ=1.23 ppm (peak 8), respectively. These peaks are attributed to the protons in their amine groups. Upon polymerization, these peaks should disappear and be replaced by the guanidino peaks similar to the one shown by the GHCl in **Figure 4-2iii** (peak 9 at δ=7.162 ppm). This is indeed demonstrated by the spectra of the resulting polymers in **Figure 4-2 iv** and **v.** The broad peaks for the AEE based polymer (peak **13)** and the HMDA based polymer (peak **17)** are attributed to the guanidino group (H^1 on $C=NH_2^+$) in the range of 6.20-8.20 ppm. The reason that these two peaks showed a

low-intensity appearance and broadening may be due to relaxation of nitrogen and slow exchange rate of the proton on $C=NH_2^+$ with other protons [61]. In order to further prove our proposed chemical structure of the guanidinium functionalized polymers, C^{13} NMR was performed on both polymers. The peaks 21 and 25 (**Figure 4-3i** and **ii**) at δ=156.3-157.9 ppm were the corresponding peaks for the guanidino group. They were relatively stronger here and again matched well with similar structures in literature [41] illustrating the presence of the guanidinium group within our synthesized polymers.

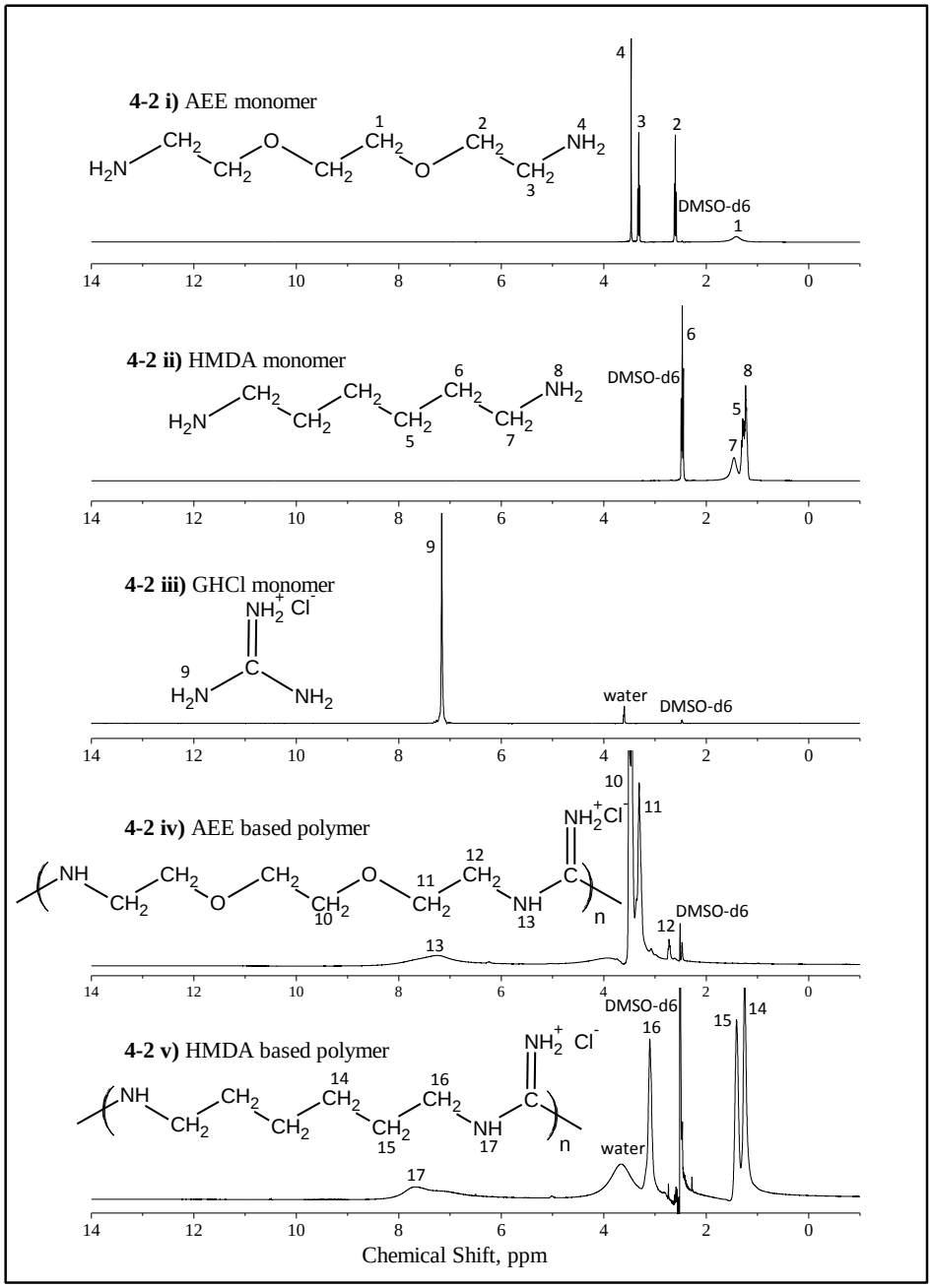

Figure 4-2: ^{1}H-NMR spectra of (i) AEE monomer, (ii) HMDA monomer, (iii) GHCl monomer, (iv) AEE based polymer and (v) HMDA based guanidine polymer [49]

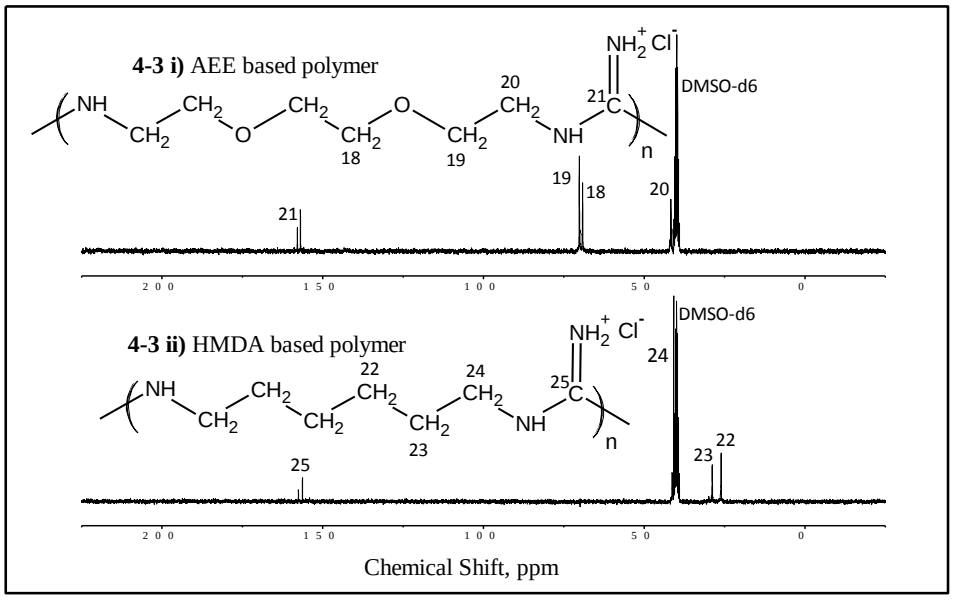

Figure 4-3: ^{13}C-NMR spectra of (i) AEE based polymer and (ii) HMDA based polymer [49]

4.4 Characterization of Composite Membrane

The FTIR spectra of the pristine porous PTFE substrate and the impregnated composite membranes were shown in **Figure 4-4a**. Compared with the pristine PTFE membrane, the composite membranes showed two new peaks at 3320 and 1630 cm^{-1}. The broad band at 3320 cm^{-1} was associated with stretching vibration of the N-H bonds, and the one at 1630 cm^{-1} was assigned to vibrations of C=N in the guanidinium groups. The peak at 1200 cm^{-1} associated with the underlying C–F group in the PTFE was observed in all the samples. The results show that successful

incorporation of the guanidinium moieties into the porous PTFE substrate has been achieved.

The above result was further confirmed by the Raman Spectra in **Figure 4-4b**. Raman peaks obtained from the pristine PTFE membrane were compared to those from the top and bottom surfaces of the HMDA based composite membrane. In agreement with the literature [54], **Figure 4-4b** clearly indicated the characteristic Raman peaks for the guanidine polymer against the background of the underlying PTFE. The broad band between 3100 and 3450 cm^{-1} were attributed to $-NH_2$ stretching vibrations while the large peak at around 2910 cm^{-1} was denoted to aliphatic C-H symmetric stretching bands. The peak at 1610 cm^{-1} was attributed to -NH vibrations, while both the bands at 1310 and 1450 cm^{-1} were assigned to the bending vibrations of the $-CH_2$ groups on the alky chains. The top surface of the composite membrane showed a higher intensity for all of these peaks probably indicating that a polymer surface layer which was understandably slightly thicker than the layer on the bottom surface.

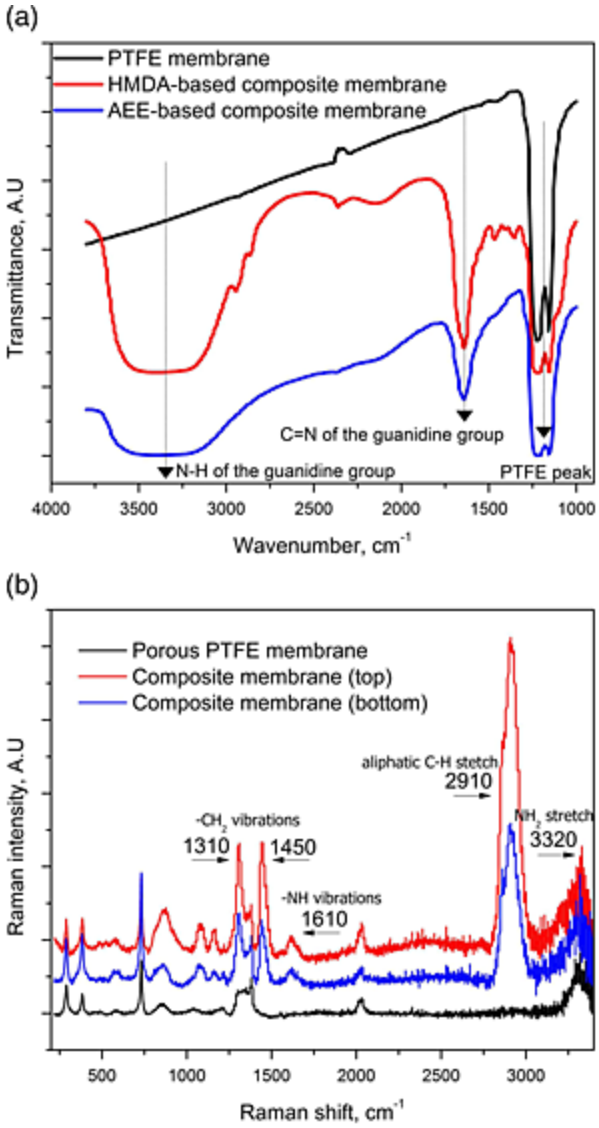

Figure 4-4: (a) FTIR and (b) Raman spectra of the porous PTFE- and HMDA-based composite membrane [49]

Microscopic morphologies of the pristine PTFE and composite membranes were shown in **Figure 4-5.** **Figure 4-5a** shows that the surface of the PTFE film

was rough and porous, which will facilitate impregnation of the guanidinium based polymers. **Figure 4-5b** demonstrates a partial impregnation of the pores on the surface. Herein a high weight percentage of the AEE based guanidinium polymer solution (15%) was used to make the composite membrane (denoted as AGM1 as shown in **Table 2**); therefore, high viscosity of the polymer solution makes it difficult to plug all the pores of the porous PTFE. Decreasing the polymer weight percentage to 7.5% lowers the viscosity of the HMDA and AEE based polymer solutions utilized in **Figure 4-5c** and **d**. Hence, the polymer solution could relatively easily penetrate and fill all the pores within the PTFE, and then a dense composite membrane with a continuous polymer surface layer can be formed (**Figure 4-5c and d**). Additionally, EP was added to the polymer solution in the samples shown in **Figure 4-5c & 4d,** therefore the impregnated polymers in the porous PTFE were crosslinked. The crosslinking of the guanidinium based polymers in the composite membranes also facilitated anchoring the ion exchange moieties to the porous substrate, as will be discussed in the next chapter. The appearance of the cluster and pleat might be attributed to handling the membrane under high energy electron beam and the subsequent dehydration and shrinkage of the AEM.

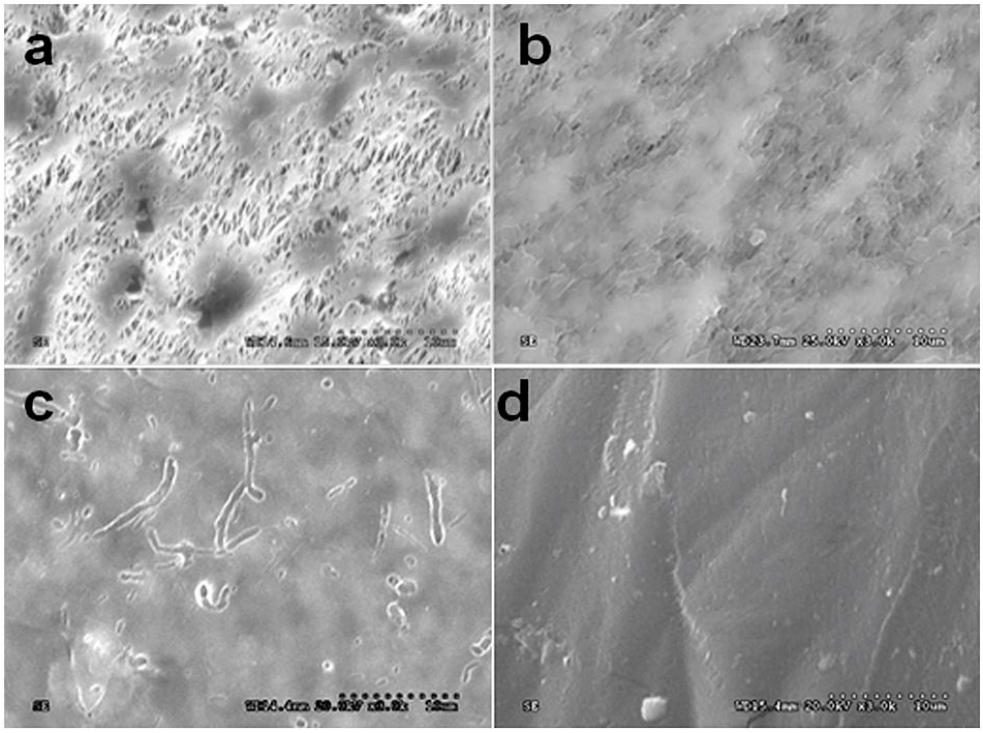

Figure 4-5: SEM images of membranes: a) Porous PTFE substrate, b) Partially penetrated composite membrane, AGM1, using 15% AEE-based polymer solution. c) Fully impregnated and crosslinked membrane, HGMC, using 7.5% HMDA-based polymer solution, and d) Fully impregnated and crosslinked membrane, AGMC, using 7.5% AEE-based polymer solution. [49]

Table 4-1 compared the EDX results between the pristine PTFE and the AEE based guanidinium composite membrane (denoted as AGMC corresponding to **Figure 4-5d**). The AGMC sample refers to a composite membrane synthesized using 7.5 wt% of AEE based polymer with EP as crosslinking agent. **Table 4-1** clearly show a significant increase in carbon and nitrogen contents and a

corresponding drop in the F content in the composite membrane. This further demonstrated that the polymer has successfully penetrated into the pores of the PTFE matrix.

Table 4-1: EDX results for pristine PTFE substrate and fully impregnated AEE based composite membrane (AGMC) [49]

	PTFE substrate		Composite membrane	
Element	*Wt. %*	*At. %*	*Wt. %*	*At. %*
C K	33.61	49.91	71.68	80.66
N K	02.30	02.93	09.91	09.57
O K	01.79	02.00	09.00	07.60
F K	44.83	42.08	01.63	01.16
ClK	00.60	00.30	00.14	00.05
AgL	16.87	02.79	07.64	00.96

One of the advantages of using the PTFE substrate as reinforcement for weaker polyelectrolytes is the strong structural integrity it imparts to the composite membrane. To observe this the porous PTFE substrate and composite membrane were subject to uniaxial tensile testing.

The PTFE substrate in **Figure 4-6** imparts a greater amount of total strain to the membrane but incorporation of crosslinked guanidinium based polymer to its porous network reduces this by making the membrane stronger and increasing its peak stress from 7.5 MPa to 13.8 MPa. The composite membrane is stronger by virtue of the crosslinked membrane embedded in the substrates pores, yet as enough elasticity from the PTFE for use in the membrane electrode assembly of fuel cells.

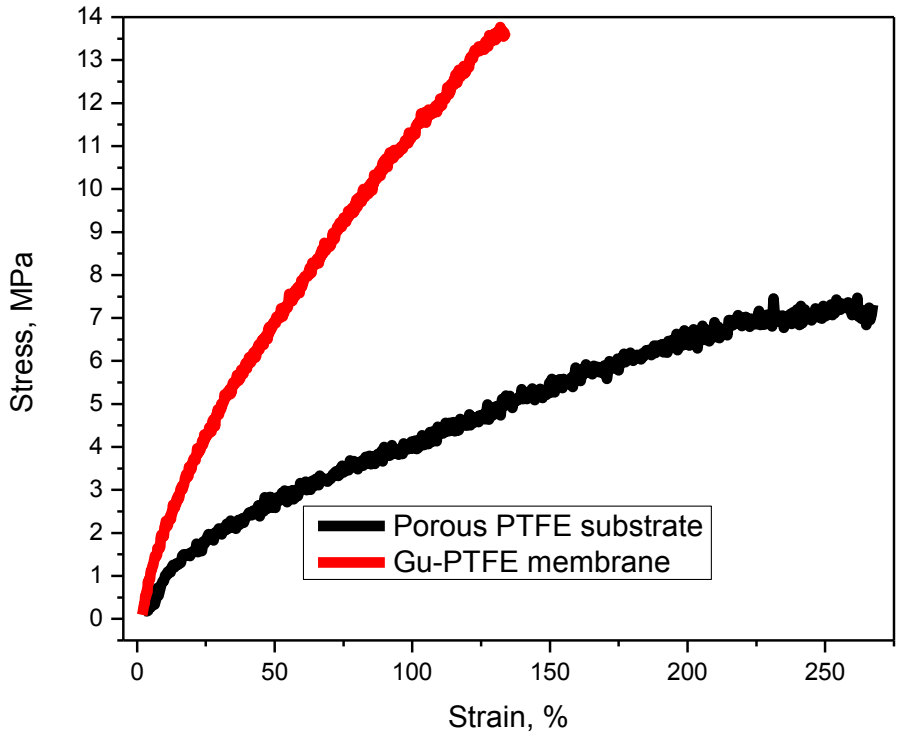

Figure 4-6: Tensile tests of Porous PTFE and composite Gu-PTFE membrane

Thermo-gravimmetric analysis (TGA) and differential thermo-gravimmetric analysis (DTG) were conducted to assess the short term thermal stability of the guanidinium based polymers and membranes. Starting from low temperatures, almost all the TGA curves (except for the PTFE film) in **Figure 4-7a** show an initial weight loss due to absorbed water, and then followed by a slow degradation region. This is particularly evident for the non-crosslinked polymers. Since the heating rate was high (10 ^{o}C min^{-1}) and the guanidinium groups in the polymers could retain water due to their strong hydrophilicity, further removal of the absorbed water could be delayed to higher temperatures. Therefore, the slow degradation region also included a major contribution from the remaining absorbed moisture. The above two-stage of water removal, particularly for the non-crosslinked based polymers, may indicate a commensurate variety of water "states" in the membranes. Different water states have been proposed to exist in Nafion membranes [62], corresponding to different internal environments. For our membranes, water molecules that do not interact strongly with the polymer matrix exhibit liquid-water dynamics corresponding to the initial or first-stage water loss in the TGA analysis, whereas water bound to the polymer hydrophilic groups, those located at the polymer/liquid-water interface or trapped within the polymer chains, exhibit slower dynamics within the slow degradation region.

Upon further increasing the temperature, the polymers encounter degradation of the quaternary guanidinium groups which began at *ca.* 325 ^{o}C and matched well

with reported values [31, 34]. For the AEE based polymer samples, this eventually leads to complete decomposition. The HMDA based guanidinium polymers showed better heat stability and their macromolecule breakdown started at a much higher temperature, *ca.* 445 ^{o}C. The existence of these two plateaus and the shape of the curves for the two HMDA based guanidinium polymer samples agreed well with literature [61]. The same profile was presented by the HGMC* composite membrane followed by an additional PTFE decomposition. **Table 4-2** showed the crosslinked samples and membranes generally experienced lesser weight loss. For example, a look at the Δm =20% column clearly showed that the non-crosslinked samples reach this mass loss at much lower temperatures, indicating poor thermal stability. Also, the composite membrane (HGMC*) had by far the greatest thermal stability owing to the presence of the stable PTFE substrate.

The DTA curves in **Figure 4-7b** were used to reveal more details about the decomposition regions of the crosslinked HMDA based polymer and composite membrane. They clearly illustrated at least two minima. The first sharp minimum, pertaining to the above mentioned guanidinium functional group degradation, took place between 300-400 ^{o}C, suggesting good short term thermal stability. **Figure 4-7b** further showed convincing amounts of polymer impregnation in the composite membrane because its DTA curve matched well with the underlying polymer curve. The last (third) minimum point was attributed to the PTFE degradation and was

smaller in size, suggesting that the imbedded polymer exists in a large majority (estimated at 86.5 wt %) in the composite membrane.

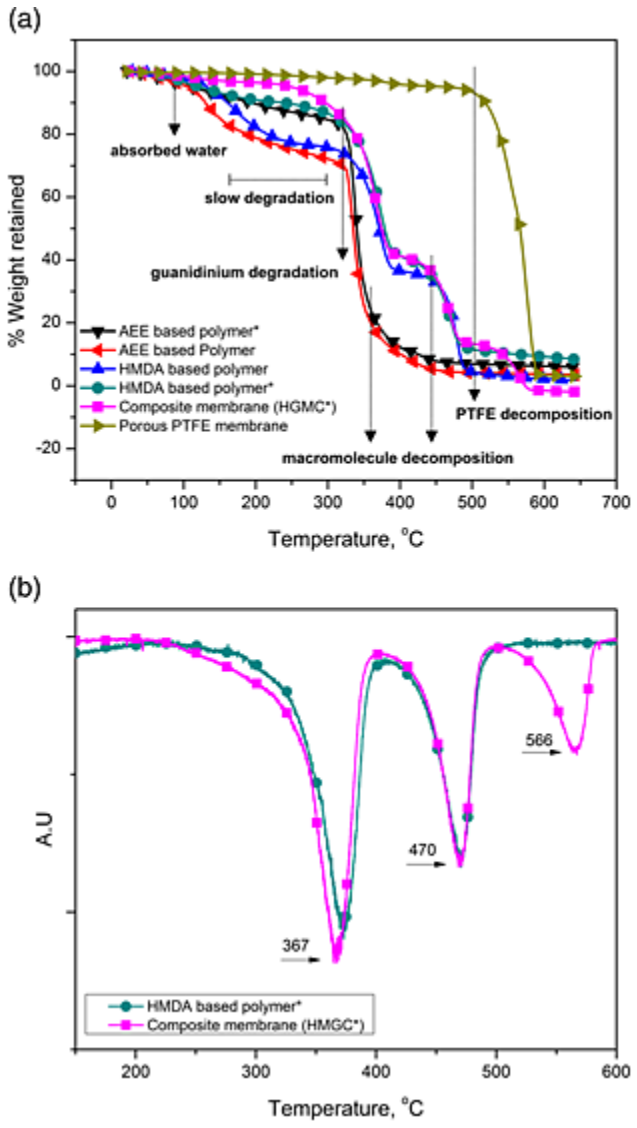

Figure 4-7: (a) TGA and (b) DTG curves for different polymers (*: crosslinked) [49]

Table 4-2: Temperature (°C) of mass changes (Δm) for different samples calculated from TGA curves. (*: crosslinked samples) [49]

Sample	Δm = 2%	Δm = 5%	Δm = 10%	Δm = 20%	Δm = 50%
AEE based polymer*	65.27	110.1	194.7	325.8	340.1
AEE based Polymer	64.74	107.9	130.1	189.2	335.2
HMDA based polymer	91.74	132.6	161.0	216.5	371.1
HMDA based polymer*	80.76	122.1	236.1	336.1	378.7
Composite membrane (HGMC*)	113.2	250.2	296.6	337.7	374.5
Porous PTFE membrane	297.3	463.5	518.2	538.1	566.3

3.5 Characterization of Blended Membranes

FTIR spectra of the synthesized blend polymers and some of the starting materials are illustrated in **Figure 4-8**. The main peak (Peak 1) of the guanidinium group is at 1564 cm^{-1} (C=N vibrations) and the broad band (Peak 2) due to the stretching vibration of N-H bonds appears at 3300 cm^{-1}. The broadband (Peak 2) is often interchangeably denoted as N-H or OH^- for many AEM materials in literature. Hence we find that activation of the material in aq. KOH augments the intensity of Peak 2, causing the ratio of Peak 2: Peak 1 to rise by a factor of almost 2. Similarly, chitosan curve also had a peak around 3300 cm^{-1} attributed to its –OH group [63]. In addition, the peak at 2878 cm^{-1} is attributed to $-CH_3$ which is the strongest for

the sample modified with sodium stearate (sample 4). The other sharp peak of the Gu(L) polymer is at 1560 cm^{-1} from the band of $\nu_a COO^-$ [64] in the stearate.

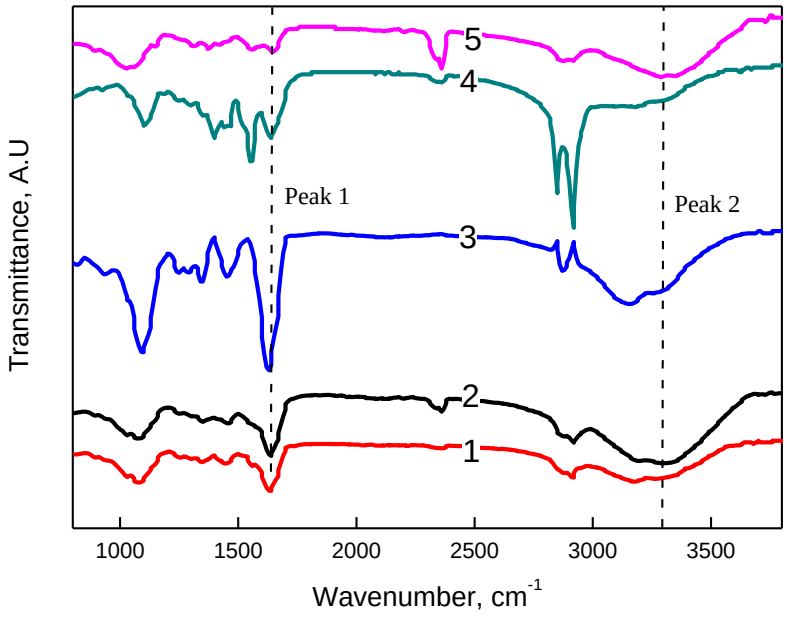

Figure 4-8: FTIR spectra of different membranes and their starting materials: 1) non-activated Gu-Chi5.6 polymer, 2) activated Gu-Chi5.6 polymer, 3) Gu prepolymer, 4) Gu(L) polymer, and 5) Chitosan. Gu, Chi, and (L) stand for guanidinium, Chitosan, and lipophilic, respectively

SEM microstructures of different blend membranes are taken to understand phase mixing in the blend membranes. **Figure 4-9** (**a-c**), corresponding to different guanidinium-chitosan blend membranes, show that certain periodic troughs were

present on the membrane surface. However, they appear only as surface defects confirmed by very low methanol permeability values discovered in the next section. These could in fact be the result of domains of the dispersing phase brought about by Ostwald ripening or coalescence (through Brownian motion), or combination of the two mechanisms [65]. The microstructures are further exacerbated by uneven dehydration and shrinkage of the polymer components, particularly at the chitosan-guanidinium interface in the polymer blend, under the high energy electron beam in the SEM chamber. The general size of the dispersed chitosan rich domains marked by the yellow dotted circles becomes smaller and less spherical yet the quantity seems greater for the highest chitosan content, i.e., Gu-Chi5.6 (**Figure 4-9b**), which might signify greater shear forces while blending due to the higher chitosan content. In **Figure 4-9a** the domain size (diameter) is around 10 µm while in **Figure 4-9b** the domains reduce to around 6 µm albeit their numbers increase dramatically reflecting the higher quantity of chitosan. One reason for using chitosan was because of its superior film making properties, and increase in the number of chitosan anchoring domains could provide a stronger (greater strength, **Figure 4-10**) and tighter structure (lower permeability, **Figure 7**). However, they would serve as 'relatively' inactive sites and cause a reduction in the ionic conductivity. Reaction of sodium stearate with the prepolymer seems to improve the structure in **Figure 4-9c** leading to uniform spherical domains but with the highest domain size (ranging to slightly lower than 15 µm). However, this time the

bulk material also incorporates the inactive sodium stearate component (for better strength) and we envision that it will exhibit lower ionic conductivity as confirmed in the next section.

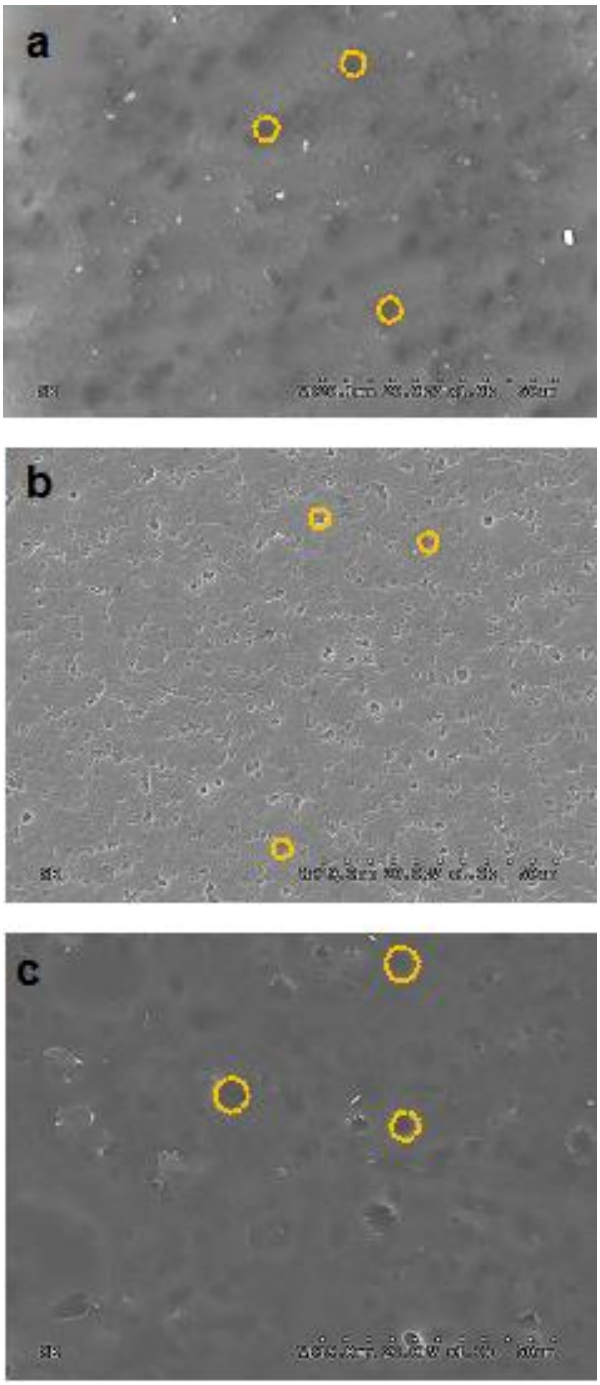

Figure 4-9: SEM micrographs of blend membranes, a) Gu-Chi2.2 b) Gu-Chi5.6 c) Gu(L)-Chi2.5

To study mechanical properties of the blend membranes, tensile tests were conducted. The results for the three blend polymers are shown in **Figure 4-10** and are further compiled in **Table 4-3.** As expected, increasing chitosan content to the blend drastically increased the tensile strength of the membranes from approx. 4 MPa for Gu-Chi2.2 to approx. 25 MPa for Gu-Chi5.6. This was essentially six times increase in strength by only 2-3 times increase in mass of chitosan. The modified prepolymer with sodium stearate had the same effect; however, it also rendered the membrane a greater deal of rigidity demonstrated by the much higher modulus but yet smaller strain (**Table 4-3**).

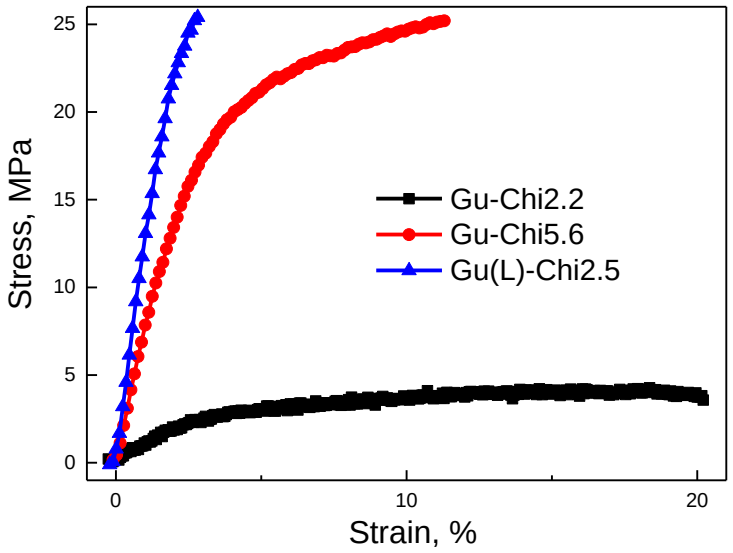

Figure 4-10: Tensile test results of various blended membranes

Table 4-3: Summary of mechanical properties for different membranes from the tensile tests

Sample membrane	Peak Load N	Peak Stress MPa	Strain At Break %	Modulus MPa
Gu-Chi2.2	0.321	4.3	18.4	105.95
Gu-Chi5.6	3.112	25.2	11.3	790.17
Gu(L)-Chi2.5	1.778	25.4	2.8	1339.58
Porous PTFE	0.624	7.5	269.7	8.31
Gu-PTFE	1.927	13.8	132	19.91

3.6 Chemical (Hydroxide) Stability:

Small pieces of the crosslinked guanidinium functionalized polymers were studied by immersing them in 5 M aq. KOH at 55 ^{o}C. They were taken out at regular time intervals, washed with DI water, wiped dry with tissue paper, and then studied using complementary techniques of Raman (**Figure 4-11**) and FTIR (**Figure 4-12**) spectroscopy to detect any degradation or changes in chemical structures. During the test, all of the samples appeared to lose some weight. They also became a little lighter in color and less transparent. The Raman spectra for the AEE and HMDA based guanidinium functionalized polymers were presented in **Figure 4-11a and b**, respectively. The results exhibit similar peaks to the composite membranes

shown in **Fig. 3b**. They also showed no significant change in peak positions or their relative intensities even after an exposure of 30 h to 5M KOH at 55ºC.

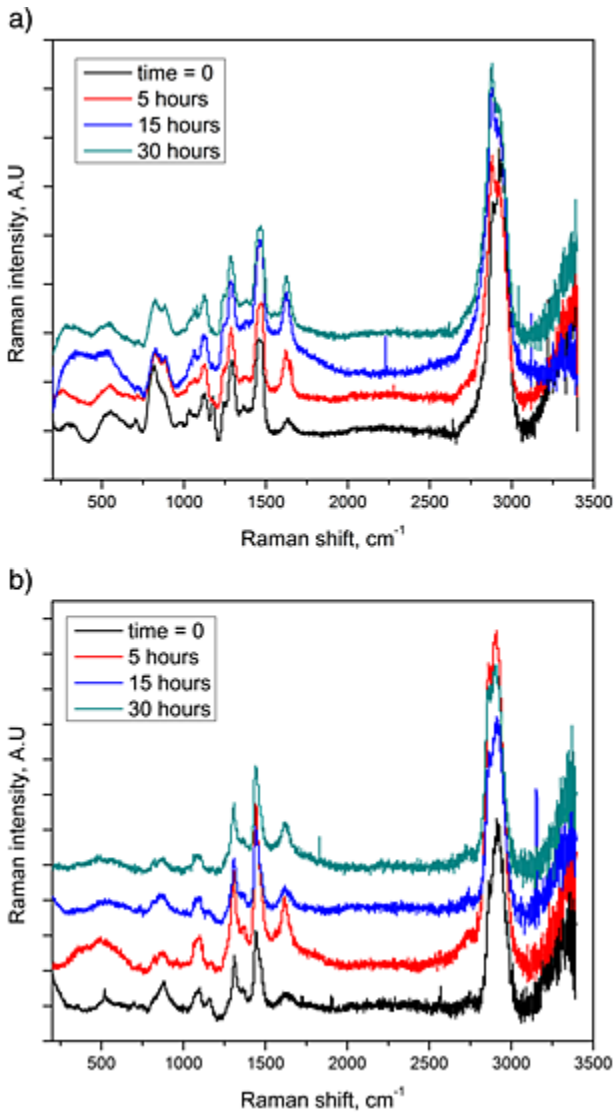

Figure 4-11: Raman spectra of a) AEE and b) HMDA-based guanidinium polymers exposed to 5 M aq. KOH at 55°C for different time intervals [49]

FTIR spectra of both AEE (**Figure 4-12a**) and HMDA based polymers (**Figure 4-12b)** did not show any remarkable change either, even though the exposure time has been extended to 50 h. The peak at *ca.* 1630 cm^{-1} corresponding to δ_{NH} showed a trend of decreasing intensity for both polymers relative to the N-H stretch broad band at 3320 cm^{-1}. For the HMDA type in **Figure 4-12b**, a new peak appeared at *ca.* 2400 cm^{-1} and had a trend of slowly increasing in intensity with exposure time. It lies in the frequency range of characteristic C-N stretch. This implies that there was some amount of degradation with the amine groups but the main guanidinium carbon atom is still stable. These stability results are substantial especially if compared to the commercial Tokuyama A201 membrane in **Figure 4-12c** which was exposed to the same conditions for the purpose of establishing a reference. There was an evident change from exposure time 30 to 50 h. The peaks *ca.* at 1359 cm^{-1} and 1442 cm^{-1} increased in intensity and a new broad peak at around 3100 cm^{-1} instead of the twin peaks at 2800 cm^{-1} and 2910 cm^{-1} appeared. The commercial A201 membrane was composed of a linear hydrocarbon backbone with quaternary ammonium group [66]. Key modes of degradation of the quaternary-ammonium groups are either through the Hoffman elimination reaction [48] or direct nucleophilic displacement at the cationic sites [46, 67]. The former involves the attack of hydroxyl ions on the beta-hydrogen of the ammonium, while the latter can occur on the carbon located in the alpha or beta position of the ammonium. Both degradation mechanisms lead to formation of alkenes [37] which

were exactly ascribed to the new peak at *ca.* 3100 cm^{-1} in **Figure 4-12c**. This observation confirms the above-mentioned degradation mechanism of quaternary ammonium groups.

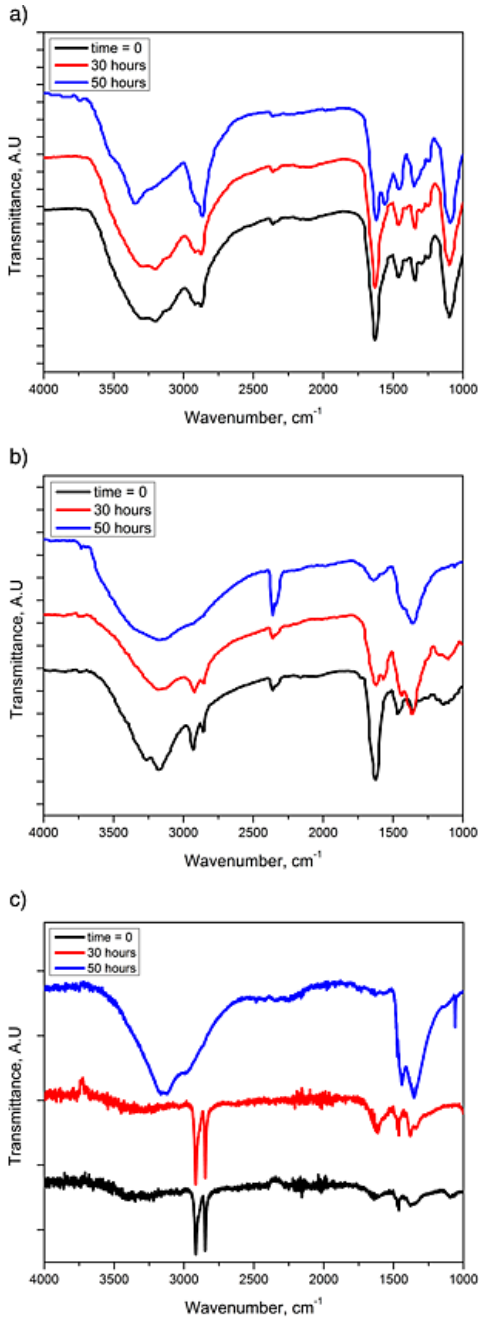

Figure 4-12: FTIR spectra of a) AEE-based guanidinium polymer, b) HMDA-based guanidinium polymer, and c) commercial Tokuyama A201 after exposure to 5 M aq. KOH at 55°C for different time intervals [49]

Chemical degradation of AEMs stems largely from nucleophilic attack of hydroxide ions on the fixed cationic sites, which results directly in a loss of ion-exchange groups, and a subsequent decrease in OH- conductivity. Degradation mechanisms of AEMS have virtually always been studied on quaternary-ammonium groups, even though research on new ion exchange groups has increased dramatically [17, 40-43]. Though recent membrane degradation studies [23, 44, 45] on quaternary ammonium groups have provided some fundamental understandings that may be applied to other types of AEMs, but with considerable limitation. For example, membrane conditions that lead to poor solvation of OH^- ions may enhance chemical degradation of the cations. Chemical stability is less dependent on modification of the alkyl groups that attach to the cationic moieties [46]. Of course, the above statements may be valid for non-quaternary-ammonium AEMs in some sense, as the nucleophilic attack by OH^- ions contributes to the chemical degradation in most of cases. However in our membranes, due to remarkable charge delocalization (over one carbon and three nitrogen atoms) and disappearance of hydrogen attached to the three nitrogen atoms in the fully crosslinked polymers (**Figure 3-1**), it appeared that either the Hoffman elimination or direct nucleophilic displacement reactions would not likely occur during membrane degradation.

This charge delocalization in the guanidinium hydroxides also provides a high degree of thermal and basic stability [35, 41]. Hence, the results demonstrated

that the guanidinium group by virtue of its resonance stabilization of the π-system and its "Y-delocalization" resulted in stabilization comparable to cyclic aromatics such as benzene [68] and their chemical stability was superior to ammonium based AEMs such as the A201.

3.7 Conclusion

The fabricated composite and hybrid blended AEMs are analyzed in this chapter. The condensation polymerization to obtain the base guanidine polymer is successfully performed as indicated by the NMR results. This prepolymer is then used to fabricate composite and hybrid blended membranes.

This prepolymer is then dissolved in solution and is used to penetrate the pores of the PTFE substrate for the composite membrane. SEM/EDX and spectroscopic analysis show complete impregnation was achieved. Similarly, the prepolymer blended with chitosan resulted in dense hybrid blended membranes. The PTFE base and chitosan blend components play essential part in strengthening the obtained AEMs.

The polymer and hence membranes also show exceptional thermal and chemical stability. The chemical stability especially is promising considering the extreme conditions used for testing. The synthesized guanidinium material infact performed better than the Tokuyama A201 commercial AEM.

Chapter 5

Electrochemical Study of AEMs

5.1 Introduction

The first step for characterization of newly developed AEMs is to test their chemical, thermal and mechanical properties. Having done that successfully in the previous chapter, they can be confidently applied to a fuel cell system. Having said that it is still important to investigate how good the electrochemical properties of the AEMs are, otherwise performance in a fuel cell might not be optimum. Some of these properties are illustrated in **Figure 5-1** below:

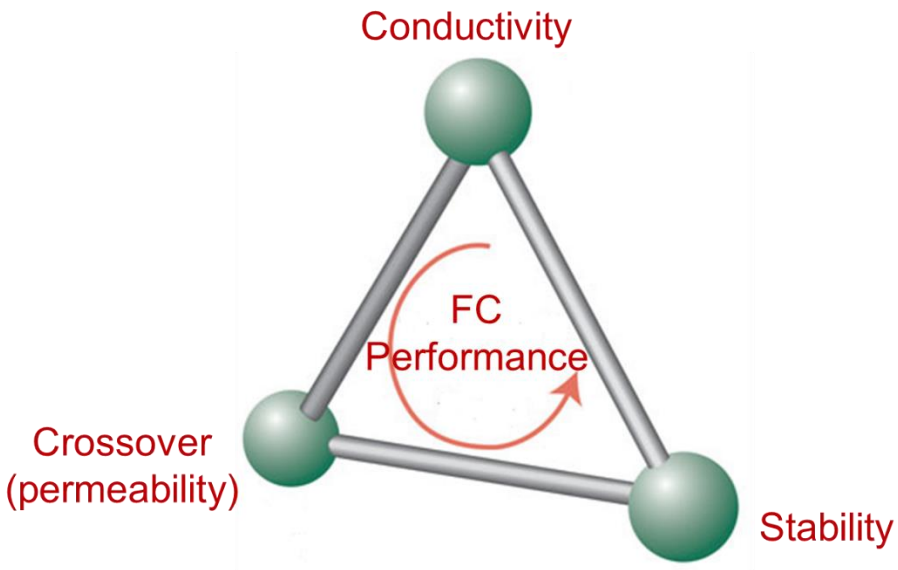

Figure 5-1: Important membrane properties for good fuel cell performance

2.5.4 Anionic Conductivity, Water/Alkali uptake & Dimensional Stability

After activation to their hydroxide form, the membranes were repeatedly washed and submerged in DI water for 2 d to remove any traces of residual KOH so that the anionic conductivity measured wasn't affected by it. Strictly speaking, the conductivity may not be solely due from the guanidinium cations as the hydroxide form of the membrane would react with CO_2 in the air during the impedance experiment. Thus conductivity values recorded are likely to be a result from a mixture of alkaline anions (OH^- and either HCO_3^-/CO_3^{2-}) [69, 70].

The anion conductivities of the AEM strips (approx. 5 cm x 2 cm, DI water, 20 ^oC) were estimated from AC impedance spectroscopy data by the commonly employed four point probe technique [71] using the PARSTAT 2273 frequency response analyzer. Electrochemical impedance spectroscopy (EIS) was performed by imposing a small sinusoidal (AC signal) voltage, 10 mV, across the membrane sample at frequencies between 1 milli Hz to 1 kHz and measuring the resultant current response. The real impedance value at the real intercept in the Nyquist plot was taken as the resistance of the membrane [71-73]. This was then used to calculate the anionic conductivity, σ, by employing the following formula:

$$\sigma = \frac{L}{Zre \times A}$$

where L is the length between sense electrodes (1 cm), Zre is the real impedance response at high frequency, and A is the membrane area available for anion conduction (thickness x width). Sample Nyquist plots are illustrated in Fig 2b. For purpose of reference, Nyquist plot of Nafion 112 (in DI water, 20 ^{o}C) was also plotted and was used to obtain a conductivity value of 10.2 mS cm^{-1} which is comparable to that found in literature [74].

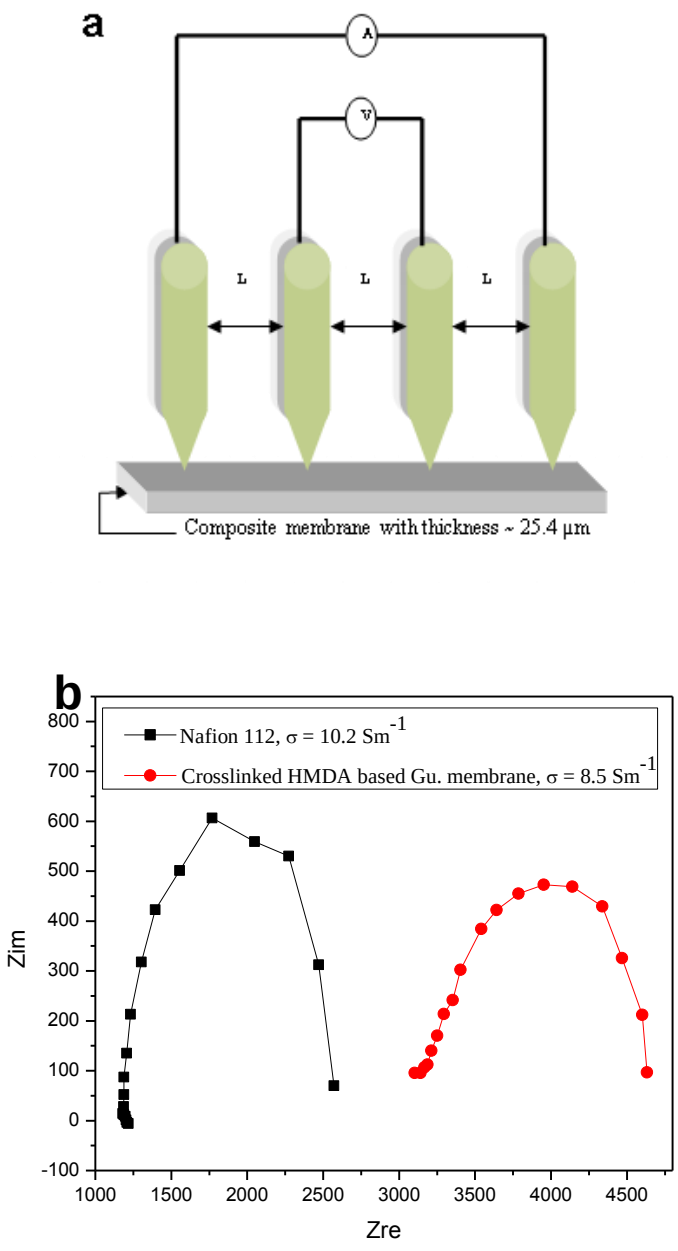

Figure 5-2: Four-probe membrane conductivity measurement: (a) experiment setup and (b) Nyquist plots to measure σ for Nafion 112 & HGMC (thickness = 50.8 & 25.4 µm respectively)

Similarly, dry strips of membranes were taken and their weight was measured before they were immersed for 48 h in deionized water for measurement of water uptake (*Wu*) and in 1M KOH for alkali uptake (*Au*). The water and alkali uptake of the membranes was thus calculated based on the weight gain as seen widely in literature [75-77]. Besides, the dimensional change (ΔL) in both water and alkali were also recorded by tracking the change in distance specified positions before ($L1$) and after ($L2$) the samples were soaked in deionized water or 1M KOH for 48 h.

$$Wu = \frac{Mw - Mo}{Mo} \qquad Au = \frac{Ma - Mo}{Mo} \qquad \Delta L\% = \frac{L2 - L1}{L1} \times 100$$

where, Mo is weight of the dry membrane while Mw and Au are the weights of the corresponding water and alkali swollen membranes respectively.

2.5.5 Methanol Permeability & Selectivity

Methanol permeability measurement is based on the Gasa method [78] which employed a permeation cell derived from Walker et al [79]. 25g of methanol was sealed inside a permeation cell and was only allowed to diffuse through a circular opening of a membrane (diameter = 0.6 cm). **Figure 5-2** shows the schematic and actual setup of the permeability test. One set of measurements were conducted at room temperature (22 ^{o}C). For an elevated temperature (60 ^{o}C) the cell was kept inside an oven. The oven had an internal volume of 0.3 m^3 and convective air flow was created by a fan inside the oven to ensure constant

concentration difference for methanol to permeate through the membrane. The mass of methanol inside the vials as a function of time was measured and the equation below was adopted from J. Zhou et al. [75] for easy comparison with literature of the permeability (P) of the various membranes:

$$P = \frac{N \times l}{VP \times A \times t}$$

where N = number of moles of methanol lost (moles), l = thickness of the membrane, VP=saturated vapor pressure of methanol at 22 ^{o}C or 60 ^{o}C (Pa), A = membrane area for methanol permeation (cm^2), and t = time (days).

The selectivity of the membranes was tabulated according to the following relations:

$$Sm = \frac{\sigma}{P};\ Sr = \frac{Sm}{Sn}$$

where Sm = selectivity of each membrane, σ = anionic conductivity, P = methanol permeability, Sr = relative selectivity factor, and Sn = permeability of Nafion (N117).

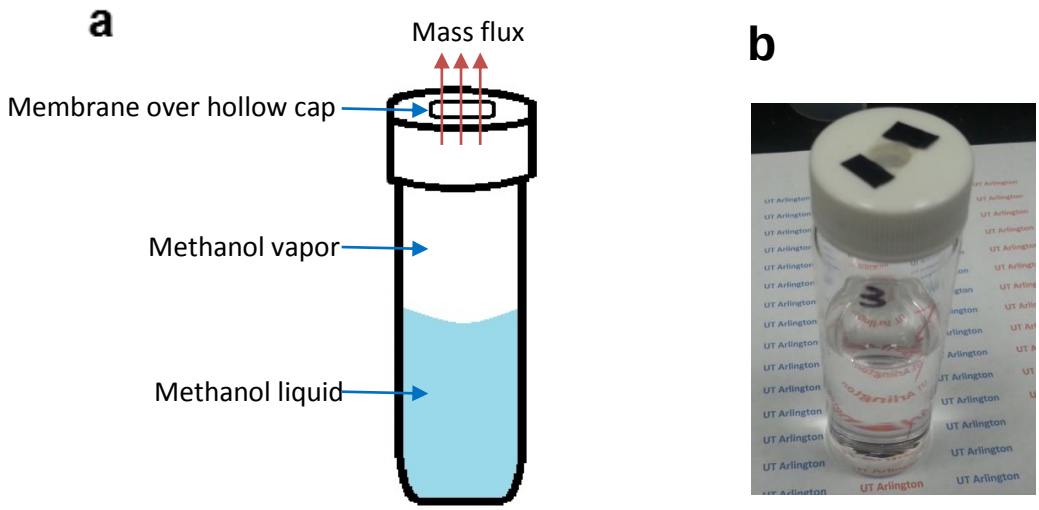

Figure 5-3: Schematic (l) & actual (r) setup of the permeability test

5.3 Membrane Properties

5.3.1 Anionic Conductivities & Water Uptake of Composite membrane

The properties of three AEE based (AGM) and two HMDA (HGM) based composite membranes were shown in **Table 5-1**. AGM1 were prepared from a polymer solution with a larger weight percentage (15%, shown in **Fig. 4-5b**) with a higher viscosity. This reduced the effectiveness of the polymer infiltration process leading to a lower anionic conductivity (30.7 mS cm^{-1}) when compared to AGM2 (56.6 Sm^{-1}) fabricated using a dilute polymer solution (7.5wt%).

Table 5-1: Weight % of polymer, ionic conductivity (σ), water uptake (WU) and ion-exchange-capacity (IEC) of membranes

Sample	Wt% of polymer in solution	σ, mS cm^{-1}	WU %	IEC, mmoles/g
AGM1	15	30.7	38.67	0.143
AGM2	7.5	56.6	54.18	0.303
AGMC*	7.5	78.9	63.21	0.239
HGM1	7.5	27.7	48.21	0.118
HGMC*	7.5	84.7	62.48	0.458

(AGM: AEE based composite guanidinium membrane; HGM: HMDA based composite membrane; C*: crosslinked samples) [49]

According to our previous studies [59, 60], fabrication of the composite membranes relies on surface tension to drag polymer solution into the pores and then impregnate the PTFE films. Hence, an appropriate viscosity is essential for successful membrane fabrication. AGMC (corresponding to **Figure 4-5d**) prepared from the crosslinked AEE based guanidinium polymer exhibited interesting outcomes. Compared to AGM2, it showed higher conductivity (78.9 mS cm^{-1}). The crosslinked HMDA based guanidinium membrane, HGMC (corresponding to **Figure 4-5c**), also showed a substantial increase in conductivity (84.7 mS cm^{-1}) compared to the noncrosslinked HGM1 (27.2 mS cm^{-1}). These are very impressive values considering that our crosslinked structures did not provide substantial

increase in charge concentration (see **Figure 3-1** for structures). Strictly speaking, the conductivity is not solely due from the OH^- ions as the membrane in hydroxide form may react with CO_2 in the air during the impedance experiment. Thus conductivity values recorded are likely to be a combined result from a mixture of alkaline anions (OH^- and either HCO_3^-/CO_3^{2-}).

Our initial attempt for using crosslinking was to reduce membrane swelling and provide mechanical integrity across the porous substrate. The surprisingly higher conductivity may result from more effective impregnation and retention of the polymer into the pores of the PTFE substrate. For example, it was estimated from the TGA curve (**Figure 4-7a**) that the amount of crosslinked polymer HGMC impregnated into the PTFE substrate was *ca.* 86.5wt% of the whole composite membrane. We propose that the crosslinking process aids the polymer impregnation due to the following three reasons: 1) Crosslinking agent affects the viscosity of the polymer solution to be deposited and helps by better wetting of the PTFE substrate; 2) Crosslinking helps in anchoring the polymer with guanidinium moieties to the pores of the PTFE film; 3) Crosslinking also prevents loss of polymers during the process of alkalization and repeated washing after that.

Hence it is believed that the higher ionic conductivity of the crosslinked membranes is mainly due to optimum impregnation of the polymers to the PTFE substrate. This is more prominent for the HMDA based membranes. For example, the HGMC has the highest IEC value which supports our argument. Its water uptake

value is also high even though it was crosslinked, implying a higher content of polymer was incorporated. During the synthesis, the HMDA based polymer was found to easily wet the PTFE substrate and therefore yield better impregnation. The AGMC seems to follow the same trend particularly in ionic conductivity and water uptake although the effect is less pronounced. Figure 5-4 further illustrates these observations.

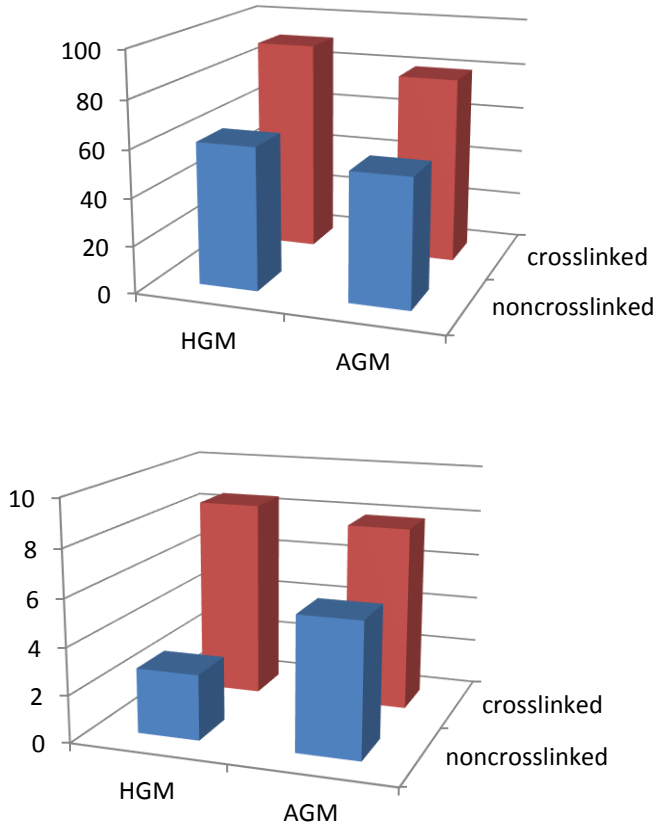

Figure 5-4: (top) Water uptake (%) and (bottom) Conductivity (S m^{-1}) for various crosslinked and noncrosslinked membranes

It should be noted, however, that the IEC values are generally lower when compared to those found in literature because of the presence of the PTFE substrate. However, IEC was not a decisive factor in membrane conductivity since Nafion has a low IEC (0.91 mmol g^{-1} [80]) but a good conductivity at 20 ^{o}C (100 mS cm^{-1}) [74]. Membrane conductivity is also highly dependent on the basicity of ion exchange groups. Strong basic groups lead to an augmentation of both the number of dissociated hydroxides and water uptake, thus facilitating ion conductivity under otherwise similar conditions. The strong basicity offered by the guanidinium groups in our membranes serves the same purpose.

5.3.2 Anionic Conductivies & Water Uptake of Hybrid Blend Membranes

Ionic conductivity of the blend membranes was measured using a four-probe AC method. In **Figure 5-5a,** amongst the three blend membranes, Gu-Chi2.2 with the greatest proportion of guanidinium ion exchange group shows the highest conductivity at 21 mS cm^{-1}, followed by Gu-Chi5.6 at 15 mS cm^{-1}. The lipophilic Gu(L)-Chi2.5 expectantly yields only 12 mS cm^{-1} because of the presence of both the stearate group and chitosan. The values, albeit a little low, are reasonable considering the lower guanidinium content by virtue of the other blend components, but also because of the slower migration rate of OH^- ions (generally taken as nearly half of H^+ ion migration rates [81, 82]). In fact the conductivity value for the commercial Tokuyama A201 was the lowest at 11 mS cm^{-1}. The reason for these consistently low values may be related to the process of CO_2 quickly equilibrating

with the AEMs, which could be critically dependent on atmospheric CO_2 concentration and temperature [69, 70]. To verify this we also tested a previously fabricated [83] Guanidinium-PTFE composite membrane (Gu-PTFE) and the conductivity value proved to be at least 30% lower than the last reported results. Thus strictly speaking, conductivity values recorded herein are likely to be affected by the presence of carbonate (either HCO_3^-/CO_3^{2-}) anions. Despite the 30% drop, the conductivity of the Gu-PTFE is understandably the highest since it primarily includes the guanidinium-based polymer impregnated over a highly porous PTFE substrate (porosity value > 85%) and is devoid of any other blending additions. However, apart from taking repeated readings for a sense of reproducibility, care was taken to use the same handling conditions for the 4-probe conductivity measurements in order to make a fair comparison.

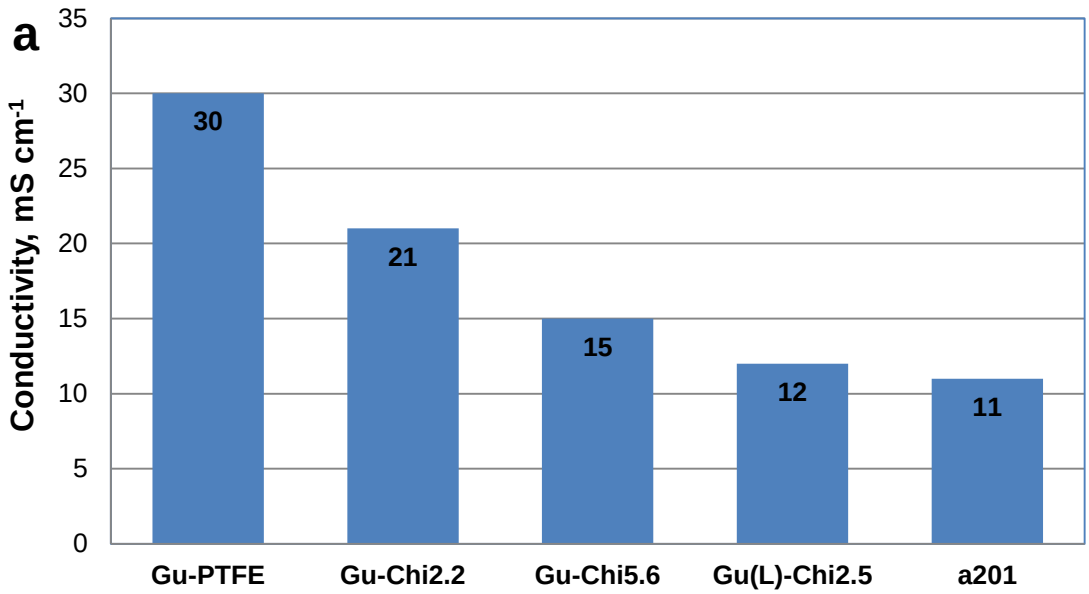

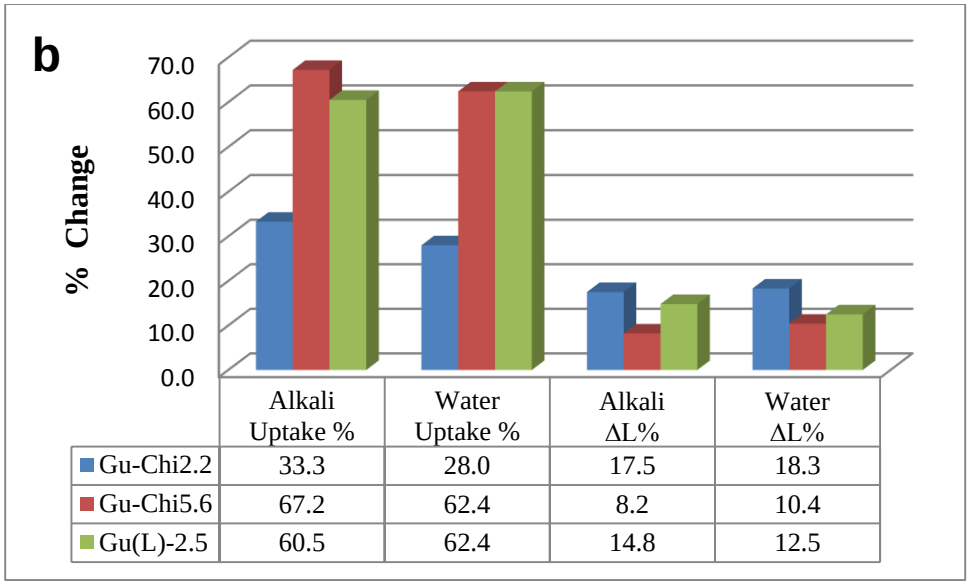

	Alkali Uptake %	Water Uptake %	Alkali ΔL%	Water ΔL%
Gu-Chi2.2	33.3	28.0	17.5	18.3
Gu-Chi5.6	67.2	62.4	8.2	10.4
Gu(L)-2.5	60.5	62.4	14.8	12.5

Figure 5-5: a) Conductivity and b) water/alkali uptake and swelling results of different blend membranes [84]

Higher water uptake is known to facilitate hydroxide transport [85] by generating solvated ionic species and broadening associated ion transfer channels, thereby facilitating their migration. However, in these blend membranes along with the guanidinium ion exchange group, the chitosan and sodium stearate components are also thought to participate in absorbing water. This was seen as soon as they're added to aqueous solutions. They form a thick suspension and slightly swell up in solution while they were vigorously mechanically stirred for a few hours. Hence, it is found in **Figure 5-5b** that Gu-Chi5.6 and Gu(L)-Chi2.5 show higher alkali and water uptake values without appreciable rise in their anionic conductivities. Gu-Chi2.2 on the other hand shows lesser, yet still significant, water and alkali uptake (approx. 30%), and has the highest anionic conductivity amongst the blend membranes. Due to the different polymer structures and chemistry, the blend elements would exhibit different degrees of swelling while larger amounts of the main ion exchange groups are known for contributing to the most significant swelling in membranes [34]. This explains the case for Gu-Chi2.2 which has the largest proportion of guanidinium and thus the highest conductivity (21 mS cm^{-1} in **Figure 5-5a**), but also suffers from the greatest swelling (around 18% elongation in **Figure 5-5b**) among the three blend membranes.

To understand the observed combined membrane properties, the supramolecular interactions of the functional groups used in this study and the hydroxide conduction mechanism are illustrated in **Figure 5-6**. Hydroxide

conduction is postulated to occur mainly through the Grotthuss mechanism by the formation and cleavage of the bonds as it diffuses through the hydrogen-bonded network of water molecules [86]. The hydroxyl groups on chitosan, especially the highly solvated guanidinium ion exchange groups, are believed to lead to a further increase in the formation and cleavage of bonds of the diffusing hyper-coordinating water molecule when it is in close proximity to these groups due to their strong electronegativity. In the same way, surface site hopping of hydroxyl anions facilitated by the hydration shell around the guanidinium groups in the membrane is also shown by the purple arrows. These claims are supported by the fact that more chitosan component (**Figure 5-5b**) leads to increased water/alkali uptake and a reasonable anionic conductivity (**Figure 5-5a**) despite diluting the main guaindinium ion exchange groups. Lastly, chitosan is capable of making not only intramolecular hydrogen bonds with itself but also intermolecular bonds with the guanidinium-based polymer chains (shown in **Figure 5-6**), thus providing invaluable integrity to the blend membranes demonstrated by the tensile testing results in the previous section. These strong intermolecular bonds are also important to reduce dissolution and swelling of membrane materials while a fuel cell is in operation as proven by the membrane swelling data in **Figure 5-5b**.

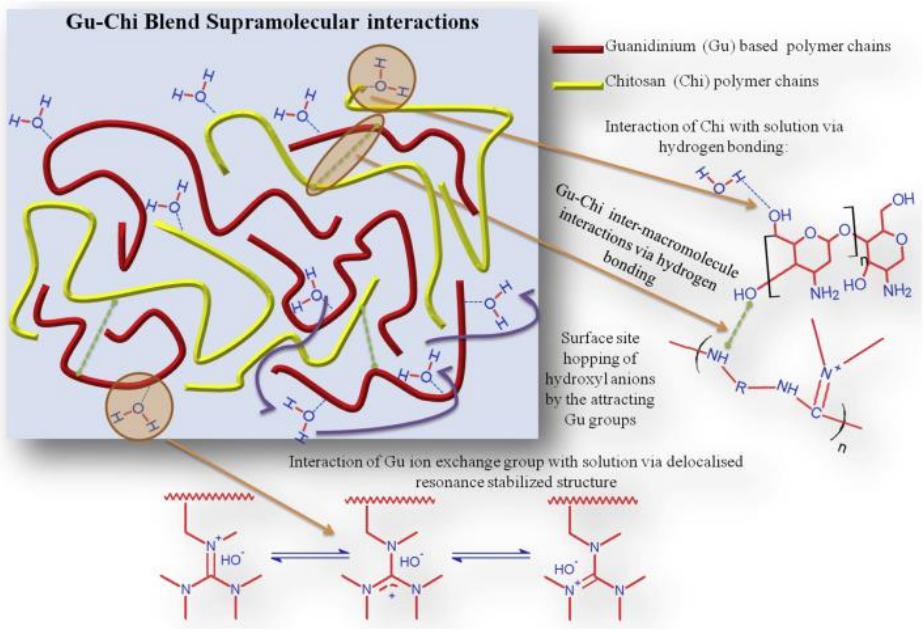

Figure 5-6: Guanidinium-Chitosan Blend interactions and intermolecular forces

5.3.3 Study of Membrane Permeability

Further studies were conducted to understand the methanol permeability through the membranes and the mass loss of methanol (for duration of around 48 h) was used to estimate the amount of methanol permeated through various membranes. **Figure 5-7a & b** compare the permeability of different membranes at 22 ^{o}C and 55 ^{o}C, respectively. Two commercial samples, namely Nafion 117 and the Tokuyama A201, were used as references for comparison and to validate the experimental results. The Guanidinium-PTFE (Gu-PTFE) membrane was again used for comparison of permeability. Indeed, the highest permeability was demonstrated by the two commercial references (Nafion N117 at room temperature

and Tokuyama A201 at 55ºC). This just reiterates the problem of fuel crossover using Nafion for direct methanol fuel cells, despite their high proton conductivity. Another reason for using Nafion was to check experimental values with Zhou et al. [75] who used a Nafion reference in their report as well. The permeability value of the Nafion sample is in good agreement with the reported values [75], and its temperature dependence is less abrupt than the blend membranes. Nevertheless, the permeability values of the blend membranes fabricated in this work are approximately an order lower than those of Nafion. For instance all the fabricated membranes, both composite and blended, allowed lesser moles of methanol through them thereby exhibiting lower methanol permeability. This difference is made further obvious at 55 ºC in **Figure 5-7b** where all the permeability values are understandably augmented because of the higher temperature. For the blends, the presence of the two components of chitosan and guandinium groups, yielding a possible domain structure illustrated in the SEM images (**Figure 4-9**), leads to sharper increase in permeability with a rise in temperature compared to Nafion. Each constituent depending on their nature would respond differently upon being exposed to heat leading to a less tight structure. However, their permeability values are still better than both Nafion and the composite membrane suggesting the polymer blend membranes are more homogenous than the Gu-PTFE composite membrane even at higher temperatures. Another observation was the slight reduction in methanol permeability from Gu-Chi2.2 to Gu-Chi5.6 at both the 22 ºC

and 55 ^{o}C ranges. It seems increasing the blend portion of the higher molecular weight and stronger chitosan additive would slowly lead to a more homogenous blend. This can be inferred by looking at domain size reduction for Gu-Chi5.6 in the SEM microstructures (**Figure 4-9**). On the other hand, the lipophilic membrane, Gu(L)-Chi2.5, shows the smallest permeability values at both 22 ^{o}C and 55 ^{o}C. Also, activated Gu-Chi5.6 (hydroxide form) was also tested and showed a similar permeability especially at 22 ^{o}C (but slightly increases at 55 ^{o}C) to the non-activated counterpart, demonstrating that the activation process is not too detrimental to membrane tightness.

The selectivity factor (ionic conductivity/methanol permeability) is an important parameter often used to evaluate the potential of ion exchange membranes for application in direct methanol fuel cells [75, 87]. The relative selectivity, a ratio of each membrane's selectivity factor to that of Nafion N117, is plotted in **Figure 5-8** together with that of Nafion membrane. All the blend Gu-Chi membranes and the composite Gu-PTFE membrane show higher selectivity than Nafion and Tokuyama A201, except for Gu-Chi2.2 which is also comparable to A201. The composite Gu-PTFE membrane shows the best selectivity by virtue of the dominant effect of its much higher ionic conductivity. Even for the blended membranes fabricated in this study, the results imply that their lower methanol permeability, not only would potentially solve one of the underlying problems associated with direct methanol fuel cells, but would also compensate their lower

anionic conductivities. Among the blends, Gu(L)-Chi2.5 turns out to have the best selectivity due to its very low methanol permeability. The reason is addition of the long alkyl chains of the stearate group to the base polymer. This provides integrity and homogeneity to the matrix and is corroborated by the higher strength in **Figure 4-10** and lower permeability in **Figure 5-7**. These results are further supported by the strengthened matrix in **Figure 4-9c,** which was punctuated by spherically uniform dispersed chitosan rich phase possessing excellent intrinsic film forming properties leading to a very leak-proof Gu(L)-Chi2.5 membrane.

A comparative analysis of **Figures 4-10**, **5-5**, and **5-7, 5-8** suggests that the blend membranes, Gu-Chi2.2 and Gu-Chi5.6, display a desirable combination of mechanical and electrochemical properties; therefore, further fuel cell test was conducted using these two membranes. On the other hand, in Gu(L)-Chi2.5 though the stearate group helps increase the molecular weight of the prepolymer giving a slightly more homogenous blend demonstrated by lesser surface defects on the microstructure (**Figure 4-9c)**; however, the membrane is more rigid (**Figure 4-10**), which may lead to brittleness. In addition, according to **Figure 5-5,** the Gu(L)-Chi2.5 sample shows the lowest conductivity among all the blend membranes. Its conductivity value is only about 50% of that of the Gu-Chi2.2 even if they have similar weight fractions of chitosan. Hence, no further fuel cell test was performed on this membrane.

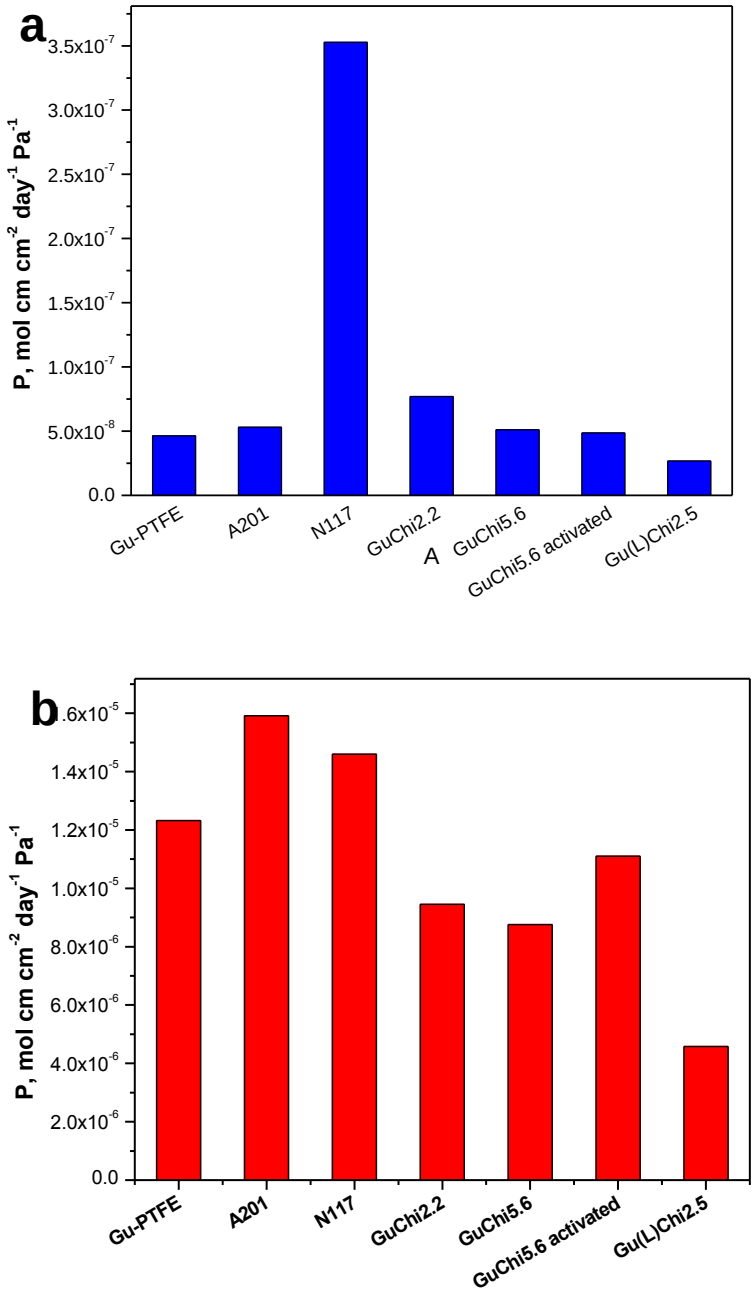

Figure 5-7: Permeability of methanol in different membranes at a) 22 ^{o}C and b) 55 ^{o}C [84]

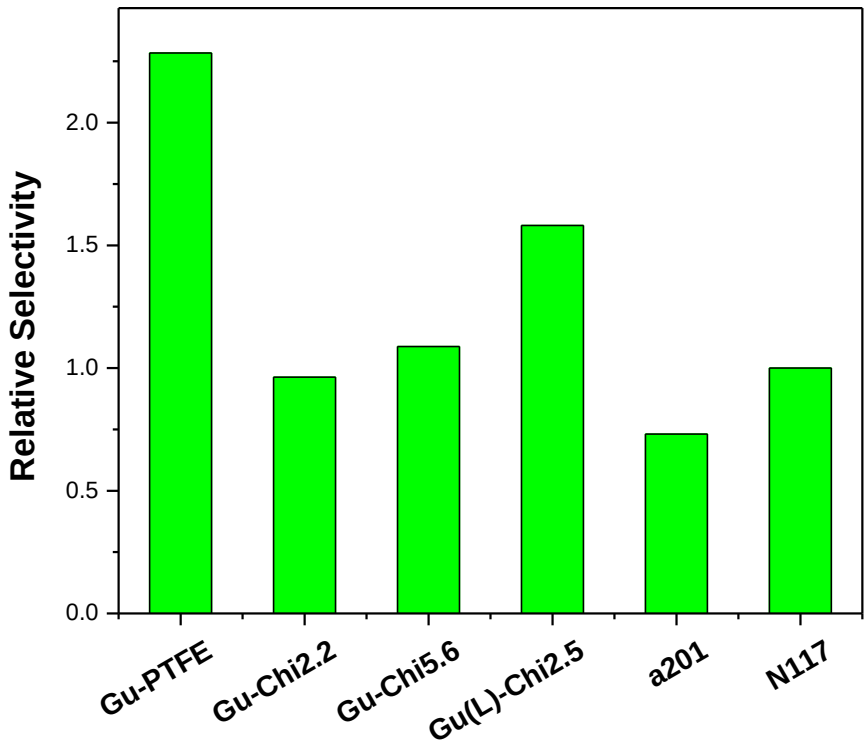

Figure 5-8: Relative Selectivity factor of different membranes at room temperature (*relative to Nafion N117) [84]

5.4 MEA Fabrication

The ionomer solution (5 wt%) was prepared by dissolving our own formulated prepolymer synthesized in Section 2.1 in a mixed solvents of ethanol and DI water. Catalyst inks were prepared by mixing TKK Pt/C catalyst (46.7% Pt) with the ionomer solution in a mass ratio of 3 (Pt):100 (polymer). Subsequently, the Pt/C-ionomer slurry was sprayed onto a Toray 090 carbon paper to achieve a Pt loading of 1 mg cm^{-2}. The solvent was allowed to evaporate and the electrodes were placed in an oven at 80 ◦C for 1 h. After washing with DI water, the ionomer in the electrodes were converted to OH^- form by immersing in 1 M KOH (aq) for 48 h. The prepared electrodes (active area = 1 x 1 cm^2) together with a membrane were sandwiched between two gaskets (thickness = 0.15 mm) and assembled into a graphite fuel cell fixture with parallel flow fields.

A Lab Alliance pulse-free pump was used to supply the fuel cell with 3M methanol together with 1M KOH at 1 mL min^{-1} into the anode and oxygen as an oxidant into the cathode. The produced current was monitored using a Princeton Applied Research PARSTAT 2273 potentiostat. All the fuel cells were conducted at room temperature.

5.5 Methanol Fuel Cell Study

The schematic for the DMAFC operation is illustrated in **Figure 5-9** and the results for evaluating different membranes are shown in **Figure 5-10**. Methanol at the anode releases six protons along with six electrons and CO_2. The released electrons pass through an external circuit to reach the cathode. Simultaneously, the OH^- diffuses through the membrane to the cathode to react with oxygen and the returning electron. At the cathode, CO_2 and water are the products.

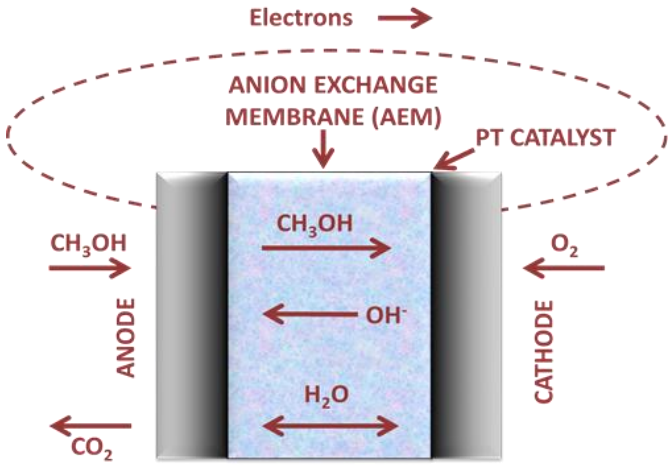

Figure 5-9: Schematic of direct methanol fuel cell

Table 5-2 shows that the incorporation of lesser amounts of chitosan yields better open circuit voltage (OCV) for the fuel cell. This is understandable since it implies a higher proportion of the active guanidinium ion exchange group. Similarly incorporation of the sodium stearate group to the structure produces the same effect. GuChi2.2 produced the highest OCV (0.69V), even much higher than

the commercial A201 (0.47V). Selected polarization curves are plotted in **Figure 5-10a** to further highlight this illustrate this point.

Table 5-2: Fuel cell OCV changes with different compositions

Sample	OCV (V)
A201 (commercial)	0.47
Gu-PTFE Composite	0.57
Gu-Chi2.2	0.69
Gu-Chi2.5	0.49
Gu-Chi5.6	0.37
Gu(L)-Chi5.6	0.41

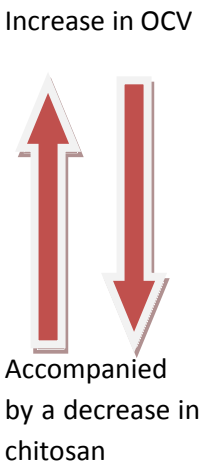

Figure 5-10a shows that the blend membranes with less chitosan yield better fuel cell performance and higher open circuit voltage (OCV). This is understandable since it implies a higher proportion of the active guanidinium ion exchange group. GuChi2.2 produced the highest OCV (0.69V), even much higher than the commercial A201 (0.47V). Hence, both the Gu-Chi membranes fabricated from Scheme 1 show good performance compared to Tokuyama A201. The OCV is highlighted here as it is directly affected by the quality of the membrane and extent of fuel crossover etc. Besides, the power density of the GuChi2.2 membrane is about 1.6 times higher than those of the other two membranes as shown in **Figure**

5-10b. It is admitted that the fuel cell performance is fairly low since no optimization has been conducted on the triple phase boundary of catalyst layers, MEAs, cell hardware, and even the operation conditions (i.e., methanol concentration, fuel and oxygen flow rate, temperature etc.). Besides, pure Pt catalysts, instead of Pt alloys, were employed in the anode for methanol oxidation, which could cause additional overpotential. The exact dominating factor that contributes to the observed fuel cell performance in **Figure 5-10** may be beyond the scope of this study; however, relatively to the Tokuyama A201, the synthesized guanidinium based AEMs show a better combination of low fuel crossover, ionic conductivity, and mechanical strength, therefore appearing as a good alternative to current commercial membranes.

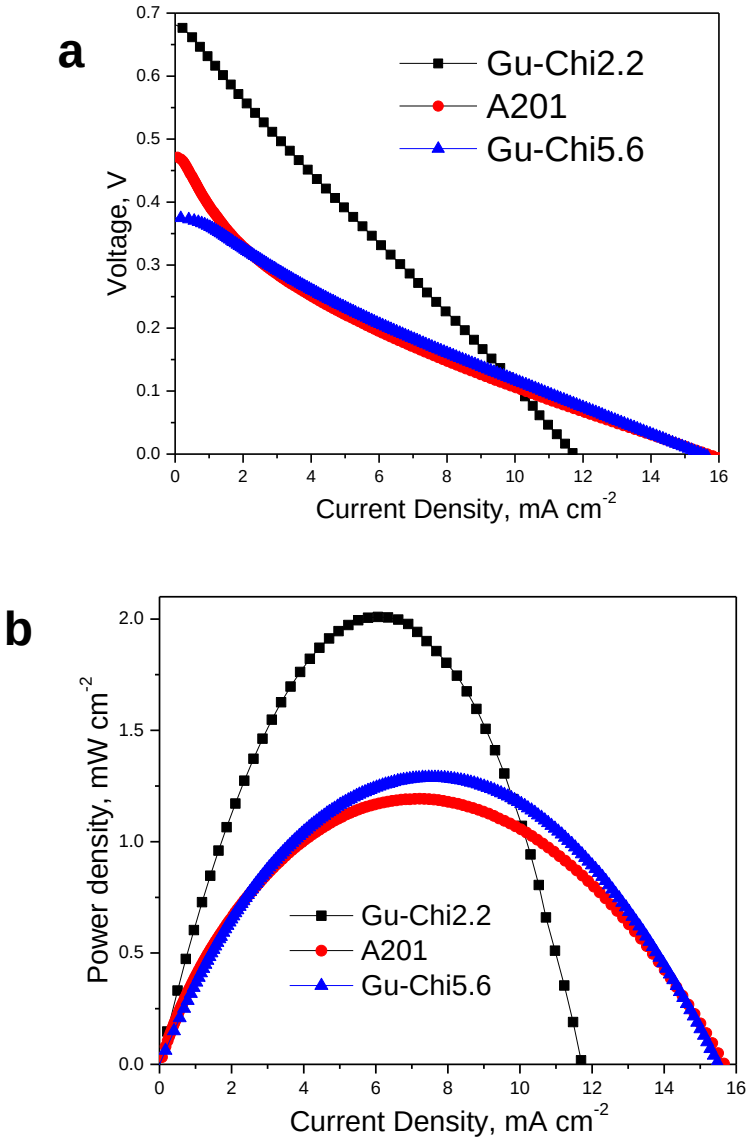

Figure 5-10: Cell Polarization & OCV changes with chitosan content ii) Power Density curves comparing fuel cell performance of different blended AEMs with commercial A201 membrane. The thickness of Gu-Chi2.2 and Gu-Chi5.6 are 55 and 75 μm, respectively [84]

We envision more enhancements in performance by quaternizing the chitosan in the membranes [88] thereby augmenting the already high hydroxide conductivity provided by the guanidinium anion exchangers. The process would involve crosslinking which would also boost the mechanical properties of the membranes and reduce the membrane swelling/dissolution. In addition, the mechanism of hydroxide transport is still not that well understood for AEMs in general and for guanidinium in particular. Further investigation is already under way to assess the long term stability and work is near completion to probe the micro and nanoscale phase changes with guanidinium acting as an anion exchanger.

5.6 Conclusion

All the guanidinium based membranes show high anionic conductivity due to the strong basic nature and resonance structure of guanidinium group. The composite membranes especially showed the highest anionic conductivity values. It shows that the guanidinium prepolymer forms a well-connected network through the cross-section of the porous PTFE substrate. The high water uptake values also facilitates hydroxide conduction aided by the crosslinking effect. The crosslinked samples in particular exhibit ionic conductivities (78.9 -84.7 mS cm^{-1}) comparable to Nafion at room temperature. In addition, the composite membranes do not suffer

from any rule of mixtures as the guanidinium polymer is not mixed with another polymer as in the case of the hybrid blended membranes.

However, due to the difficulty of fabricating composite membranes of larger sizes because of the extremely hydrophobic nature of PTFE, Guanidinium-Chitosan blend AEMs are also tested. They reveal decent performance demonstrated by their use in DMAFCs. They prove to be a promising alternative to the existing commercial membranes because of their ease of fabrication and versatility. In these membranes, chitosan has excellent film forming properties and can provide the much needed reinforcement to the blend membranes while the guanidinium groups act as the ion exchange group. Furthermore, modifying the membranes with the stearate groups could lead to better integrity and lower fuel crossover. Hence, the performance of all the fabricated membranes was found to be comparable to the commercial Tokoyama A201 membrane, with the GuChi2.2 actually better in the DMAFC. This is promising because our preliminary work [83] on their chemical stability has shown that the guanidinium group used in the backbone of the polymer structure significantly enhances the membrane stability against chemical attack of hydroxyl groups. Therefore, the developed membranes pose great promise for DMAFC applications.

Chapter 6

Micro/Nano Phase Analysis of Guanidinium based AEMs

6.1 Introduction

The role of an AEM is to conduct hydroxyl ions from the cathode to the anode where reduction and oxidation of O_2 and methanol occur. This transport of hydroxyl ions has to be at very high rates and should also be highly selective. If this is not the case, then the corresponding fuel cell will not exhibit performance of any practical significance. As it is, the conduction of large bulky anion is slower than those of hydronium ions in PEMs. Hence, there is an urgent need to understand the mechanism of hydroxide transport through AEMs in order to tune their respective hydroxide conductivities accordingly. This chapter proposes to probe the membranes on the micro and nano levels using Raman spectroscopy and AFM techniques to see if there is any preexisting or in-situ phase network to facilitate such hydroxide transport for fuel cell applications.

Since the development and commercialization of AEMs especially for high end applications such as fuel cells are relatively new, there are only a few studies on this subject. Hence with the limited number of analytic or numeric models currently in literature, debates concerning the exact mechanism for hydroxide transport are at large. Most of our understanding comes from analogies with proton exchange membranes.

Thus it is imperative to first have a look at the wealth of literature surrounding PEMs. The debate with respect to PEM, centers on the description of the mechanism of the transport processes for the hydrogen proton (H^+), typically in the form of hydronium (H_3O^+), in the membranes. The main discussed H^+ transport mechanisms can be lumped into a combination of Grotthuss mechanism, surface site hopping along sulfonic acid side chains, diffusion, migration, and convective processes [89-94]. These processed have been explained and replicated using techniques such as detailed statistical mechanics, lumped physics and ab initio molecular dynamics (AIMD) models [89-94]. Arguments about their relative contributions continue but during the last decade this much has been confirmed using a variety of experimental techniques that the H^+ transport coefficient (proton conductivity) depends strongly on environmental factors such as temperature, pressure and relative humidity.

For this study, we opt to study the effect of relative humidity or alternatively hydration since it is thought to play a major role in both proton and hydroxide mechanisms discussed above. But we first want an understanding of the general preexisting phase structure of the guandinium based materials. Since, the polymer is not susceptible to any interpretable XRD results, Raman Mapping is used as an alternative. Additionally, we can ascertain the extent of blending for the hybrid blend membranes at the micron level. For the nanoscale, AFM is used to probe the

structure along with any effects from the degree of hydration. Finally a simulation is attempted to better understand the experimental findings.

6.2 Microstructure Raman Chemical Mapping

Raman spectrographs and mapping are conducted using a Thermo Scientific DXR Raman Spectroscope. Initially, the guanidinium prepolymer and chitosan starting material are examined to mark their main functional peaks. These are illustrated in **Figure 6-1**.

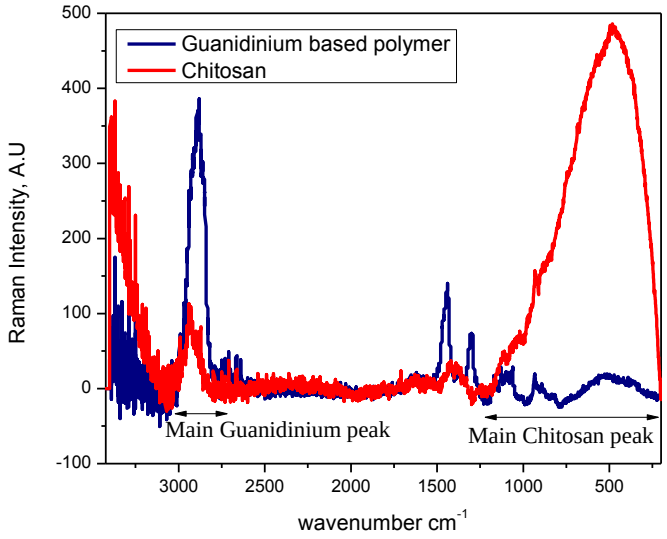

Figure 6-1: Raman Spectrographs of Guanidinium based polymer and chitosan starting materials

The maps are then correspondingly obtained by using a ratio of these peaks. Initially the blended polyelectrolyte is examined with a certain step size. The step size refers to the movement in distance (x.y) directions of the laser to reach its next scan location for collecting the spectra. When specifying the step size, it is important to keep the aperture in mind. It is a good idea to keep the step size equal to the aperture size (25 μm). In fact, it is also possible to 'over step' the map to obtain an even smoother profile. For the maps presented in this dissertation, each are obtained with a total of 20 spectra. That is, the sample is scanned 20 times, and each scan location is separated by the selected step size for that map. This complete movement for the 20 spectra separated by the step size gives the total map area. **Table 6-1** shows the general operating parameters of the Raman spectroscope and **Table 6-2** gives the individual conditions for each map, especially the relation of step size with total scan area.

Table 6-1: General operating parameters for the Raman Spectroscope

Exposure time:	2.00 sec
Number of exposures:	3
Laser:	780 nm
Laser power level:	50.0 mW
Grating:	400 lines/mm
Spectrograph aperture:	25 µm slit
Number of spectra for mapping:	20

Table 6-2: Conditions for Raman mapping

Figure #	Sample	Step Size (x.y)	Map size (x.y)
6-3a	Hybrid Blended Gu-Chi5.6	250x250 µm	1000x750 µm
6-3b		1250x125 µm	500x350 µm
6-3c		25x25 µm	100x70 µm
6-4	Guanidinium Prepolymer	25x25 µm	100x70 µm

After the complete 20 spectra are collected from the scan area, this whole area is then mapped with the **area ratio of Main Guanidinium peak/Main Chitosan peak** labelled in **Figure 6-1**. Hence, this gives a map corresponding to the ratio of these two peaks.

Thus, the maps are actually telling us how effective the homogeneity of the polymer blend in the membrane is. This effectiveness which is actually the value of the ratio pointed out in the preceding paragraph, is represented on the scale bar at the bottom of each **Figure 6-2 a-c**. The left box is a 2D map and this is reproduced on the right in 3D with the intensity of the ratio as the z-axis.

The results in **Figure 6-2** show that overall the blending is homogenous with regions of slight gradients marked in the map. This is reasonable as small differences of the peak area intensities are not only reflective of slight changes in blended composition on the microscopic scale but also indicative of experiment artifacts related to the sample surface flatness and fluorescence for example. In addition there are minor circular regions of higher percentage of guandinium main peak signal (violet) and also higher percentage of chitosan main peak signal (grey). These are attributed to the domain structures detected in the SEM images.

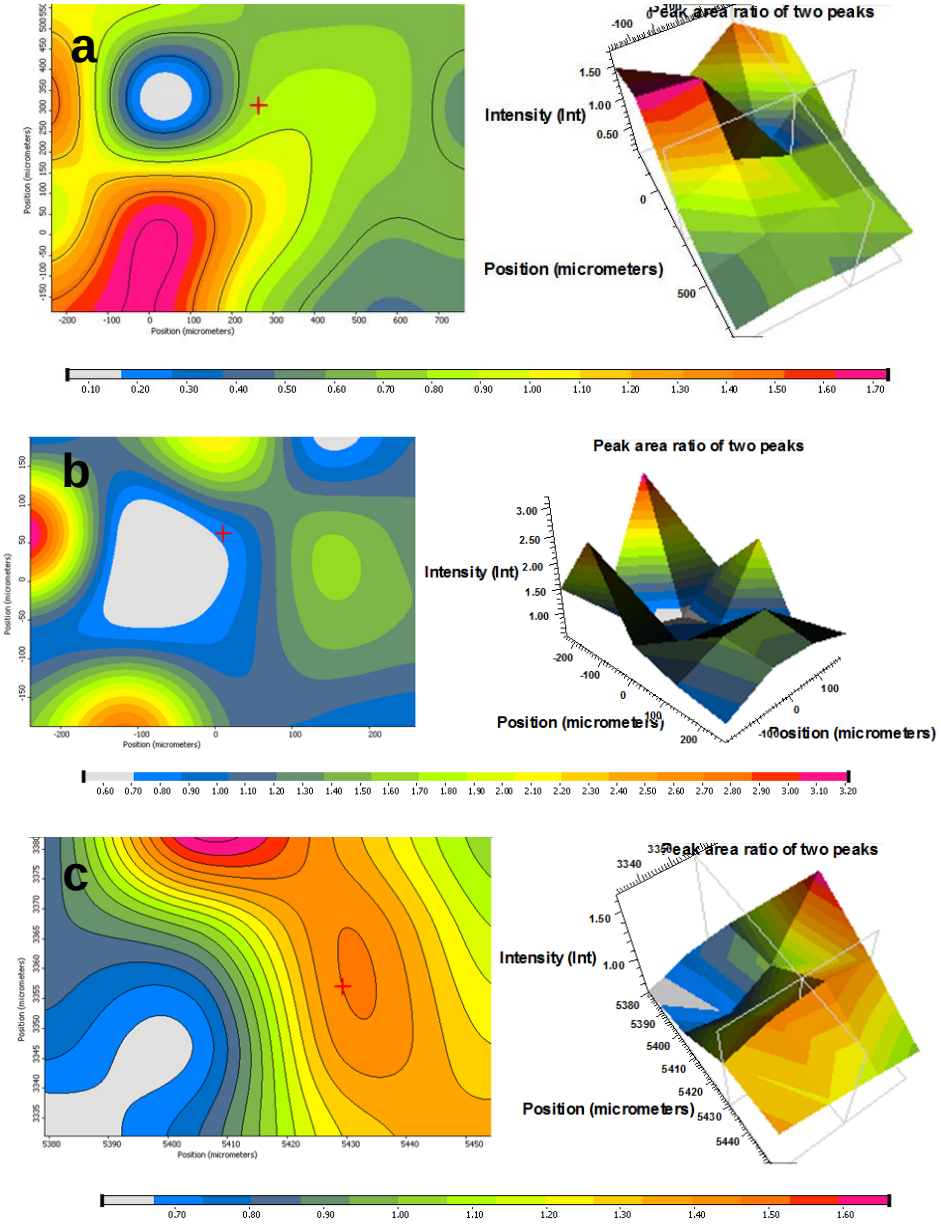

Figure 6-2: Raman Mapping of hybrid blend Gu-Chi5.6 membrane; a) step size = 250µm x250µm & scan area = 1000µmx750µm b) step size = 125 µmx125µm & scan size = 500 µm*375 µm c) step size = 25µm*25 µm and scan size = 100 µm *75 µm

As a reference the prepolymer is also mapped in similar fashion as the blended polymer above. If the same peak area ratio is taken we should end up with an almost homogenous map subject to experimental/sample artifacts. This is exactly what we have in **Figure 6-3**. The ring of colors is due to the sample unevenness near the edge.

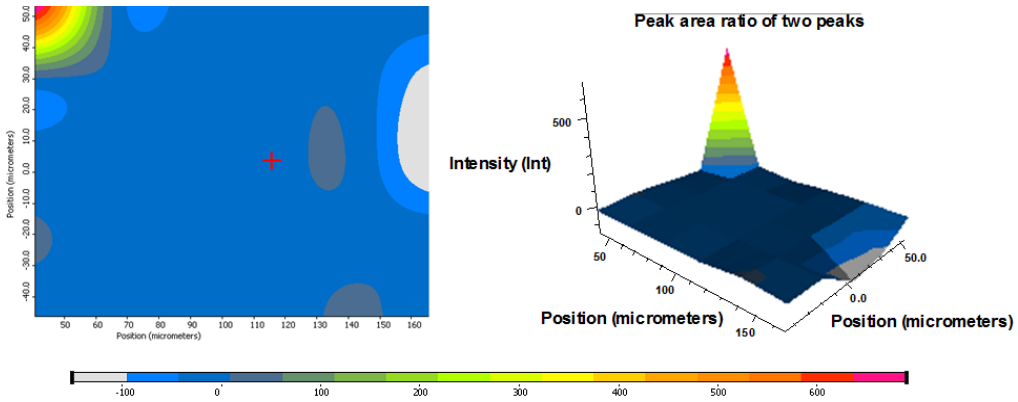

Figure 6-3: Raman mapping of guanidinium based prepolymer:

25µmx25µm and scan size = 100µmx75µm

6.3 Nanostructure AFM Study

AFM is a very useful tool which has been used to study PEM membranes [95-97] and their cluster-network or water channel model. In the latter, sulfonic acid functional group self-organize into arrays of hydrophilic water channels around the hydrophobic polymer backbone. The channels provide passage through which small ions can be easily transported while the polymer backbone provides mechanical integrity. To the best of our knowledge, we have not yet seen any

detailed AFM study of AEMs particularly in conditions similar to here where the membrane structure is probed with drastic changes in their hydration levels.

6.3.1 Experimental Setup

A Park XE 70 AFM was used in non-contact mode. Images were generated in topography, error signal, amplitude and phase mode.

Two set of samples were tested. One was a film from guanidinium based prepolymer and the other was the Guanidinium-Chitosan hybrid blend membrane (Gu-Chi2.2). The sample were fully hydrated under water and then extracted. Immediately afterwards their surface was quickly examined under the microscope. After taking out the samples and affixing them to the sample holder assembly and setting up the microscope approximately 15 minutes passed before the image was obtained. This represents the fully hydrated or wet condition, fresh out of water. The samples are then reexamined after a gap of 25 minutes putting the total time after extraction from water to 40 minutes. The images obtained at this stage represent the semi-hydrated condition. Finally the samples are dried over night at 50 ^{o}C and examined under the AFM to study their structure in the dry state.

6.3.2 Results & Discussion

The images for the guanidinium polymer are shown below in **Figure 6-4** and their 3D morphology are illustrated below them in **Figure 6-5**. The nanostructure for the wet sample is visibly inundated by long parallel channels. The 3D structure shows that these channels separated by height differences which pose

as their boundaries. We envision the ravines or glens separated and bordered by ridges as the channels responsible for anionic conduction. This hypothesis is not much different from the water channel model in PEMs. Indeed, this is supported by the image of the semi-hydrated membrane. After sometime (40 minutes), the number of these ravines decrease giving a reasonable explanation to the loss of conductivity with a drop in humidity in several studies. These results are not hence, just extendable to other guanidinium based material and AEMs but also to PEM (save for the difference in the nature of conducting ions being hydronium in that case).

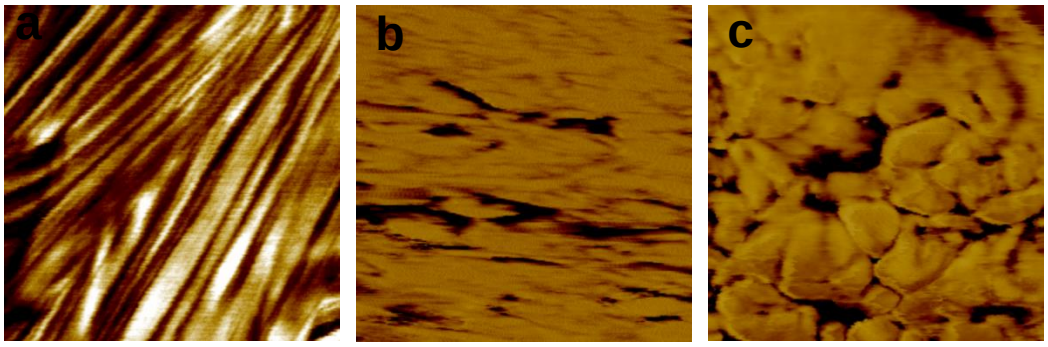

Figure 6-4: AFM images of Prepolymer; a) Wet; b) Semi Wet; c) Dry

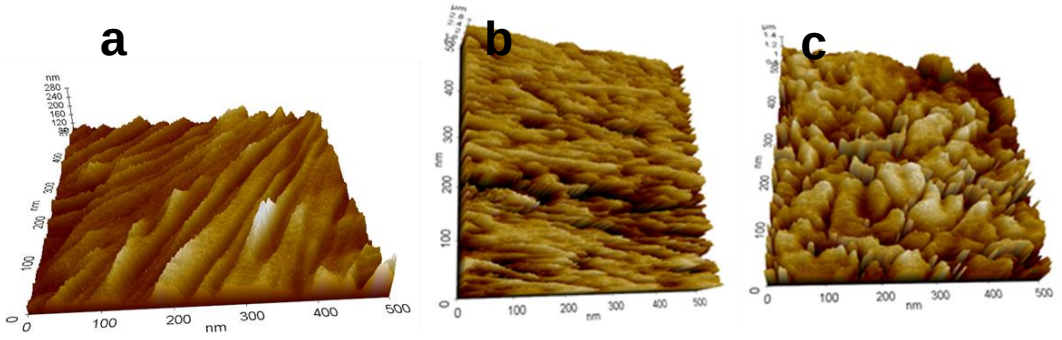

Figure 6-5: (3D view of) AFM images of Prepolymer; a) Wet; b) Semi Wet; c) Dry

Finally with the dry sample, it is noticed that the columnar patterns and ravines coalesce and disappear to give way to a more random equiaxed granular structure. Hence, the dry membrane displayed random structure; however, increasing membrane water uptake produced aligned channels, which are attributed to water-assisted π-stacking of the planar shaped guanidinium groups [98]. The diameters of the channels are ca. 27 – 30 nm and 15 – 23 nm, respectively, at water take of 50% and 25%. This face-to-face alignment of guanidinium plans offers facilitated charge transport as well as great stabilizing effects (as shown by the results in Chapter 5).

The repeatability of this change from highly orientated channels to random granular structure with loss of hydration is again demonstrated in **Figure 6-6** for the hybrid blended Gu-Chi2.2 membrane.

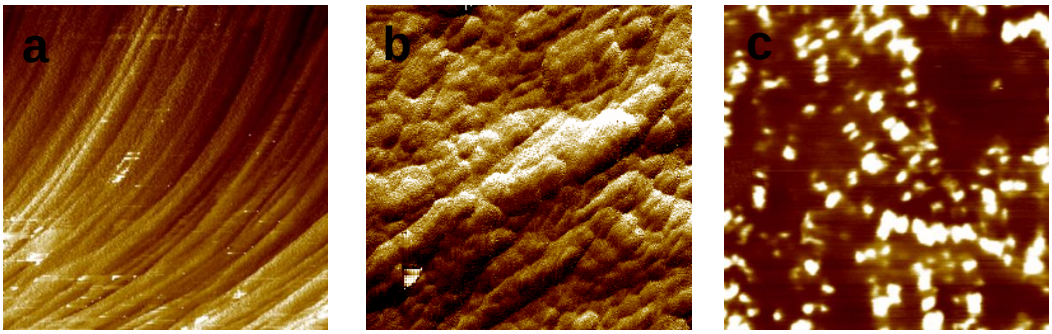

Figure 6-6: AFM images of hybrid Gu-Chi2.5 membrane; a) Wet; b) Semi Wet c) Dry

We go a step further and use the XEI software on the AFM to do a quantitative study of the conducting channels in the guandininum based polymer film. A 'Threshold grain detection algorithm' is used. In this method, a group of pixels surrounded by the other pixels are larger (or smaller) than the upper (or lower) Threshold values are recognized as grains. This is demonstrated for the wet sample in **Figure 6-7** and the grain information which in this case are the ravens of conducting channels is collected in **Table 6-3**. Similar analysis are carried out on the semi-hydrated and dry samples and data from these three is summarized in **Table 6-4**.

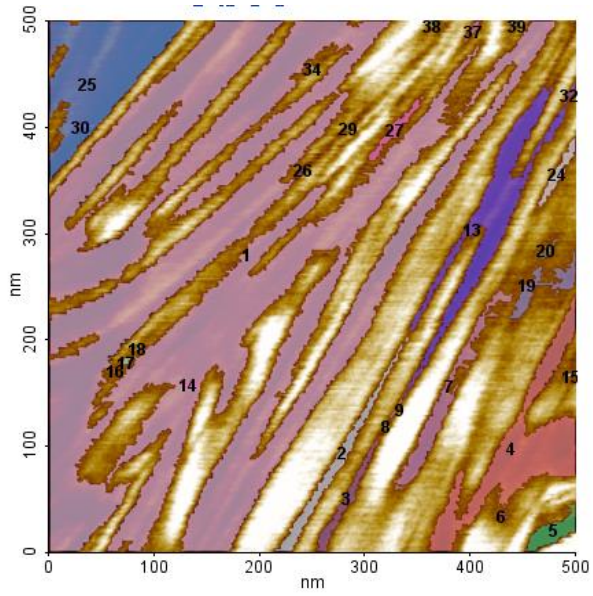

Figure 6-7: Threshold grain detection of wet prepolymer film

Table 6-3: Grain data of wet prepolymer film from threshold analysis

Grain	Area(µm²)	Vol(deg×m·m)	Length(nm)	Peri(µm)
Mean	4.301E-3	2.198E-13	94.160	0.599
Std.	1.62E-2	8.253E-13	145.850	1.881
1	8.76E-2	4.463E-12	690.672	10.201
2	1.961E-3	1.033E-13	237.881	0.598
3	9.651E-4	5.149E-14	119.923	0.329
4	7.755E-3	4.002E-13	276.683	1.108
5	8.926E-4	4.23E-14	64.925	0.181
6	6.104E-5	3.366E-15	13.672	0.040
7	2.499E-3	1.33E-13	215.385	0.703
8	3.433E-5	1.867E-15	8.286	0.022
9	6.104E-5	3.343E-15	21.126	0.043
13	6.752E-3	3.52E-13	324.254	1.456
14	3.052E-5	1.649E-15	21.573	0.039
15	2.289E-5	1.263E-15	8.735	0.017
16	2.67E-5	1.472E-15	8.735	0.026
17	4.959E-5	2.722E-15	11.049	0.032
18	2.289E-5	1.259E-15	8.286	0.021
19	1.141E-3	6.226E-14	88.388	0.383
20	1.945E-4	1.064E-14	29.813	0.100
24	5.684E-4	3.06E-14	75.138	0.194
25	8.717E-3	4.299E-13	196.811	0.707
26	7.629E-5	4.123E-15	21.126	0.050

6.4 Numerical Study of Transport Channels

6.4.1 Setup for Simulation

The guanidinium membrane structure is recreated and its conductivities are simulated using a numerical study. Here, in this chapter, we build on what is learnt from the previous two sections specifically from the AFM images. In short, a mesh is created with fixed number of seeds from which the anion conducting channels grow. These channels can grow randomly and end up representing the polymer film in its dry state (**Figure 6-4c**). Alternatively, the (orientation or preferred direction) of their growth can be controlled by a factor *N* which ranges from 0-100 to depict the semi wet and wet states of the polymer film (**Figure 6-4a&b**). At the same time, the total volume fraction (*Vc*) of these channels as a function of total mesh area can be varied too. In this way we can explore, structures similar and also intermediate to those summarized by the AFM analysis in Table:

Table 6-4: Summary of data from AFM grain analysis

Sample	% A of valleys	% V of valleys
Wet pristine Gu Polymer	67	62
Semi Wet pristine Gu Polymer	23	17
Dry pristine Gu Polymer	15	3

A commercial computational fluid dynamics (CFD) software was used to simulate the single particle phase transition for different particle size and morphology. The codes used in the CFD software to describe the equations and properties of the material are described in detail in Appendix A.

The simulation of electrochemical reaction based on a single-domain, control-volume approach was performed on the reconstructed 3D domain. Since the reconstructed membrane structures automatically tracks the interfaces between different phases; physical equations describing transport properties in different phases are easily implemented. Transport of hydroxyl is driven by gradient of ionic potential (ϕ) in the following equation:

$$\nabla \cdot \left(k \nabla \phi \right) = 0$$

k is the effective ionic conductivity which is dependent on the micro-morphology of the membrane structure. At the two boundaries perpendicular to the transport direction (i.e., the left and right boundaries), one layer of transport cells is added to the computational domain, for ease of implementation of the boundary conditions. Fixed overpotential values were applied as the boundary conditions.

6.4.2 Simulating Ionic Transport Channels

Figure 6-8 shows an example of the ionic flux which is used to simulate the polymer channel structures in **Figure 6-9**.

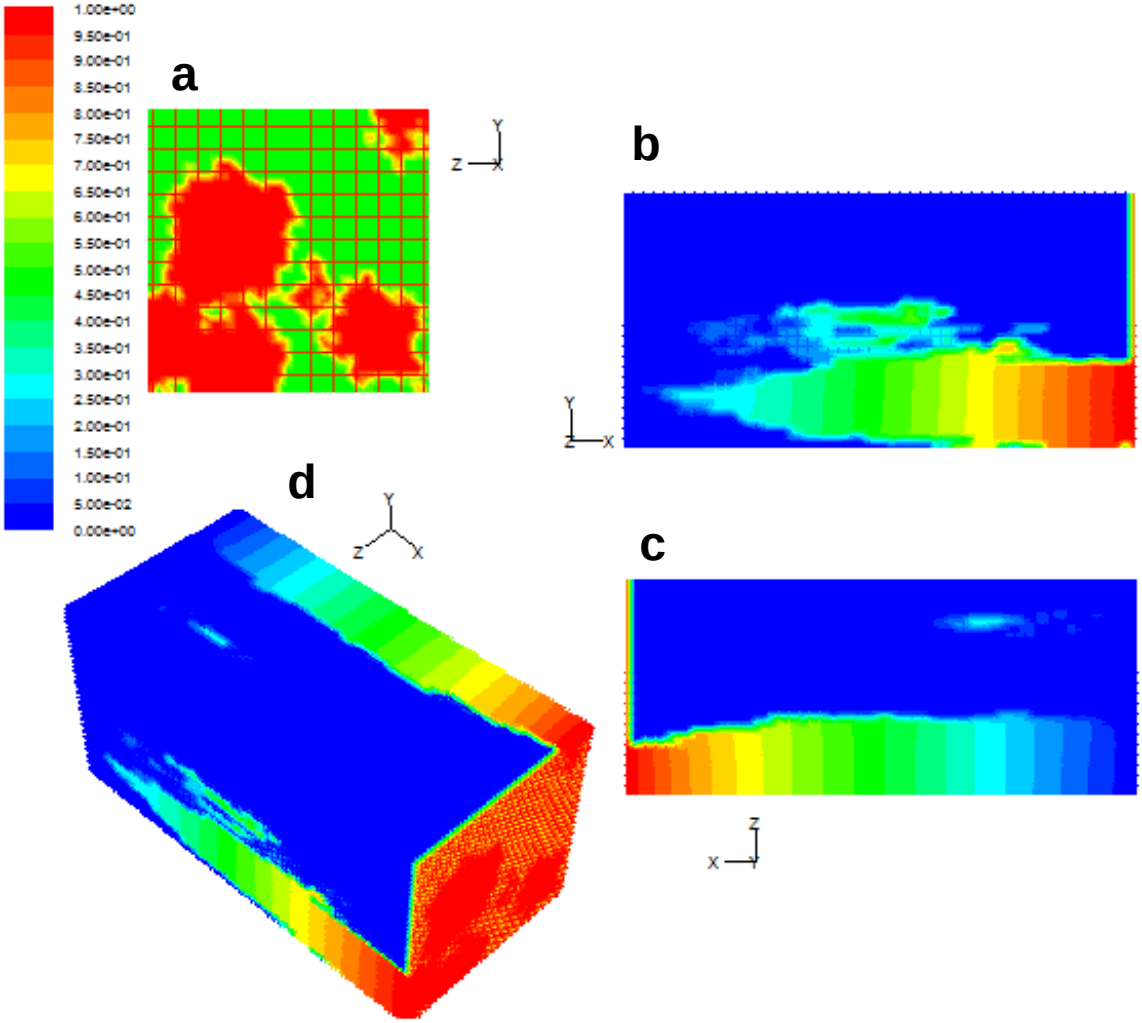

Figure 6-8: Ionic flux simulated for membrane with Vc= 61, N=90; View:

a) right side b) top c) front d) isometric

Only the three simulated structures which resemble the conditions of the AFM images in Figure are reproduced here in isometric view. The front, right and top views of each are included in appendix B for a closer examination. The structures use the same parameters of Vc as noted in Table for the actual guanidinium polymer film. The orientation bias N is chosen qualitatively by inferring the AFM images again; with N=90 corresponding to the well-defined channeled wet polymer structure, N=34 corresponding to the moderately orientated semi-wet structure and n=1 going to the random dry polymer structure. Indeed the simulated and actual polymer structures do resemble each other especially for the wet and semi wet conditions. For the dry conditions, it is difficult to simulate meaningful structures with Vc = 3 which is why Vc was taken as 20 but N was kept low alternatively.

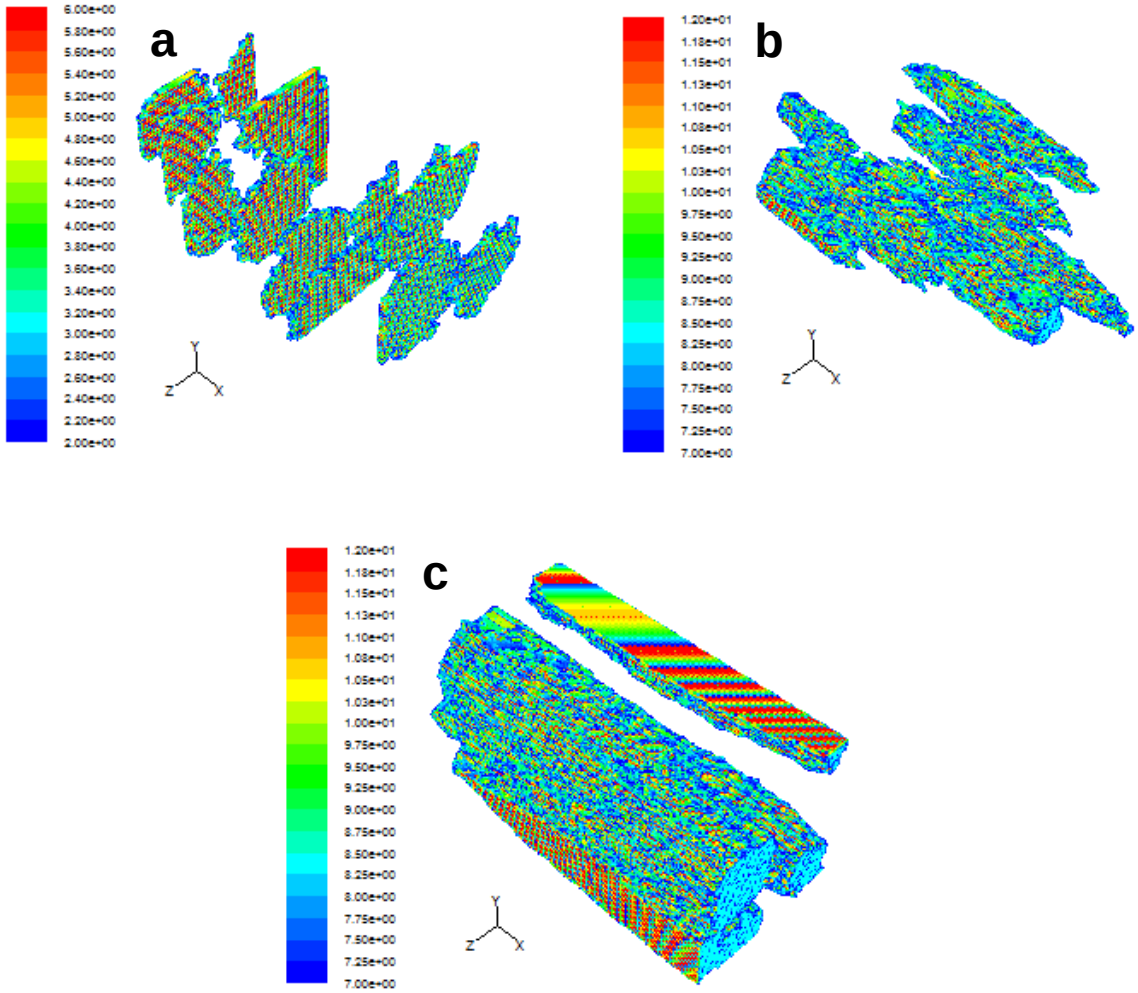

Figure 6-9: Isometric generated structures for membranes with a) $V_c = 20$; N=1; b) $V_c = 20$; N=34; $V_c = 61$; N=90

6.4.3 Simulated Ionic Conductivities

Using different combinations of N and Vc a number of structures (omitted here to avoid redundancy) were generated. These structures were used to calculate the ionic conductivity. Ionic conduction was obtained by simulating a potential

difference between the two ends of the mesh. Refer to appendix A for the exact code.

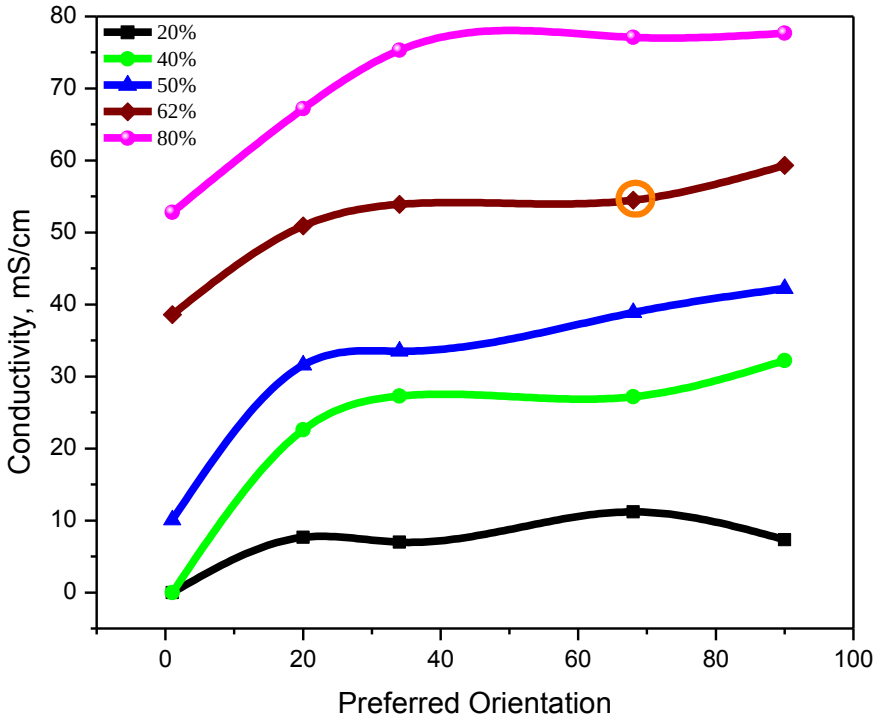

Figure 6-10: Ionic Conductivity vs N for different V_c

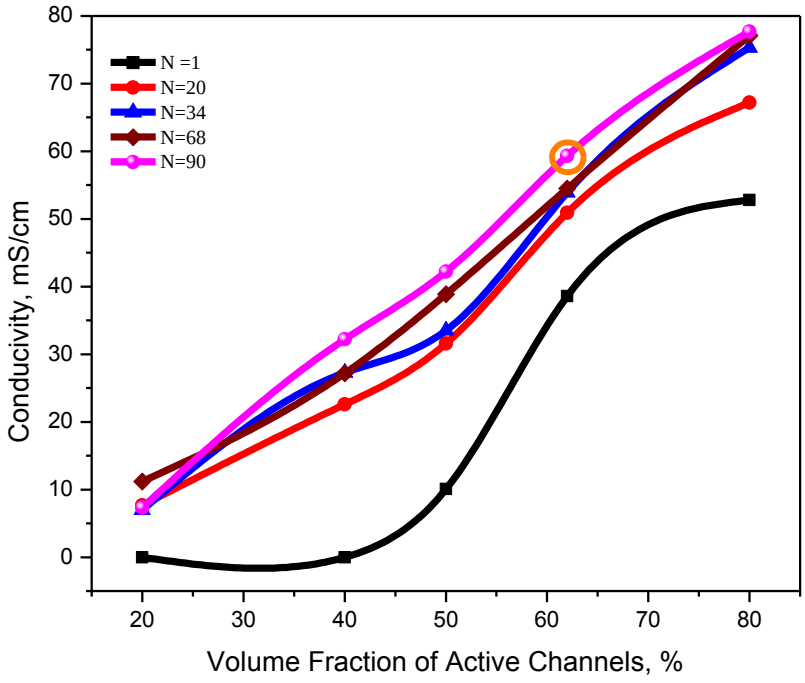

Figure 6-11: Ionic Conductivity vs V_c for different N

Figure 6-10 shows the increase in ionic conductivity with increased preferred orientation bias (i.e a tendency to form parallel channels) for fractions of active channel volume while **Figure 6-11** shows the increase in ionic conductivity with increase of total volume fraction of these channels and shows the important of highly orientated channels for achieving higher conductivities. The orange circle on both these with V_c = 61 & N=90 represent the data point for the wet state in **Figure 6-4c**. It shows a reasonable value of around 60 mS cm^{-1} for the anionic conductivity. This compares well with our previous published findings on the

composite membrane that shows conductivities ranging from 57-85 mS cm^{-1} and is the best estimate for the anionic conductivity of the base polymer. All in all, the results projected by the simulated conductivities corroborate the earlier hypothesis that the parallel ravines in the AFM structure are modes of hydroxide transport for this anion exchange membrane system.

6.5 Conclusion

The Raman mapping shows signs of phase segregation at the microscale for the Gu-Chi blend membrane. This is reasonable considering only physical mixing was used to blend two very different polymers. The AFM structure at the nanoscale shows an interesting ravine-ridged structure under high degrees of hydration. This micro and nanoscale picture is presented in the schematic below:

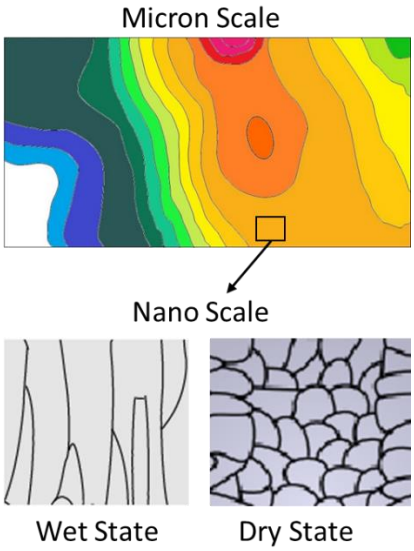

Figure 6-12: Schematic of micro and nanostructure of prepolymer film.

Figure 6-13 summarizes the findings for the nanoscale study of the channels and simulations. It is found that similar channels besides existing in PEMs also exist in some systems of nature. **Figure 6-13** relates the nanostructure of the membranes to the tree trunks. A (250nm x 250nm) AFM scan of the wet prepolymer film is overlapped with a microstructure of the sapwood section of a tree log or trunk and it almost perfectly matches. The analogy is clear: Sapwood is that outer section of the tree that is alive and transports the water and nutrients similar to the channels in our wet membrane which transport the ions for the fuel cell reaction to generate energy. Towards the inner side (heartwood) this transport quickly ceases and eventually the driest (pith) section of the trunk does not help any transport process but only provides the function of mechanical support. Similarly our 'dry' membranes also provide negligible anionic conduction through the EIS process.

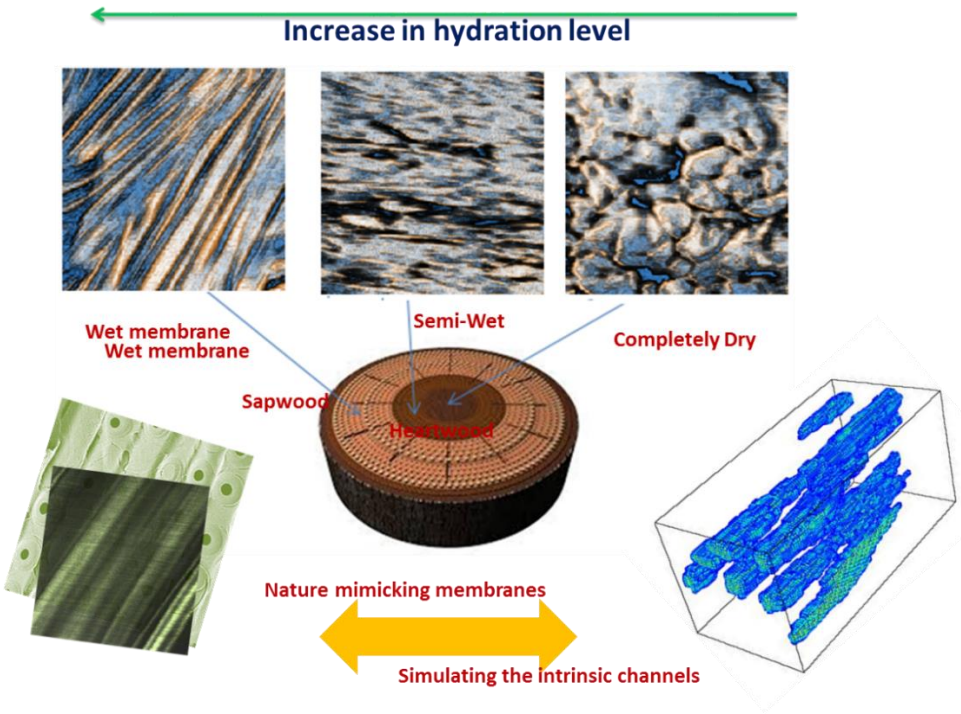

Figure 6-13: Summary of findings at the nanoscale for the guanidinium membrane

The simulated structures and reasonable conductivities thus obtained support the claim that these channels are crucial to hydroxide transport. It may be beneficial to discuss the guandinium functional group for a better understanding of how and why these channels form in the first place. Guanidinium is a planer ion [96] that is well known to form weak hydrogen bonds around its edge. However, it also known to form strongly-held hydrogen-bonded ion pairs to protein carboxylate groups. It also possesses a hydrophobic face and hence the orientation of the ion is important for its interaction with water and other species. It could be argued that it

is this preferred orientation that leads to the channel rearrangements seen in the simulations and AFM structures in wet conditions.

Chapter 7

Conclusion

One of the main motivations to develop fuel cells is that they offer the cleanest power generation possible. Besides other advantages such as quiet operation and efficient energy conversion for steady interrupted electrical supply they can also be used in hybrid configurations to provide varying power demands such as automotive applications. However, they have faced serious constraints in terms of cost and performance. This dissertation has attempted to by-pass these constraints by adopting and modifying the AFC fuel cells system known to possess the fastest kinetics under 200 °C.

In essence, the fuel cell system used here is called the Alkaline Anion Exchange Membrane Fuel Cell. This is able to use the fast kinetics of AFCs by virtue of their superior electro-kinetics. The guanidinium functional group plays a key role in the AEMs described in this dissertation. The prepolymer which forms the basis of the AEMs has the guanidinium group incorporated directly into its polymer backbone through a polycondensation reaction between a guanidine salt and two different diamines. This is to ensure maximum stability. Our hypothesis is confirmed when we compare it against a commercial Tokuyama A201 membrane which is based on the traditional quaternary ammonium group. Vibrational spectroscopy showed that under extreme conditions of 5 M KOH solution at 55°C

for 50 h. our synthesized material exhibited superior stability compared to the commercial quaternary ammonium A201. The reason is attributed to the remarkable charge delocalization (over one carbon and three nitrogen atoms) and disappearance of hydrogen attached to the three nitrogen atoms in the fully crosslinked polymers, which makes both Hoffman elimination or direct nucleophilic displacement reactions unlikely to occur during membrane degradation. This charge delocalization in the guanidinium hydroxides also provides a high degree of thermal and basic stability [35, 41]. Hence, the results demonstrate that the guanidinium group by virtue of its resonance stabilization of the π-system and its "Y-delocalization" result in stabilization comparable to cyclic aromatics such as benzene [67].

A series of two contrasting types of AEMs are fabricated from the guanidine based prepolymer after it is subject to minor post modification such as crosslinking or tethering a lipophilic element to its main chain for suitable physio-chemical and mechanical properties. In addition, to achieve these optimum properties along with the required electrochemical performance, the membranes are eventually fabricated using two different approaches.

The composite membrane is fabricated by incorporating guanidinium based polymer solution into a porous polytetrafluoroethylene (PTFE) film. Polymer crosslinking helps reinforce the mechanical strength of the membranes and interlock the guanidinium moieties to the porous PTFE. SEM, FTIR & Raman

convincingly show complete impregnation of the microporous pores of the PTFE substrate by the prepared polymer solution.

The hybrid blend membranes were obtained by blending the prepolymer with chitosan, another strengthening agent. Chitosan is chosen for not just its compatibility with the prepolymer but also its excellent film forming abilities. Hence, a polymer slurry which is obtained with the evaporation of most of the solvent is effectively deposited as film through the application of a doctor blade and subsequent heat treatment.

Whereas the composite membrane displayed an outstanding ionic conductivity 80 mS cm^{-1} (at 20°C in deionized water), the hybrid blend membranes exhibited relatively lower values due to the effect from the blend components. These values are slightly below those recorded for the PEM Nafion and are exceptional considering the difference in the relative transport coefficients of D_{H^+} (9.3 x 10^{-9} m^2/s) and D_{OH^-} (5.3 x 10^{-9} m^2/s) in liquid water at 25°C [96]. It should be noted, however, that the IEC values are generally lower when compared to those found in literature because of the presence of the PTFE substrate. However, IEC is not a decisive factor in membrane conductivity since Nafion has a low IEC (0.91 mmol g^{-1} [79]) but a good conductivity at 20 ^oC (100 mS cm^{-1}) [73]. Membrane conductivity is also highly dependent on the basicity of ion exchange groups. Strong basic groups lead to an augmentation of both the number of dissociated hydroxides and water uptake, thus facilitating ion conductivity under otherwise

similar conditions. The strong basicity offered by the guanidinium groups in our membranes serves the same purpose. Hence, even the drop of ionic conductivities for the blend membranes is not significant considering the amount and effect of the blend components.

However, the selectivity (ratio of ionic conductivity to methanol permeability) of the hybrid blend membranes is found to be superior even when compared to commercial membranes. Similarly, when used in a direct methanol alkaline fuel cells (DMAFCs) it fared even better than a commercial AEM reference reaching to an OCV of 0.69 V compared to the 0.47V of Tokuyama A201 at room temperature. Overall, the developed membranes demonstrate superior performance and therefore pose great promise for direct methanol anion exchange fuel cell (DMAFC) applications.

The blend membrane along with the base guanidinium prepolymer film was thus subject to a final micro and nanophase analysis to gauge a better understanding of the hydroxide conduction process which is not that well established in literature so far. Additionally Raman mapping was used to get an idea of the blend homogeneity as well. Together with AFM for nanoscale imaging we were able to get a better understanding of the structure of the membranes. Furthermore, the hydroxide transport process is highlighted when studied for effect of degree of hydration. It is postulated by studying AFM images that there is phase separation before under wet conditions leading to formation of thin ravines or hydroxide

conducting channels similar to those previously studied and modelled with PEM membranes. These channels are also studied for better understanding and backing with the help of a simulation. The mechanism hypothesized may be transferrable to other guanidinium based membranes and extendible to other types of AEMs as well.

7.1 Future Work

The concentration of this dissertation of aimed towards developing a series of high performance stable AEMs. This was adequately demonstrated in Chapters 3 to 6.However, despite various polymer strengthening methods used here, there is still room to improve the mechanical properties of the polymer and subsequent membranes made from them. It is recommended to test higher reinforcements (chitosan) proportions in blend the blend ratios and to perhaps use some stronger engineering polymers to strengthen the blend e.g. Polysulfones. However, these strong high molecular weight polymers are usually soluble in only a very small range of solvents and their compatibility with the guanidine prepolymer must be assessed before they can be physically or chemically combined with it.

Also on the device development side, namely the direct alkaline methanol fuel cell could not be optimized as it requires a detail study on the membrane electrode assembly (MEA) which is beyond the scope of this dissertation. This

optimization itself would open several research avenues which should be investigated in the future. These are summarized below:

- Optimizing the Pt or Pt alloy catalyst. This includes making the catalyst slurry with appropriate guandinium based ionomer content to establish the best triple phase boundary during fuel cell operation. The deposition and heat treatment of this slurry over the electrodes must also be determined in the most repeatable manner.
- Along with optimization of the MEA, its incorporation and sealing within the fuel cell assembly should be done via hot pressing to enable long term operation.
- Once, the perfect fuel cell assembly is accomplished, the effect of operating variables such as catalyst loading, oxygen and methanol flow rates and temperature should be investigated
- The fuel cell test should be run for longer time periods to assess the stability in-situ stability of the membranes.
- Lastly, when adequate performance is obtained through Pt catalysts, the use of cheaper non-noble catalysts should be investigated which is one of the important implications of this work.

Appendix A

Code for Simulating Membrane Structure

```
#include "global_var.h"
# include "udf.h"
# include "id.h"
# include "mem.h"
# include "sg.h"
# include <stdio.h>
# include <stdlib.h>
# include <time.h>


#define n_seed 15 /* LiFePO4 seeds*/

#define a_length 10.0e-9  /* length of side in a unit cell 1*/

#define lx 100.0  /* mesh # along x direction */
#define ly 50.0  /* mesh # along y direction */
#define lz 50.0  /* mesh # along y direction */

#define par_diff 0.50e-7 /* assumed membrane conductivity */


#define wt_c 0.10  /* carbon weight percentage */
#define wt_active 0.80  /* active material weight percentage */
#define wt_binder 0.10  /* binder weight percentage */
#define porosity 0.50 /* electrode porosity */
#define c_coating 0.08 /* carbon coating fraction on LiFePO4 */

#define e_carbon 0.85  /* porosity of carbon */
#define Rho_c 2.2  /* density of carbon in g/cm3 */
#define Rho_active 3.6  /* density of active materials in g/cm3 JES 154(5) A389 2007*/
#define Rho_binder 1.76  /* density of binder in g/cm3 , Journal of The Electrochemical
Society, 158(1) A51-A57 (2011)*/


/* C_UDSI(c,t,0) seed position */



/* C_UDSI(c,t,1) Beta, 2 phase (LiFePO4) volume fraction */
/* C_UDSI(c,t,2) index to dishtinguish components */
/* C_UDSI(c,t,3) electrolyte */
/* C_UDSI(c,t,4) phai_e */
```

```
/* C_UDSI(c,t,5) electrons */
/* C_UDSI(c,t,6) d2ce/dx2, second derivative */
/* C_UDSI(c,t,7) d2ce/dy2, second derivative */

/* C_UDSI(c,t,8) seeds */
/* C_UDSI(c,t,9) before treatment of LiFePO4*/
/* C_UDSI(c,t,10) after treatment of LifePO4 */
/* C_UDSI(c,t,11) after adding carbon coating */
/* C_UDSI(c,t,12) after adding carbon and binder */

/* C_UDSI(c,t,16) two layer of C_UDSI(c,t,9) */
/* C_UDSI(c,t,17) two layer of C_UDSI(c,t,10)*/
/* C_UDSI(c,t,18) two layer of C_UDSI(c,t,11)*/
/* C_UDSI(c,t,19) two layer of C_UDSI(c,t,12)*/

/* C_UDSI(c,t,20) particles */
/* C_UDSI(c,t,21) particles diffusivity */


/*******************************************************/
DEFINE_INIT(init,d)
{
cell_t c;
Thread *t;
FILE *fUDS0,*fUDS1,*fUDS4;

int n,i,j,ip_up,ip_op,k,kkk,ip,ky,iii,kx,jj,kz,ii,xx,yy,zz,i_dd,i_up,n_part,i_tt;

int nnn=90; /* value that controls orientation */

int c_up[599000],c_op[250000],i_a[250001],i_b[250001];
double rr,sum_r,i_c[250001],xxx,yyy,zzz;

int active_total_occupied,n_carbon_total_occupied,i_lifepo4,i_ccoat,tt;

int r=5;

active_total_occupied=50000; /* # of polymer unit cells */

n=(int)(lx)*(int)(ly)*(int)(lz);
```

```
for (i=0;i<=(n-1);i++) {i_a[i]=0;i_b[i]=0;c_op[i]=0;c_up[i]=0;} /* set cell initial values to
zero */

/****************************************** putting seeds
******************************************/

srand(time(NULL));
for (j=0;j<=(n_seed-1);j++)
{iii=(int)(n*(real)(rand())/((real)(RAND_MAX)+1.0e-10));
i_a[iii]=12;}  /* end of putting LiFePO4 seeds */

thread_loop_c(t,d)
{begin_c_loop_all(c,t)
{C_UDSI(c,t,0)=i_a[c];}  /* record seed position */
end_c_loop_all(c,t)}

/*********************************************  grows polymers on seeds
*****************************************/

 ip_op=0; /* ocupied cells numbers */

 for (k=0;k<=(n-1);k++) {if (i_a[k]==12) {c_op[ip_op]=k;ip_op++;} } /* record the cell # of
occupied cells*/

 for (j=0;j<=(active_total_occupied-1-n_seed);j++)
{
  ip_up=0; /* un_ocupied cell numbers */

          for (kkk=0;kkk<=(ip_op-1);kkk++)
          {

          ky=c_op[kkk]/(int)(ly)/(int)(lx);
          kz=(c_op[kkk]-ky*(int)(ly)*(int)(lx))/(int)(lx);
          kx=c_op[kkk]-ky*(int)(ly)*(int)(lx)-kz*(int)(lx);

          ip=(kx-1)+(kz)*(int)(lx)+(ky)*(int)(ly)*(int)(lx);
          if (((kx-1)>=0)&&(i_a[ip]==0))  {for (k=1;k<=nnn;k++) {c_up[ip_up]=ip; ip_up++;}}

          ip=(kx+1)+(kz)*(int)(lx)+(ky)*(int)(ly)*(int)(lx);
          if (((kx+1)<=((int)(lx)-1))&&(i_a[ip]==0))  {for (k=1;k<=nnn;k++) {c_up[ip_up]=ip;
ip_up++;}}
```

```
        ip=(kx)+(kz-1)*(int)(lx)+(ky)*(int)(ly)*(int)(lx);
        if (((kz-1)>=0)&&(i_a[ip]==0))  {c_up[ip_up]=ip; ip_up++;}

        ip=(kx)+(kz+1)*(int)(lx)+(ky)*(int)(ly)*(int)(lx);
        if (((kz+1)<=((int)(lz)-1))&&(i_a[ip]==0)) {c_up[ip_up]=ip; ip_up++;}

        ip=(kx)+(kz)*(int)(lx)+(ky-1)*(int)(ly)*(int)(lx);
        if (((ky-1)>=0)&&(i_a[ip]==0))  {c_up[ip_up]=ip; ip_up++;}

        ip=(kx)+(kz)*(int)(lx)+(ky+1)*(int)(ly)*(int)(lx);
        if (((ky+1)<=((int)(ly)-1))&&(i_a[ip]==0))  {c_up[ip_up]=ip; ip_up++;}

        } /* end of kkk */

iii=c_up[(int)((ip_up-1)*(real)(rand())/((real)(RAND_MAX)+1.0e-10))];
i_a[iii]=12;

c_op[ip_op]=iii;
ip_op++;

} /* end of j */

thread_loop_c(t,d)
{begin_c_loop_all(c,t)
{C_UDSI(c,t,1)=i_a[c];}
end_c_loop_all(c,t)}

/************************************************** particle orientation
above **********************************/
}


/*************** DEFINE_on_demand - remove unmeaningful cells after complet
simulation **********************/
DEFINE_ON_DEMAND(left_right_boudries)
{

Domain *domain;
cell_t c;
Thread *t;

int kx,ky,kz;
```

```
domain= Get_Domain(1);
thread_loop_c(t,domain)
{
 begin_c_loop_all(c,t)
 {
                    ky=c/(int)(ly)/(int)(lx);
                    kz=(c-ky*(int)(ly)*(int)(lx))/(int)(lx);
                    kx=c-ky*(int)(ly)*(int)(lx)-kz*(int)(lx);

                    if ((kx==0)||(kx==((int)(lx)-1)))
                    {C_UDSI(c,t,1)=5;}
 }

  end_c_loop_all(c,t)
}


thread_loop_c(t,domain)
{
 begin_c_loop_all(c,t)
 {

                    if ((C_UDSI(c,t,1)==12)||(C_UDSI(c,t,1)==5))
                    C_UDSI_DIFF(c,t,2)=par_diff;
                    else
      C_UDSI_DIFF(c,t,2)=1.0e-30;
 }

  end_c_loop_all(c,t)
}

}

/*********************************************************************
********/
DEFINE_DIFFUSIVITY(diff_UDS2,c,t,i)
{
double diff;

if ((C_UDSI(c,t,1)==12)||(C_UDSI(c,t,1)==5)) diff=par_diff;
```

```
else
diff=0.0*1.0e-30;

return diff;
} /* end of define */


/************************************************
*****************************************/
DEFINE_ON_DEMAND(new_app_diff_cal)
{
Domain *domain;
cell_t c;
Thread *t;
real i_a[250002],i_c[250002];
int kz,ky,kx,nlx,nly,nlz,iii;
real ionic1,ionic2;
real x[ND_ND];

FILE *fUDS0;
fUDS0=fopen("app_diff_new.txt","w");
nlx=(int)(lx);
nly=(int)(ly);
nlz=(int)(lz);

domain= Get_Domain(1);

/******************************** substitute C-UDSI(c,t,1) with i_a(i)
*********************************/
thread_loop_c(t,domain)
{
          C_CENTROID(x,0,t);
 begin_c_loop_all(c,t)
  {
  i_a[c]=C_UDSI(c,t,2);  /* ionic*/
  i_c[c]=C_UDSI_DIFF(c,t,2);  /* ionic diff*/

 }
  end_c_loop_all(c,t)
}
```

```
/*************************************************************************
**********************/
kx=0;

ionic1=0.0; /* flux */

 for (kz=0;kz<=(nlz-1);kz++)
   for (ky=0;ky<=(nly-1);ky++)
          {
           iii=kx+kz*nlx+ky*nly*nlx;
           ionic1=ionic1+ a_length* a_length*i_c[iii]*(i_a[iii]-0.0)/x[0];
          } /*end for kz*/

kx=(nlx-1);

ionic2=0.0;

 for (kz=0;kz<=(nlz-1);kz++)
   for (ky=0;ky<=(nly-1);ky++)
          {
           iii=kx+kz*nlx+ky*nly*nlx;

           ionic2=ionic2+ a_length* a_length*i_c[iii]*(i_a[iii]-1.0)/x[0];
          } /*end for kz*/


 fprintf(fUDS0,"ionic1    flux       %12.8e\n",ionic1);
  fprintf(fUDS0,"ionic2 flux        %12.8e\n",ionic2);

                      fprintf(fUDS0,"conducivity@left         %18.9e\n",ionic1/(nly*nlz*
a_length* a_length)*nlx* a_length/1.0);
                                              fprintf(fUDS0,"conducivity@right
         %18.9e\n", ionic2/(nly*nlz* a_length* a_length)*nlx* a_length/1.0);

fclose(fUDS0);

} /* end*/



/*************************************************************************
**********************/
```

```
DEFINE_SOURCE(uds2,c,t,dS,eqn)

{
real x[ND_ND];
real source;

if ((C_UDSI(c,t,1)==12)||(C_UDSI(c,t,1)==5)) source=dS[eqn]=0.0;

else
{source=-1.0e30*C_UDSI(c,t,2)+1.0e30*0.0; dS[eqn]=-1.0e30; }

return source;
}
```

Appendix B

Simulated Structures

Top View

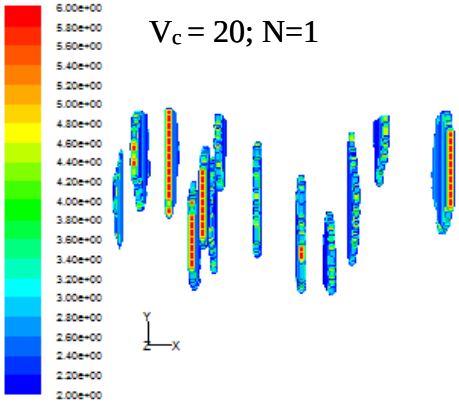

V_c = 20; N=1

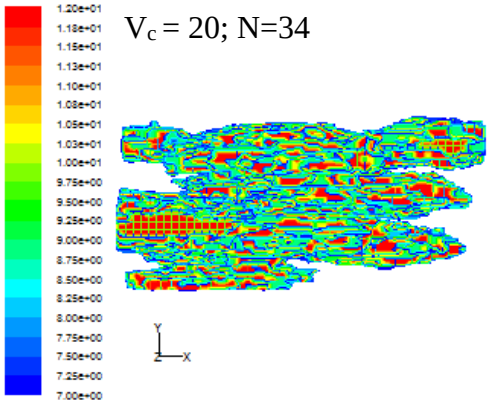

V_c = 20; N=34

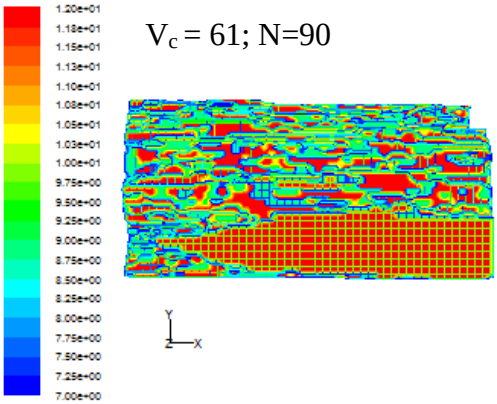

V_c = 61; N=90

Right Side View

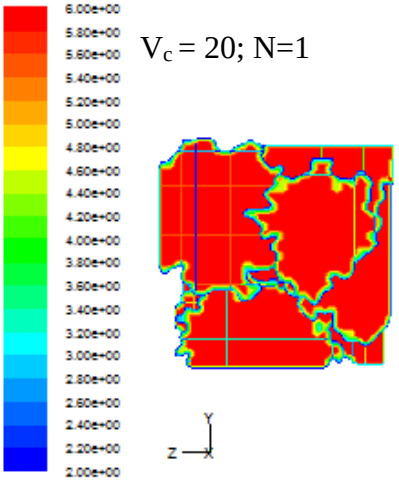

$V_c = 20$; N=1

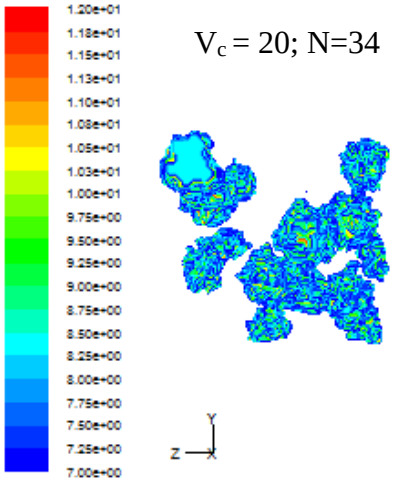

$V_c = 20$; N=34

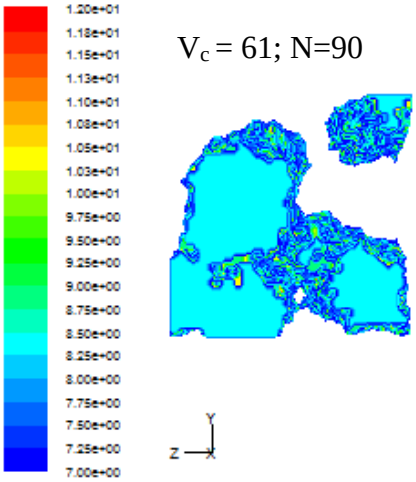

$V_c = 61$; N=90

Front View

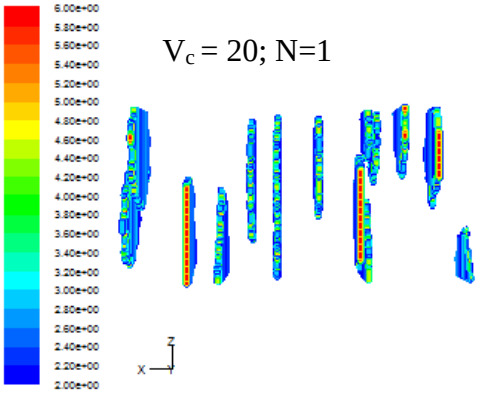

V_c = 20; N=1

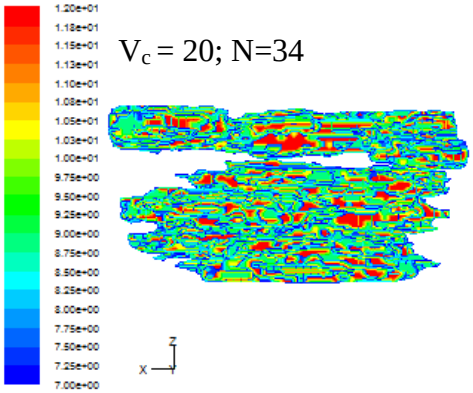

V_c = 20; N=34

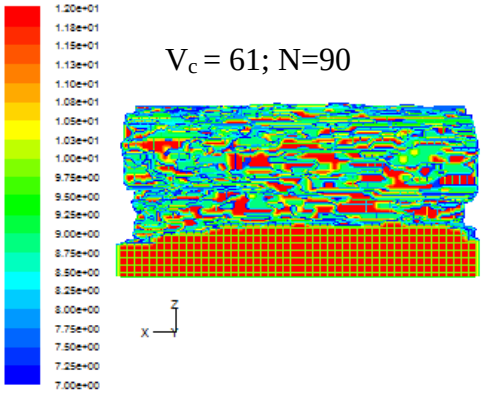

V_c = 61; N=90

References

1. Winter, M. and R.J. Brodd, *What Are Batteries, Fuel Cells, and Supercapacitors?* Chemical Reviews, 2004. **104**(10): p. 4245-4270.
2. Graziano, G., *Contrasting the denaturing effect of guanidinium chloride with the stabilizing effect of guanidinium sulfate.* Physical Chemistry Chemical Physics, 2011. **13**(25): p. 12008-12014.
3. http://www.fuelcell.no/principle_history_eng.htm
4. Yan, J. and M.A. Hickner, *Anion Exchange Membranes by Bromination of Benzylmethyl-Containing Poly(sulfone)s.* Macromolecules, 2010. **43**(5): p. 2349-2356.
5. ARGES, et al., *The chalkboard: Anion exchange membrane fuel cells*. Vol. 19. 2010, Pennington, NJ, ETATS-UNIS: Electrochemical Society. 5.
6. Varcoe, J.R. and R.C. Slade, *Prospects for Alkaline Anion-Exchange Membranes in Low Temperature Fuel Cells.* Fuel Cells, 2005. **5**(2): p. 187-200.
7. Gasteiger, H.A., et al., *Activity benchmarks and requirements for Pt, Pt-alloy, and non-Pt oxygen reduction catalysts for PEMFCs.* Applied Catalysis B: Environmental, 2005. **56**(1–2): p. 9-35.
8. de Leon, C.P., et al., *Direct borohydride fuel cells.* Journal of Power Sources, 2006. **155**(2): p. 172-181.

9. Anastasijević, N.A., V. Vesović, and R.R. Adžić, *Determination of the kinetic parameters of the oxygen reduction reaction using the rotating ring-disk electrode.* Journal of Electroanalytical Chemistry and Interfacial Electrochemistry, 1987. **229**(1): p. 305-316.

10. Spendelow, J.S. and A. Wieckowski, *Electrocatalysis of oxygen reduction and small alcohol oxidation in alkaline media.* Physical Chemistry Chemical Physics, 2007. **9**(21): p. 2654-2675.

11. Blizanac, B.B., P.N. Ross, and N.M. Markovic, *Oxygen electroreduction on Ag(1 1 1): The pH effect.* Electrochimica Acta, 2007. **52**(6): p. 2264-2271.

12. Tripković, A.V., et al., *Methanol electrooxidation on supported Pt and PtRu catalysts in acid and alkaline solutions.* Electrochimica Acta, 2002. **47**(22–23): p. 3707-3714.

13. Matsuoka, K., et al., *Alkaline direct alcohol fuel cells using an anion exchange membrane.* Journal of Power Sources, 2005. **150**: p. 27-31.

14. Yeung, K. and A. Tseung, *The Reduction of Oxygen on Teflon-Bonded Perovskite Oxide Electrodes.* Journal of The Electrochemical Society, 1978. **125**(6): p. 878-882.

15. Guo, M., et al., *Synthesis and characterization of novel anion exchange membranes based on imidazolium-type ionic liquid for alkaline fuel cells.* Journal of Membrane Science, 2010. **362**(1–2): p. 97-104.

16. Hosseini, S.M., S.S. Madaeni, and A.R. Khodabakhshi, *Preparation and characterization of ABS/HIPS heterogeneous anion exchange membrane filled with activated carbon.* Journal of Applied Polymer Science, 2010. **118**(6): p. 3371-3383.

17. Gu, S., et al., *A Soluble and Highly Conductive Ionomer for High-Performance Hydroxide Exchange Membrane Fuel Cells.* Angewandte Chemie International Edition, 2009. **48**(35): p. 6499-6502.

18. Wang, J., et al., *Synthesis of Soluble Poly(arylene ether sulfone) Ionomers with Pendant Quaternary Ammonium Groups for Anion Exchange Membranes.* Macromolecules, 2009. **42**(22): p. 8711-8717.

19. Robertson, N.J., et al., *Tunable High Performance Cross-Linked Alkaline Anion Exchange Membranes for Fuel Cell Applications.* Journal of the American Chemical Society, 2010. **132**(10): p. 3400-3404.

20. Bauer, B., H. Strathmann, and F. Effenberger, *Anion-exchange membranes with improved alkaline stability.* Desalination, 1990. **79**(2): p. 125-144.

21. Sata, T., et al., *Change of anion exchange membranes in an aqueous sodium hydroxide solution at high temperature.* Journal of Membrane Science, 1996. **112**(2): p. 161-170.

22. Hwang, G.-J. and H. Ohya, *Preparation of anion-exchange membrane based on block copolymers: Part 1. Amination of the chloromethylated copolymers.* Journal of Membrane Science, 1998. **140**(2): p. 195-203.

23. Komkova, E.N., et al., *Anion-exchange membranes containing diamines: preparation and stability in alkaline solution.* Journal of Membrane Science, 2004. **244**(1-2): p. 25-34.

24. Hibbs, M.R., et al., *Transport Properties of Hydroxide and Proton Conducting Membranes.* Chemistry of Materials, 2008. **20**(7): p. 2566-2573.

25. Li, L. and Y. Wang, *Quaternized polyethersulfone Cardo anion exchange membranes for direct methanol alkaline fuel cells.* Journal of Membrane Science, 2005. **262**(1-2): p. 1-4.

26. Couture, G., et al., *Polymeric materials as anion-exchange membranes for alkaline fuel cells.* Progress in Polymer Science, 2011. **36**(11): p. 1521-1557.

27. Tanaka, M., et al., *Anion Conductive Aromatic Ionomers Containing Fluorenyl Groups.* Macromolecules, 2010. **43**(6): p. 2657-2659.

28. Xiong, Y., et al., *Performance of organic–inorganic hybrid anion-exchange membranes for alkaline direct methanol fuel cells.* Journal of Power Sources, 2009. **186**(2): p. 328-333.

29. Pan, J., et al., *High-Performance Alkaline Polymer Electrolyte for Fuel Cell Applications.* Advanced Functional Materials, 2010. **20**(2): p. 312-319.

30. Lee, S.H. and J.C. Rasaiah, *Proton transfer and the mobilities of the H[sup +] and OH[sup -] ions from studies of a dissociating model for water*. The Journal of Chemical Physics, 2011. **135**(12): p. 124505-10.

31. Lin, X., et al., *Alkali resistant and conductive guanidinium-based anion-exchange membranes for alkaline polymer electrolyte fuel cells.* Journal of Power Sources, 2012. **217**(0): p. 373-380.

32. Wang, J., S. Li, and S. Zhang, *Novel Hydroxide-Conducting Polyelectrolyte Composed of an Poly(arylene ether sulfone) Containing Pendant Quaternary Guanidinium Groups for Alkaline Fuel Cell Applications.* Macromolecules, 2010. **43**(8): p. 3890-3896.

33. Kim, D.S., et al., *Guanidinium-Functionalized Anion Exchange Polymer Electrolytes via Activated Fluorophenyl-Amine Reaction.* Chemistry of Materials, 2011. **23**(17): p. 3795-3797.

34. Qu, C., et al., *A high-performance anion exchange membrane based on bi-guanidinium bridged polysilsesquioxane for alkaline fuel cell application.* Journal of Materials Chemistry, 2012. **22**(17): p. 8203-8207.

35. Mateus, N.M.M., et al., *Synthesis and properties of tetra-alkyl-dimethylguanidinium salts as a potential new generation of ionic liquids.* Green Chemistry, 2003. **5**(3): p. 347-352.

36. Zhang, Q., S. Li, and S. Zhang, *A novel guanidinium grafted poly(aryl ether sulfone) for high-performance hydroxide exchange membranes.* Chemical Communications, 2010. **46**(40): p. 7495-7497.

37. Merle, G., M. Wessling, and K. Nijmeijer, *Anion exchange membranes for alkaline fuel cells: A review.* Journal of Membrane Science, 2011. **377**(1): p. 1-35.

38. Cope, A.C. and A.S. Mehta, *Mechanism of the Hofmann elimination reaction: an ylide intermediate in the pyrolysis of a highly branched quaternary hydroxide.* Journal of the American Chemical Society, 1963. **85**(13): p. 1949-1952.

39. Varcoe, J., S. Poynton, and R. Slade, *Alkaline anion-exchange membranes for low-temperature fuel cell application.* Handbook of Fuel Cells, 2010.

40. Zhang, F., et al., *PTFE based composite anion exchange membranes: thermally induced in situ polymerization and direct hydrazine hydrate fuel cell application.* Journal of Materials Chemistry, 2010. **20**(37): p. 8139-8146.

41. Liu, Y.-L., et al., *Preparation and applications of Nafion-functionalized multiwalled carbon nanotubes for proton exchange membrane fuel cells.* Journal of Materials Chemistry, 2010. **20**(21): p. 4409-4416.

42. Matsumoto, K., et al., *Very High Performance Alkali Anion-Exchange Membrane Fuel Cells.* Advanced Functional Materials, 2011. **21**(6): p. 1089-1094.

43. Jung, M.-s.J., C.G. Arges, and V. Ramani, *A perfluorinated anion exchange membrane with a 1,4-dimethylpiperazinium cation.* Journal of Materials Chemistry, 2011. **21**(17): p. 6158-6160.

44. Brian, R.E., et al., *Stability of Cations for Anion Exchange Membrane Fuel Cells.* ECS Transactions, 2007. **11**(1): p. 1173-1180.

45. Zhou, J., et al., *Anionic polysulfone ionomers and membranes containing fluorenyl groups for anionic fuel cells.* Journal of Power Sources, 2009. **190**(2): p. 285-292.

46. Chempath, S., et al., *Mechanism of Tetraalkylammonium Headgroup Degradation in Alkaline Fuel Cell Membranes.* The Journal of Physical Chemistry C, 2008. **112**(9): p. 3179-3182.

47. Zhang, Q., S. Li, and S. Zhang, *A novel guanidinium grafted poly (aryl ether sulfone) for high-performance hydroxide exchange membranes.* Chemical Communications, 2010. **46**(40): p. 7495-7497.

48. Varcoe, J.R. and R.C.T. Slade, *Prospects for Alkaline Anion-Exchange Membranes in Low Temperature Fuel Cells.* Fuel Cells, 2005. **5**(2): p. 187-200.

49. Sajjad, S.D., Y. Hong, and F. Liu, *Synthesis of guanidinium-based anion exchange membranes and their stability assessment.* Polymers for Advanced Technologies, 2014. **25**(1): p. 108-116.

50. Agmon, N., *Mechanism of hydroxide mobility.* Chemical Physics Letters, 2000. **319**(3): p. 247-252.

51. Tuckerman, M.E., D. Marx, and M. Parrinello, *The nature and transport mechanism of hydrated hydroxide ions in aqueous solution.* Nature, 2002. **417**(6892): p. 925-929.

52. Grew, K.N. and W.K. Chiu, *A dusty fluid model for predicting hydroxyl anion conductivity in alkaline anion exchange membranes.* Journal of the Electrochemical Society, 2010. **157**(3): p. B327-B337.

53. Qian, L., et al., *Modified guanidine polymers: synthesis and antimicrobial mechanism revealed by AFM.* Polymer, 2008. **49**(10): p. 2471-2475.

54. Rogalskyy, S., et al., *Fabrication of new antifungal polyamide-12 material.* Polymer International, 2012. **61**(5): p. 686-691.

55. Nakanishi, K., Infrared Absorption Spectroscopy, Tokyo: Nankido Company, 1962.

56. Goto, T., K. Nakanishi, and M. Ohashi, *An account on the infrared absorption of guanidiniums.* Bulletin of the Chemical Society of Japan, 1957. **30**(7): p. 723-725.

57. Stel'Mah, S., L. Bazaron, and D. Mognonov, *On the mechanism of the hexamethylenediamine and guanidine hydrochloride polycondensation.* Russian Journal of Applied Chemistry, 2010. **83**(2): p. 342-344.

58. Stel'makh Sergey Aleksandrovich, G.e., et al., *Synthesis and pH-Sensitivity of Guanidine Containing Hydrogels.* 2012.

59. Liu, F., et al., *Development of novel self-humidifying composite membranes for fuel cells.* Journal of Power Sources, 2003. **124**(1): p. 81-89.

60. Liu, F., et al., *Nafion/PTFE composite membranes for fuel cell applications.* Journal of Membrane Science, 2003. **212**(1–2): p. 213-223.

61. Zhang, Y., J. Jiang, and Y. Chen, *Synthesis and antimicrobial activity of polymeric guanidine and biguanidine salts.* Polymer, 1999. **40**(22): p. 6189-6198.

62. Kreuer, K.-D., et al., *Transport in Proton Conductors for Fuel-Cell Applications: Simulations, Elementary Reactions, and Phenomenology.* Chemical Reviews, 2004. **104**(10): p. 4637-4678.

63. Fernandes, L.L., et al., *Cytocompatibility of chitosan and collagen-chitosan scaffolds for tissue engineering.* Polímeros, 2011. **21**: p. 1-6.

64. Kovalenko, V.I., D.N. Gayfutdinova, and V.L. Furer, *Ionic layers of potassium and sodium stearates at liquid-crystal transitions according to the data from infra-red spectroscopy.* Physicochem Investig, 2002. **2**(6): p. 37.

65. Tao, Y., J. Kim, and J.M. Torkelson, *Achievement of quasi-nanostructured polymer blends by solid-state shear pulverization and compatibilization by gradient copolymer addition.* Polymer, 2006. **47**(19): p. 6773-6781.

66. Kenji Fukuta, AMFC Workshop,Tokuyama Corporation, May 8th 2011.

67. Arges, C.G., V. Ramani, and P.N. Pintauro, *Anion Exchange Membrane Fuel Cells.* The Electrochemical Society Interface, 2010. **Summer**: p. 31-35.

68. Even, U. and J. Jortner, *Spectroscopy of Large Molecules in Supersonic Expansions: Isolated Ultracold Porphyrins*, in *Intramolecular Dynamics*, J. Jortner and B. Pullman, Editors. 1982, Springer Netherlands. p. 227-240.

69. Kiss, A.M., et al., *Carbonate and bicarbonate ion transport in alkaline anion exchange membranes.* Journal of The Electrochemical Society, 2013. **160**(9): p. F994-F999.

70. Pivovar, B., *2011 Alkaline Membrane Fuel Cell Workshop Final Report.* Contract, 2012. **303**: p. 275-3000.

71. Robertson, N.J., et al., *Tunable High Performance Cross-Linked Alkaline Anion Exchange Membranes for Fuel Cell Applications.* Journal of the American Chemical Society, 2010. **132**(10): p. 3400-3404.

72. Fujimoto, C.H., et al., *Ionomeric Poly(phenylene) Prepared by Diels−Alder Polymerization: Synthesis and Physical Properties of a Novel Polyelectrolyte.* Macromolecules, 2005. **38**(12): p. 5010-5016.

73. Jeong, M.-H., K.-S. Lee, and J.-S. Lee, *Cross-Linking Density Effect of Fluorinated Aromatic Polyethers on Transport Properties.* Macromolecules, 2009. **42**(5): p. 1652-1658.

74. Slade, S., et al., *Ionic Conductivity of an Extruded Nafion 1100 EW Series of Membranes.* Journal of The Electrochemical Society, 2002. **149**(12): p. A1556-A1564.

75. Zhou, J., et al., *Crosslinked, epoxy-based anion conductive membranes for alkaline membrane fuel cells.* Journal of Membrane Science, 2010. **350**(1–2): p. 286-292.

76. Qiu, B., et al., *Alkaline imidazolium- and quaternary ammonium-functionalized anion exchange membranes for alkaline fuel cell applications.* Journal of Materials Chemistry, 2012. **22**(3): p. 1040-1045.

77. Wan, Y., et al., *Anion-exchange membranes composed of quaternized-chitosan derivatives for alkaline fuel cells.* Journal of Power Sources, 2010. **195**(12): p. 3785-3793.

78. Gasa, J.V., R. Weiss, and M.T. Shaw, *Ionic crosslinking of ionomer polymer electrolyte membranes using barium cations.* Journal of Membrane Science, 2007. **304**(1): p. 173-180.

79. Walker, M., et al., *Barrier properties of plasma-polymerized thin films.* Surface and Coatings technology, 1999. **116**: p. 996-1000.

80. Miyatake, K., H. Zhou, and M. Watanabe, *Proton Conductive Polyimide Electrolytes Containing Fluorenyl Groups: Synthesis, Properties, and Branching Effect.* Macromolecules, 2004. **37**(13): p. 4956-4960.

81. Lee, S.H. and J.C. Rasaiah, *Proton transfer and the mobilities of the H+ and OH- ions from studies of a dissociating model for water.* Journal of Chemical Physics, 2011. **135**(12).

82. Lin, X.C., et al., *Alkali resistant and conductive guanidinium-based anion-exchange membranes for alkaline polymer electrolyte fuel cells.* Journal of Power Sources, 2012. **217**: p. 373-380.

83. Sajjad, S.D., Y. Hong, and F. Liu, *Synthesis of guanidinium-based anion exchange membranes and their stability assessment.* Polymers for Advanced Technologies, 2014. **25**(1): p. 108-116.

84. Sajjad, S.D., et al., *Guanidinium based blend anion exchange membranes for direct methanol alkaline fuel cells (DMAFCs).* Journal of Power Sources, 2015. **300**: p. 95-103.

85. Ye, Y.-S., et al., *Alkali doped polyvinyl alcohol/graphene electrolyte for direct methanol alkaline fuel cells.* Journal of Power Sources, 2013. **239**(0): p. 424-432.

86. Grew, K.N. and W.K.S. Chiu, *A Dusty Fluid Model for Predicting Hydroxyl Anion Conductivity in Alkaline Anion Exchange Membranes.* Journal of The Electrochemical Society, 2010. **157**(3): p. B327-B337.

87. Kim, D.S., et al., *Copoly(arylene ether)s Containing Pendant Sulfonic Acid Groups as Proton Exchange Membranes† † NRCC Publication No. 50899.* Macromolecules, 2009. **42**(4): p. 957-963.

88. Xiong, Y., et al., *Synthesis and characterization of cross-linked quaternized poly (vinyl alcohol)/chitosan composite anion exchange membranes for fuel cells.* Journal of Power Sources, 2008. **183**(2): p. 447-453.

89. Choi, P., N.H. Jalani, and R. Datta, *Thermodynamics and proton transport in Nafion II. Proton diffusion mechanisms and conductivity.* Journal of The Electrochemical Society, 2005. **152**(3): p. E123-E130.

90. Commer, P., et al., *The effect of water content on proton transport in polymer electrolyte membranes.* Fuel Cells, 2002. **2**(3-4): p. 127-136.

91. Marx, D., *Proton transfer 200 years after von Grotthuss: Insights from ab initio simulations.* ChemPhysChem, 2006. **7**(9): p. 1848-1870.

92. Paddison, S.J. and R. Paul, *The nature of proton transport in fully hydrated Nafion®.* Physical Chemistry Chemical Physics, 2002. **4**(7): p. 1158-1163.

93. Paddison, S.J., R. Paul, and T.A. Zawodzinski, *A statistical mechanical model of proton and water transport in a proton exchange membrane.* Journal of The Electrochemical Society, 2000. **147**(2): p. 617-626.

94. Thampan, T., et al., *Modeling of conductive transport in proton-exchange membranes for fuel cells.* Journal of The Electrochemical Society, 2000. **147**(9): p. 3242-3250.

95. Aleksandrova, E., et al., *Electrochemical atomic force microscopy study of proton conductivity in a Nafion membrane.* Physical Chemistry Chemical Physics, 2007. **9**(21): p. 2735-2743.

96. Aleksandrova, E., et al., *Spatial distribution and dynamics of proton conductivity in fuel cell membranes: potential and limitations of electrochemical atomic force microscopy measurements.* Journal of Physics: Condensed Matter, 2011. **23**(23): p. 234109.

97. James, P.J., et al., *Hydration of Nafion® studied by AFM and X-ray scattering.* Journal of Materials Science, 2000. **35**(20): p. 5111-5119.

98. Wang, X., et al., *A Terphenyl Scaffold for π-Stacked Guanidinium Recognition Elements.* Organic Letters, 2007. **10**(2): p. 297-300.

Biographical Information

Syed Dawar Sajjad was born in Karachi, Pakistan and got his primary education there. He received his Bachelor of Science (BS) degree in Metallurgy and Materials Engineering from Ghulam Ishaq Institute of Engineering Sciences & Technology at Topi, Swabi in 2009. He later joined NED University in Karachi as a lecturer for a full year and played a pioneering role in developing the new Materials Science Engineering Department there.

In 2010 he joined The University of Texas at Arlington to pursue his doctoral degree and worked under supervision of Dr. Fuqiang Liu of Materials Science and Engineering and received his Ph.D. degree in 2015. His primary research area during his doctoral study was science, engineering and technology of guanidinium based anion exchange membrane fuel cells for polymer alkaline fuel cells, while he also worked on PEM fuel cell catalyst, vanadium redox flow battery and lithium ion battery materials.

He plans to work in the industry to gain more practical experience and diversify his research interests. He plans to start a business in future in the developing countries. But mostly he is keen on using his academic and research experience to give back to the society.